Influence of the Madden-Julian Oscillation and Intraseasonal Waves on Surface Wind and Convection of Tropical Atlantic Ocean

By

Wei Yu

B.A., Nanjing Institute of Meteorology, 1991

M.S., Nanjing Institute of Meteorology, 1994

M.S., Meteorology, Florida State University, 2000

M.S., Computer Sciences, Florida State University, 2002

A thesis submitted to the

Faculty of the Graduate School of the

University of Colorado in partial fulfillment

of the requirement for the degree of

Doctor of Philosophy

Department of Atmospheric and Oceanic Sciences

2011

This thesis entitled:

Influence of the Madden-Julian Oscillation and Intraseasonal waves on surface wind and convection of Tropical Atlantic Ocean

written by Wei Yu

has been approved for the Department of Atmospheric and Oceanic Sciences

_____

Weiqing Han

_____

David Gochis

Date_____

The final copy of this thesis has been examined by the signatories, and we find that both the content and the form meet acceptable presentation standards of scholarly work in the above mentioned discipline.

Yu, Wei (Ph.D., Department of Atmospheric and Oceanic Sciences)

Influence of the Madden-Julian Oscillation and Intraseasonal Waves on Surface Wind and Convection of Tropical Atlantic Ocean

Thesis directed by Associate Professor Weiqing Han

Intraseasonal variability (10-100 day periods) of surface wind and convection in the tropical Atlantic is analyzed using QuikSCAT satellite wind, outgoing longwave radiation (OLR), and precipitation for the period of 2000-2008. Similar analyses have also been performed using the European Centre for Medium-Range Weather Forecasts (ECMWF) 40-year Re-Analysis (ERA40) data from 1960-2001 and ERA-interim reanalysis products for 1990-2008. Case studies show that the MJO propagated eastward from the Indo-Pacific Ocean to the Atlantic during winter and spring of 2002, causing the observed 40-60-day wind variations in the equatorial Atlantic basin. The Isthmus of Panama is a dominant pathway for these surface wind anomalies to propagate into the Atlantic, where they can produce important climate impacts. This pathway is statistically significant based on the analysis using multi-year data.

Further analyses have been carried out to assess the relative importance of dominant atmospheric intraseasonal convective processes over the tropical Atlantic Ocean and African Monsoon region: the Madden-Julian Oscillation (MJO, which dominates the eastward-propagating signals at 20-100-day periods), quasi-biweekly (10-25 days) Kelvin waves, and 10-100-day westward propagating Rossby waves. The results show that contribution from each process varies in different regions of the tropical Atlantic Ocean and African monsoon region. In general, the eastward-propagating MJO

and quasi-biweekly Kelvin wave more frequently dominate strong convective events than Rossby waves in the African monsoon region. The westward-propagating Rossby waves, on the other hand, have larger contributions to convection in the Western Atlantic Ocean. Both the westward- and eastward-propagating signals contribute approximately equally in the Central Atlantic basin. The impacts of intraseasonal signals have evident seasonality. The MJO is stronger during November-April than May-October in all regions. The 20-100-day Rossby waves are stronger during November-April than May-October in the African monsoon region, and are equally strong for the two seasons and dominate convection variability during May-October in the Western and Central Atlantic basins. Of particular interest is that the MJO originated from the Indo-Pacific Ocean, and the quasi-biweekly Kelvin wave generated by convection in the Amazon region and western Atlantic basin can enhance as they propagate through the tropical Atlantic Ocean, amplifying their impacts on the African monsoon. On the other hand, Rossby waves can be generated either in the eastern equatorial Atlantic or West African monsoon region. They can strengthen while they propagate westward through the tropical Atlantic, producing large effects on the Western Atlantic, Caribbean Sea and Central America regions. These results imply that air-sea interaction in the Atlantic Ocean, and possibly interaction with local convective signals can modify the strengths of the MJO, Kelvin and Rossby waves, which have important implication for the prediction in the countries that surround the tropical Atlantic Ocean.

ACKNOWLEDGEMENTS

I wish to express my sincere appreciation to Dr. Weiqing Han, my major advisor, for her encouragement, valuable discussions and suggestions during the course of this study and publishing the results. I would also like to thank Dr. Eric Maloney, Dr. David Gochis, Dr. Tom Warner, Dr. David Noone and Dr. Peter Pilewskie, for serving as my committee members and their encouragements and valuable discussions during those years. Special thanks to Dr. Eric Maloney and Dr. David Gochis for their valuable discussions, suggestions and reviewing drafts for publishing the paper.

Special thanks also go to my colleagues, who are in Dr. Weiqing Han's research group (Benet E Duncan, Laurie Leah Trenary and Jih-Wang Wang), for their helpful discussions and assistance. Thanks NCAR for the financial support of my PhD study. I must also express my gratitude to Laurie Conway ── her assistance made my PhD course work and graduation procedures a lot easier. I also want to express my gratitude to my NCAR colleagues: Terri Betancourt, Dara Houliston and Ming Ge, who gave me their encouragement and support.

CONTENTS

TABLES

Table

FIGURES

Figure

CHAPTER I

INTRODUCTION

Previous studies have shown significant intraseasonal oscillations (ISOs) in the tropical Atlantic and West African sector (e.g., Park and Schubert 1993; Shapiro and Goldenberg 1993; Foltz and McPhaden 2004; Gu and Alder 2004; Gu 2009). A few processes have been suggested to be able to cause these oscillations: the global propagation of the Madden-Julian Oscillation (MJO; Madden and Julian 1971,1972) originating from the Indo-Pacific Ocean (e.g., Park and Schubert 1993; Hendon and Salby 1994; Foltz and McPhaden 2004), intraseasonal variations of convection in the African monsoon region (e.g., Grodsky and Carton 2001; Thorncroft et al. 2003; Maloney and Shaman 2008; Janicot et al. 2009; Gu 2009), and atmospheric variability from mid-latitudes (e.g., Park and Schubert 1993; Shapiro and Goldenberg 1993). The MJO and intraseasonal convection of the African monsoon, however, are not completely independent. It has been shown that the MJO can affect the intraseasonal convection of the West African monsoon (e.g., Gu and Adler 2004; Maloney and Shaman 2008).

1.1 Observations and Mechanisms of the MJO

1.1.1 Observed Features

The MJO is the most prominent mode of atmospheric intraseasonal variability in

the tropical troposphere. It is known to be convectively coupled, and have global zonal wavenumbers 1-3, with peak period at 30-90 days. The convective aspects are most apparent in the Indian and western Pacific Oceans, where the sea surface temperature (SST) is warm and known as the “warm pool”. The MJO propagates eastward in the Indo-Pacific warm pool at an averaged speed of 5 m/s (e.g., Weickmann et al., 1985; Knutson et al., 1986). Although the convectively coupled signal disappears outside of the ”warm pool”, a global eastward-propagating signal is observed in the zonal wind of the upper troposphere that moves much more rapidly as free Kelvin waves (Milliff and Madden, 1996; Matthews, 2000). The space-time schematic diagram of the large-scale features of the MJO is presented in Figure 1.1 (Madden and Julian 1972).

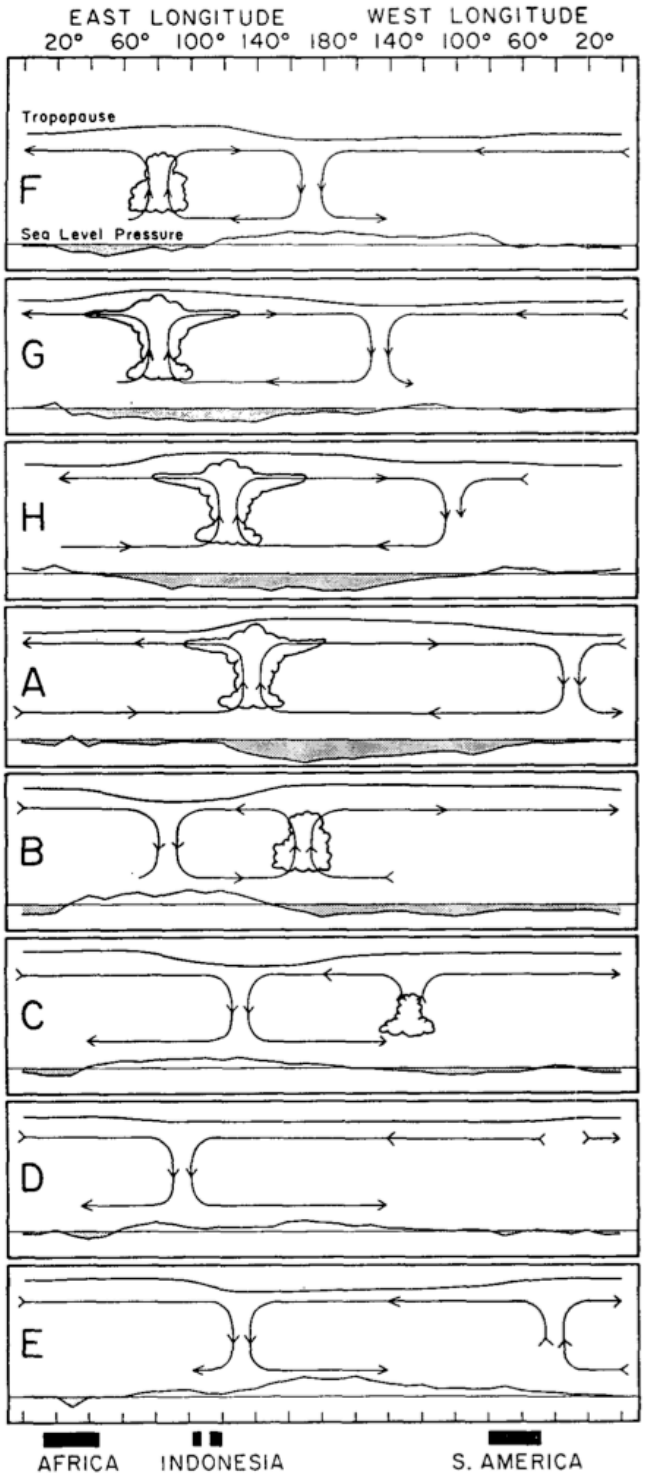

Figure 1.1. Schematic depiction of the fundamental large-scale features of the Madden-Julian Oscillation (MJO) through its life cycle (from top to bottom). Cloud symbols represent the convective center, arrows indicate the zonal circulation, and curves above and below the circulation represent perturbations in the upper troposphere and sea level pressure. From Madden and Julian [1972].

In the Indo-Pacific Ocean, the large-scale wind structure of the MJO is often described in terms of equatorial waves coupled to deep convection. East of the convective center, there are anomalous low-level easterlies and upper-level westerlies, which resemble the equatorial Kelvin wave. Immediately to the east of the convective center are low-level convergence, ascending motions and positive humidity. To the west, there are anomalous low-level westerlies (upper level easterlies) with a pair of cyclonic (anticyclonic) circulations straddling the equator at the surface (upper level), which characterize the equatorial Rossby waves (Madden, 1986). Immediately to the west of the convective center are low-level divergence, descending motions and negative humidity. Both Kelvin and Rossby wave structures have been considered dynamically essential to the MJO (Zhang 2005). Along the equator, the above fields have westward tilt in the vertical with respect to the convective center (e.g., Sperber, 2003; Kiladis et al., 2005; Zhang 2005). Such zonal asymmetry provides favorable large-scale conditions for the development of new convective systems east of the existing ones and discourages such development to the west, resulting in the eastward propagation of convection (see Zhang 2005 for a summary).

The MJO activities exhibit significant interannual variability and pronounced seasonality: the MJO is stronger and propagates eastward during boreal winter (November─April), but weaker and propagates both eastward and northward (southward) in the northern (southern) hemisphere during boreal summer (May-──October) (Wang and Rui, 1990; Madden and Julian, 1994; Hendon and Salby, 1994; Wang and Xie, 1997; Lawrence and Webster, 2001).

1.1.2 Mechanisms

Even though the existence of the MJO has been observed since the 1970s (Madden and Julian 1971, 1972), a fundamental understanding of the underlying physical mechanisms remains elusive. A number of theories exist that attempt to explain the primary observed features of the MJO.

(a) Atmospheric Response to Independent Forcing. It has been suggested that intraseasonal fluctuations in precipitation associated with the Asian summer monsoon can be a forcing source for the MJO, which are relatively stationary in space and can result from the local hydrological cycle (e.g., Yasunari, 1979; Webster, 1983). They can excite a stationary oscillation in precipitation with a period close to 50 days (Zhang 2005, and references therein). However, no statistically significant signals of intraseasonal stationary oscillation in equatorial convection can be objectively identified (Zhang and Hendon 1997). In addition, tropical stochastic forcing (e.g., Majda and Biello, 2004) and extratropical disturbances (Lau and Peng, 1987; Hsu et al., 1990; Lau et al., 1994; Matthews et al., 1996; Liebmann and Hartmann, 1984; Magana and Yanai, 1991; Matthews and Kiladis, 1999; Yanai and Lu, 1983; Yanai et al., 2000) have also been thought to be possible sources of the MJO forcing. The maximum growth in precipitation due to this stochastic forcing is, however, at zonal wave numbers greater than 4. Thus, momentum and energy transferring from synoptic-scale to planetary-scale intraseasonal perturbations play a crucial role to generate the MJO. A coupling between extratropical baroclinic disturbances and tropical barotropic intraseasonal perturbations may amplify

the latter. However, whether relationships between the extratropical and tropical intraseasonal signals are statistically significant is controversial.

(b) Atmospheric Instability. Instability theories seek mechanisms for growing, unstable modes that resemble the observed MJO. Sources of the instabilities involve deep convective processes, which are associated with moisture convergence and surface evaporation. For the moisture convergence instability theory, ‘‘Kelvin wave-CISK’’ (Lau and Peng, 1987; Chang and Lim, 1988), suggests that equatorial Kelvin wave becomes unstable when its convective heating interacts with its low-level convergence. Without additional assumptions, unstable wave-CISK Kelvin modes propagate at speeds (16-19 m/s) much faster than the MJO, and the growth rates are the greatest on smallest scales. By including the frictional effect on moisture convergence in the atmospheric boundary layer in a “moist Kelvin wave”, referred to as “frictional-convergence” theory of the MJO (Salby et al., 1994), the fast-speed and small-scale problems from wave-CISK theory have been treated. Frictional convergence in the boundary layer leads wave convergence in the lower tropical troposphere and damps small-scale wave-CISK modes. The instability of moisture convergence due to boundary layer viscosity results in slowly eastward moving, planetary-scale unstable modes. By including the equatorial Rossby wave, boundary layer dynamics can generate an unstable mode consisting of coupled Rossby-Kelvin waves (Wang and Rui, 1990; Wang and Li, 1994). A key feature of this theory is that the boundary layer convergence leading (east of) the convective center of the MJO, which has been confirmed by many studies (Hendon and Salby, 1994; Jones and Weare, 1996; Maloney and Hartmann, 1998; Kiladis et al., 2005).

In the surface evaporation mechanism, or "wind-induced surface heat exchange" (WISHE) (e.g., Emanuel, 1987) or "evaporation-wind feedback" (EWF) (Neelin et al., 1987) mechanism, the interactions between surface evaporation and the surface wind component of planetary-scale Kelvin waves provide a source of instability for the MJO (Raymond 2001; Sugiyama 2009a, b; Sobel et al. 2008, 2010).

(c) Other Factors. Recent model experiments suggest that the MJO is driven at least in part by moisture mode instability (e.g., Majda and Stechmann 2009; Raymond and Fuchs 2009; Maloney et al. 2010). A moisture mode is a balanced disturbance, whose large-scale circulations are well described by the weak temperature gradient approximation (e.g., Held and Hoskins 1985; Sobel et al. 2001) and involve those processes that control the tropical moisture field, such as surface latent heat flux and horizontal advection (e.g., Sobel et al. 2001; Majda and Klein 2003; Maloney et al. 2010). MJO is a moisture mode destabilized by increasing moisture anomalies, and the propagation of the disturbances is governed by processes that make moisture anomalies move horizontally (e.g., Sobel et al. 2001; Raymond and Fuchs, 2009; Maloney et al. 2010). The model results of Majda and Stechmann (2009) also offer an explanation for the observed dominance of eastward-propagating intraseasonal variability that the eastward-propagating modes are more strongly coupled with the equatorial moist convective processes as convectively coupled moisture mode instability. SST is very important for the large-scale organization of tropical convection and the impacts of atmosphere–ocean coupling in tropical intraseasonal oscillations have been addressed and

play important roles for the evolution, propagation and prediction of the MJO (Grabowski 2006; Linter and Neelin 2008; Fu et. al 2008; Sobel et. al 2010).

1.2 Impacts of the MJO

The MJO is climatically important because it can have significant impacts on ENSO (e.g., Moore and Kleeman 1999; McPhaden 1999; Takayabu et al. 1999; Kessler and Kleeman 2000; Zhang 2005), the Asian-Australian monsoon (e.g., Sikka and Gadgil 1980; Yasunari 1981; Krishnamurti and Subramanyam 1982; Webster 1983; Wang and Xie 1997; Lawrence and Webster 2001; Lau and Waliser 2005), the Indian Ocean Dipole (e.g., Rao and Yamagata 2004; Han et al. 2006), and tropical cyclones (e.g. Maloney and Shaman 2008).

Many previous studies have revealed the global influences of the MJO. Strong MJO signals have been observed in the North American Monsoon (NAM; e.g. Higgins and Shi 2001; Barlow and Salstein, 2006; Lorenz and Hartmann, 2006), where positive zonal wind anomalies in the Eastern Tropical Pacific are followed by anomalous precipitation in Mexico and the southwest United States several days later. Foltz and McPhaden (2004) showed that intraseasonal surface wind variability is prominent in the subtropical and mid-latitude Atlantic Ocean, where surface winds are significantly correlated with MJO signals in the Indo-Pacific Ocean. Jones and Schemm (2000) demonstrated that the South Atlantic Convergence Zone (SACZ) exhibits a wide range of intraseasonal variability, and that 30-70 day variations are directly related to the MJO.

Maloney and Hartmann (2000) showed that the MJO can affect the Atlantic, and demonstrated a link between the MJO and hurricane activity in the Gulf of Mexico and the Caribbean Sea. Given that the cold sea surface temperatures (SSTs) in the Eastern Pacific cold tongue region inhibit convection, the South American continent blocks continuous air-sea interaction, and the Andes block eastward propagation, the actual mechanisms by which the MJO influences the tropical Atlantic and the propagation of the MJO surface signatures into that basin are still not well-characterized.

Interestingly, in the equatorial Atlantic Ocean, satellite and in situ observations show significant spectral peaks at 40–60 day periods in surface winds, sea level, and thermocline depth (Han et al. 2008). Results from numerical model experiments demonstrate that this sea level and thermocline depth variability results mainly from the first and second baroclinic modes of oceanic equatorial Kelvin waves forced by 40-60-day equatorial zonal wind anomalies. The significant 40–60-day peaks in zonal and meridional winds, which appeared in both the QuikSCAT and Pilot Research Moored Array in the Tropical Atlantic (PIRATA) data, were found to be especially strong in 2002, a year when anomalously warm temperatures or a so-called ‘Atlantic Niño’ event occurred (Fu et al. 2007). Han et al. (2008) also found that 40-60-day zonal wind anomalies in the central-western equatorial Atlantic basin for the 2000–06 period were significantly correlated with sea level anomalies across the equatorial Atlantic basin, with simultaneous and lag correlation values ranging from 0.62 to 0.74 with significance above 95%. Han et al. (2008), however, did not explain the origin of the strong 40-60-day wind anomalies. Since the cold SST in the Eastern Pacific inhibits MJO convection and

the Andes block the MJO propagating into the Atlantic Ocean, the global eastward-propagating signals are shown to be in the upper troposphere through the non-convectively coupled longitudes more rapidly than the MJO (Milliff and Madden, 1996; Matthews, 2000). What is the source of the 40-60-day zonal surface wind observed in the equatorial Atlantic Ocean?

1.3 ISOs in African Monsoon Region and Their Impacts on Atlantic Ocean

Observational evidence shows that boreal summer wind and precipitation associated with the West African monsoon, which have 10-25-day and 25-60-day dominant periods, can affect the Eastern-Central Tropical Atlantic Ocean especially the Intertropical Convergence Zone (ITCZ; e.g., Grodsky and Carton 2001; Janicot and Sultan 2001; Redelsperger et al. 2002; Nicholson and Grist 2003; Thorncroft et al. 2003; Sultan and Janicot 2003a; Maloney and Shaman 2008; Mounier et al. 2008; Janicot et al. 2009). It is shown that enhanced (suppressed) 30-90-day precipitation anomalies of atmosphere are accompanied by a significant suppression (enhancement) of the Eastern North Atlantic trade winds (Maloney and Shaman 2008).

Wang and Fu (2007) showed that the convection on Amazon could affect the Atlantic ITCZ at a convectively coupled Kelvin waves with a period of 6-7.5 days. Liebmann et al. (2009 further described two mechanisms for the initiation of the convectively coupled Kelvin waves along the equator over South America and western Atlantic. One is related to the preexisting Kelvin wave in the upper level over either the

eastern Pacific or central South America. Another one with precursor convective anomalies over South America resembles the cold surges caused by a synoptic wave train propagates over South America from the South Pacific (e.g., Garreaud and Wallace 1998; Garreaud 2000; and Liebmann et al. 2009). The Pacific cases are affected by the SSTs in Central and Eastern Pacific. MJO and El Nino are more likely to contribute the Kelvin wave activities in South America (e.g., Jones 2009). Other cases are also discussed that convective anomalies over equatorial South America with no visible precursors in either the Pacific or South America, but that propagate into the Atlantic as a Kelvin wave. It indicates the existing of other mechanisms, such as the reflection of Rossby wave energy off the Andes (Kleeman 1989), or the impacts of extratropical wave activities (Hoskins and Yang 2000; Pan and Li 2008). However the propagation of the intraseasonal convectively coupled Kelvin waves in Atlantic and their impacts on African monsoon are less addressed.

Janicot et al. (2010) identified three intraseasonal modes in African monsoon precipitation by EOF analysis: the quasi-biweekly zonal dipole mode (QBZD; Mounier et al., 2008; Janicot et al., 1010), the “Sahel” mode (Sultan et al, 2003; Janicot et al., 2010), and the “African MJO” mode (Matthews, 2004; Janicot et al., 2009). The intraseasonal signals in QBZD mode propagate eastward with possibility of modulating convection over the Indian Ocean, and the mechanisms of this mode appear to be controlled both by equatorial atmospheric disturbances propagating eastwards and by radiation–atmosphere interaction processes over Africa (Mounier et al., 2008). The “Sahel” mode shows 10-25-day intraseasonal signals in African monsoon precipitation, propagating westwards until

it dissipates over the tropical Atlantic. A westward-propagating convectively coupled equatorial Rossby wave is likely to be one of the mechanisms for the "Sahel" mode (Janice et al., 2010). Additionally, the land–atmosphere and radiation–atmosphere interaction processes can also contribute to the maintenance and the westward propagation of the "Sahel" mode (Taylor, 2008 and 2011).

The "African MJO" mode (Matthews, 2004; Janicot et al., 2009 and 2010) is related to the MJO (25-90 days) detected over the Indian and West Pacific Oceans. The related precipitation grows in West and Central Africa and propagates westward, and dissipates over the western part of Africa, suggesting that a convectively coupled equatorial Rossby wave signal is dominant (Janicot et al., 2009, 2010; Lavender and Matthews, 2009). Matthews (2000) suggested that sea level pressure anomalies associated with a global dry equatorial Kelvin wave that travel at a speed of approximately 35 m/s can propagate from the Pacific into the Atlantic through the gap at Panama. Such intraseasonal Kelvin waves can be excited by MJO heating in the Eastern Hemisphere (Matthews 2000; Small et al. 2010). Matthews (2004) suggested that equatorial dry Kelvin waves and dry Rossby waves could link the MJO in the Indian sector and the "African MJO" mode, which suggests that an dry equatorial Kelvin wave response to the warm pool convection forcing propagates eastward and a dry equatorial Rossby wave response propagates westward and between them they complete a circuit of the equator and meet up 20 days later over Africa, where the negative mid-troposphere temperature anomalies associated with the Kelvin and Rossby waves favor enhancement of the deep convection.

Below 10-day period, one of the most important disturbances is the African atmospheric easterly wave (AEW), which propagates from West Africa towards the tropical North Atlantic basin and the Caribbean Sea and usually are related to the intense cyclonic activity in Atlantic during July and November (e.g., Shapiro, 1986; Goldenberg and Shapiro 1996). These waves, which have typical 3-4-day synoptic periods (Burpee, 1974), are responsible for about 60% of tropical storms, and 85% strong hurricanes (Avila and Pash, 1992, 1995; Landsea, 1993). In this study, we focus on understanding the ISO impacts in the tropical Atlantic Ocean, and thus will not discuss the effects of AEWs.

While the possible influences of atmospheric ISOs on convection and wind of tropical Atlantic Ocean have been suggested, understanding of their impacts is far from complete. In addition, the relative importance of the MJO, Rossby waves and Kelvin waves on intraseasonal surface winds and convection in different regions of the tropical Atlantic Ocean for different seasons has not been systematically studied. It is not clear whether the westward-propagating signals in the tropical Atlantic are excited only by the African monsoon precipitation, or they can also originate from the eastern Atlantic basin and subsequently enhance over the Atlantic Ocean.

1.4 Present Study

This study will document intraseasonal signals (especially surface wind and convection) in the tropical Atlantic Ocean and the effects of the MJO, Rossby waves and

quasi-biweekly Kelvin waves on the intraseasonal variability. The first part builds on the previous work (Han et al. 2008) and addresses the extent to which the MJO causes strong 40-60-day surface wind anomalies in the equatorial Atlantic. The cases during 2002 are first analyzed, and then longer records are used to explore the seasonality and statistically significant propagation pathways by which surface wind and convection associated with the MJO affect the Atlantic Ocean. The second part documents intraseasonal convection and surface wind variations in the tropical Atlantic Ocean, and explore the effects of the MJO, Rossby waves and quasi-biweekly Kelvin waves on intraseasonal variability using satellite observations and reanalysis data. The MJO and equatorial wave signals are identified based on the dispersion relation of equatorially trapped waves (Wheeler and Kiladis 1999).

CHAPTER II

OBSERVATIONS OF EASTWARD PROPAGATION OF ATMOSPHERIC INTRASEASONAL OSCILLATIONS FROM THE PACIFIC TO THE ATLANTIC

(Yu et al. 2011: JGR-Atmosphere, in press)

2.1 Data and Method

MJO propagation can be effectively diagnosed using Outgoing Long-wave Radiation (OLR) and winds (Arkin and Ardanuy 1989; Liebmann and Smith, 1996; Matthews 2000; Jones et al. 2004.). Hence, 3-day mean, QuikSCAT ocean surface wind vectors and NOAA interpolated OLR data from 2000 to 2006 are used to diagnose intraseasonal variability using 30-70-day band-pass filtered fields (Duchon 1979). To minimize the influence of missing values due to incomplete sampling and rain contamination, we averaged the 0.25^{o}x0.25^{o} resolution QuikSCAT winds onto 2.5^{o}x2.5^{o} grids and also did time interpolation for the missing values. To support inferences on convective activity provided by the OLR in both the tropical and subtropical oceans, we also analyzed the 1^{o}x1^{o} Global Precipitation Climatology Project (GPCP) precipitation data, the 2.5^{o}x2.5^{o} Climate Prediction Center (CPC) merged analysis of precipitation (CMAP) product, and 0.7^{o}x0.7^{o} European Center for Medium-Range Weather Forecasts (ECMWF) Reanalysis (ERA)-Interim precipitation data (Simmons et al. 2007; Allan et al. 2010; Xie and Arkin 1997).

To isolate the MJO signals, OLR data were filtered to 30-70-day periods and eastward wavenumbers 1-3, consistent with previous studies (Hendon and Salby 1994; Jones and Schemm 2000; Foltz and McPhaden 2004). A broad 20-100-day filter with eastward wavenumbers 1-6, following the suggestion of the U.S. Climate Variability and Predictability Research Program (CLIVAR) MJO working group (CLIVAR MJO Working Group 2009) and Wheeler and Kiladis (1999), is also applied to compare with the extracted 30-70-day MJO signals to ensure that the signals examined here are not an artifact of the narrow response function used. Intraseasonal variance, spectral coherence analysis, and correlation analysis were performed using QuikSCAT winds to demonstrate the effects of the MJO on surface winds in the tropical Atlantic Ocean. Surface winds from ERA-Interim data with 1.5 degree resolution from 1990 to 2007 and the 40-year reanalysis (ERA40) with 2.5 degree resolution for 1960-2001 were also analyzed in order to assess the robustness of the results for longer periods. Because QuikSCAT winds are not retrieved over land, we can not use the spatial filter to extract the MJO signals for QuikSCAT, and thus only filter QuikSCAT winds to 30-70 days.

2.2 Observed Intraseasonal Variability in the Tropical Atlantic

Figures 2.1a-d show Atlantic variance spectra of surface winds along the equator during 2002 from QuikSCAT and ERA-Interim data. Both zonal and meridional winds exhibit strong spectral peaks at intraseasonal periods, among which 40-60-day peaks are evident across most of the equatorial basin in both QuikSCAT and ERA-Interim data, consistent with Han et al. (2008). Strong spectral power occurs at periods greater than 80

days in the Eastern and Central Atlantic basin, which is associated with the strong seasonal variations.

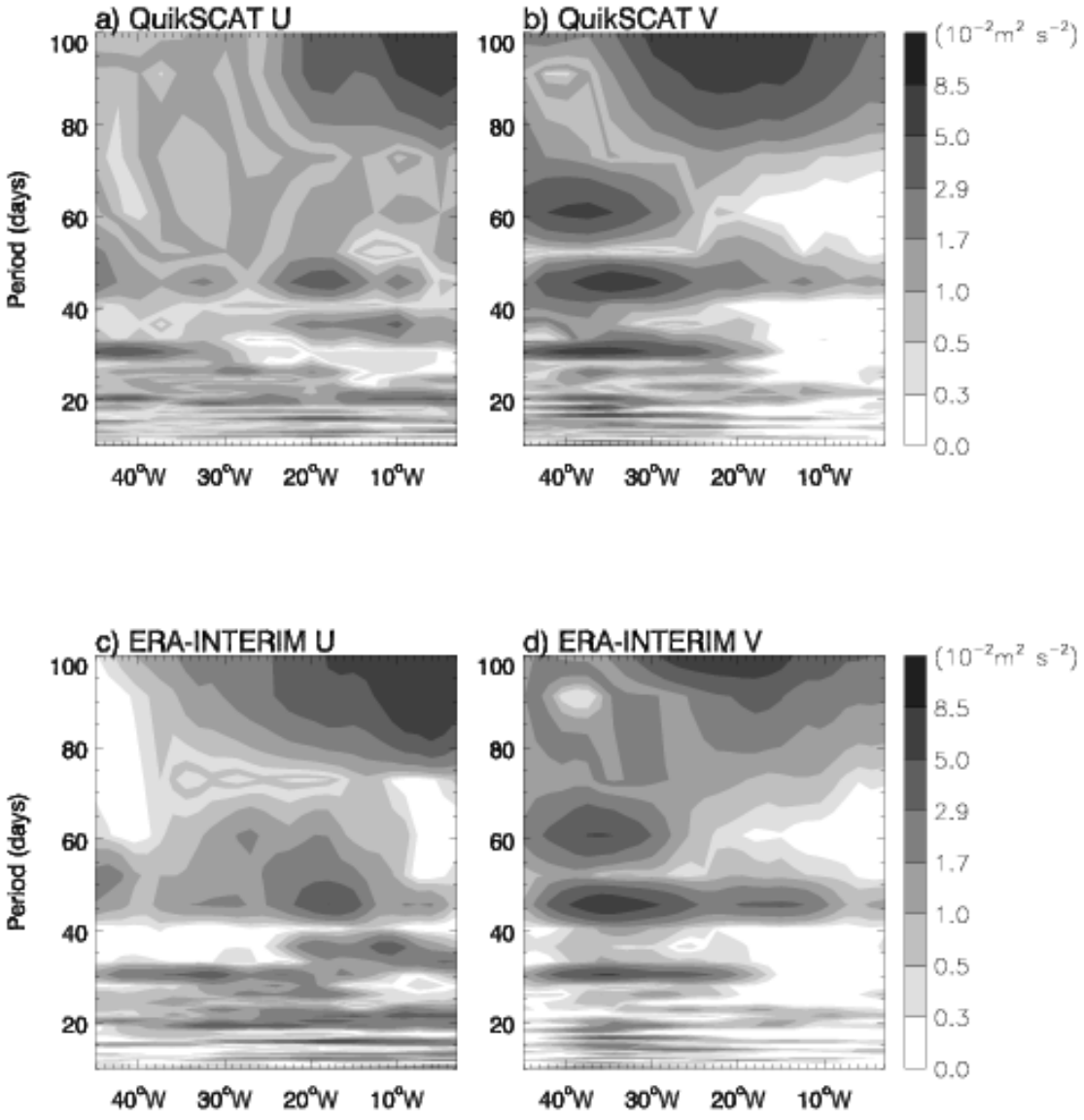

Figure 2.1. Variance spectra of surface wind (10m) along the Atlantic equator (5°S–5°N averaged) based on daily winds of 2002. a) QuikSCAT zonal wind; b) QuikSCAT meridional wind; c) ERA-Interim zonal wind; and d) ERA-Interim meridional wind.

2.3 Evidence of MJO Propagation into the Atlantic during 2002

Figure 2.2 shows longitude-time diagrams of the 30-70-day bandpass filtered QuikSCAT surface zonal wind and OLR anomalies averaged from 15^{o}S to 15^{o}N during 2002. Note that the OLR field is further bandpass filtered to zonal wavenumbers 1-3. The large-scale features and eastward propagation of the 30-70-day wind anomalies (Figure 2.2a) agree well with the MJO signals in OLR (Figure 2.2b) in terms of a consistent phase relationship and amplitude, suggesting that the 30-70-day QuikSCAT wind anomalies are largely associated with the MJO. During January-July, the maximum 30-70-day wind anomalies are observed in the Indian Ocean and Western Pacific, and subsequently propagate into the Atlantic Ocean, although the Atlantic manifestation of the wind anomalies is weaker relative to the Indo-Pacific sector. Eastward propagating MJO events occur with gradually increasing strength during boreal winter and spring of 2002, reaching a maximum in May and then becoming weaker during summer. To ensure that the narrow filtering we use does not too strongly constrain our results, we also applied a wider 20-100-day filter as a sensitivity test. Results are similar to those derived using a narrower filter, as shown in both QuikSCAT zonal wind and OLR anomalies, except that signals are higher amplitude and noisier (Figure 2.3). MJO propagation from the Indian Ocean to the Atlantic is very clear during April and May in both Figure 2.2 and Figure 2.3, with propagation speeds of approximately 4.7 m/s from the Indian Ocean to the western Pacific and 14.5 m/s from the central Pacific to the Atlantic, as indicated by their phase lines. These values generally agree with the well-documented MJO propagation speed of ~5 m/s in convective regions across the Indian and western Pacific

Oceans, and 10-15 m/s in the Western Hemisphere (e.g., Hendon and Salby 1994). The basic propagation patterns are consistent for both OLR and winds, with winds slightly lagging enhanced convection.

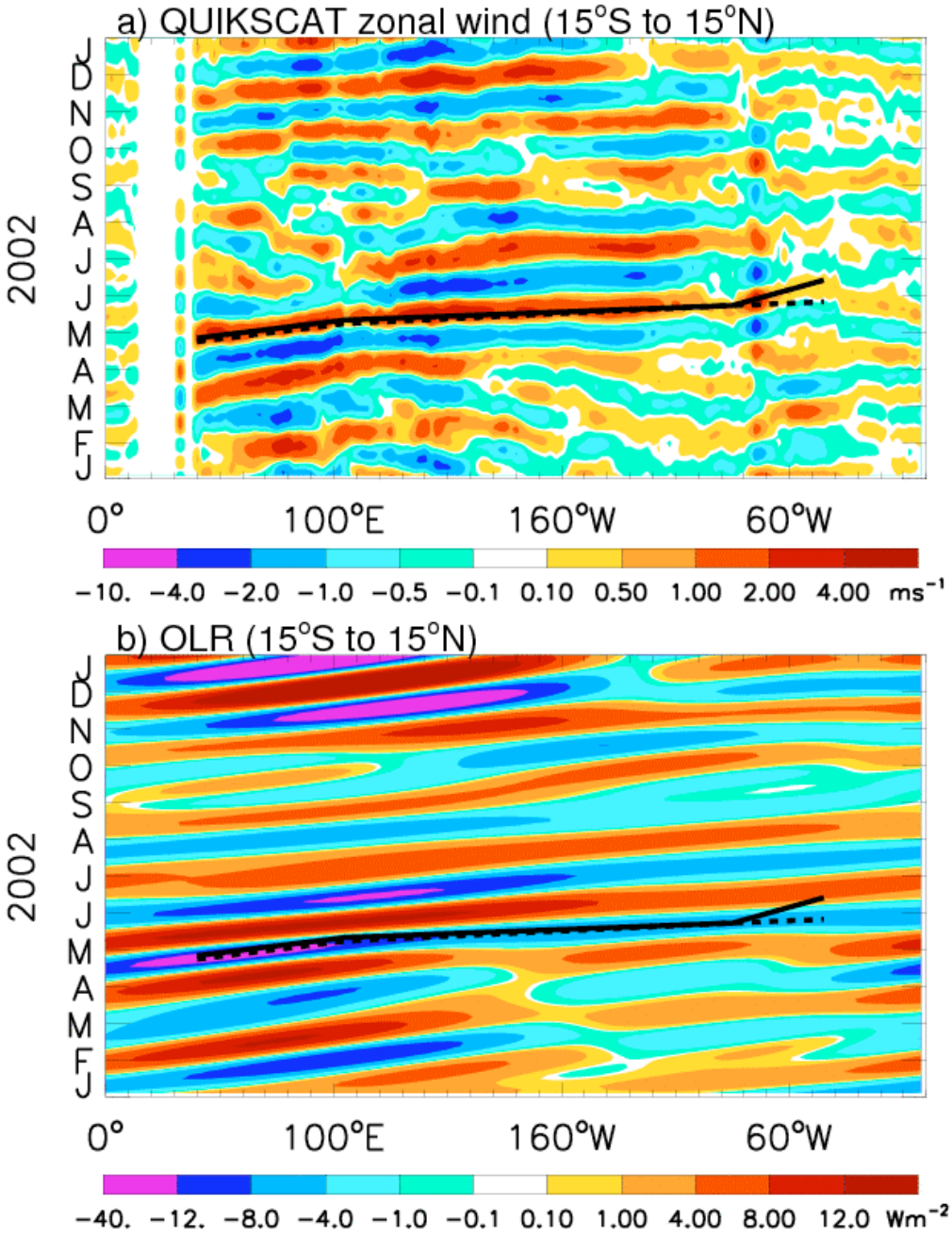

Figure 2.2. a) Longitude-time diagram of 30-70-day band-pass filtered QuikSCAT 10m zonal wind averaged from 15°S to 15°N during 2002; b) same as a) but for 30-70-day OLR data, which have been restrictively filtered to eastward wavenumbers 1-3. Two black phase lines are QuikSCAT (solid line) and OLR (dashed line).

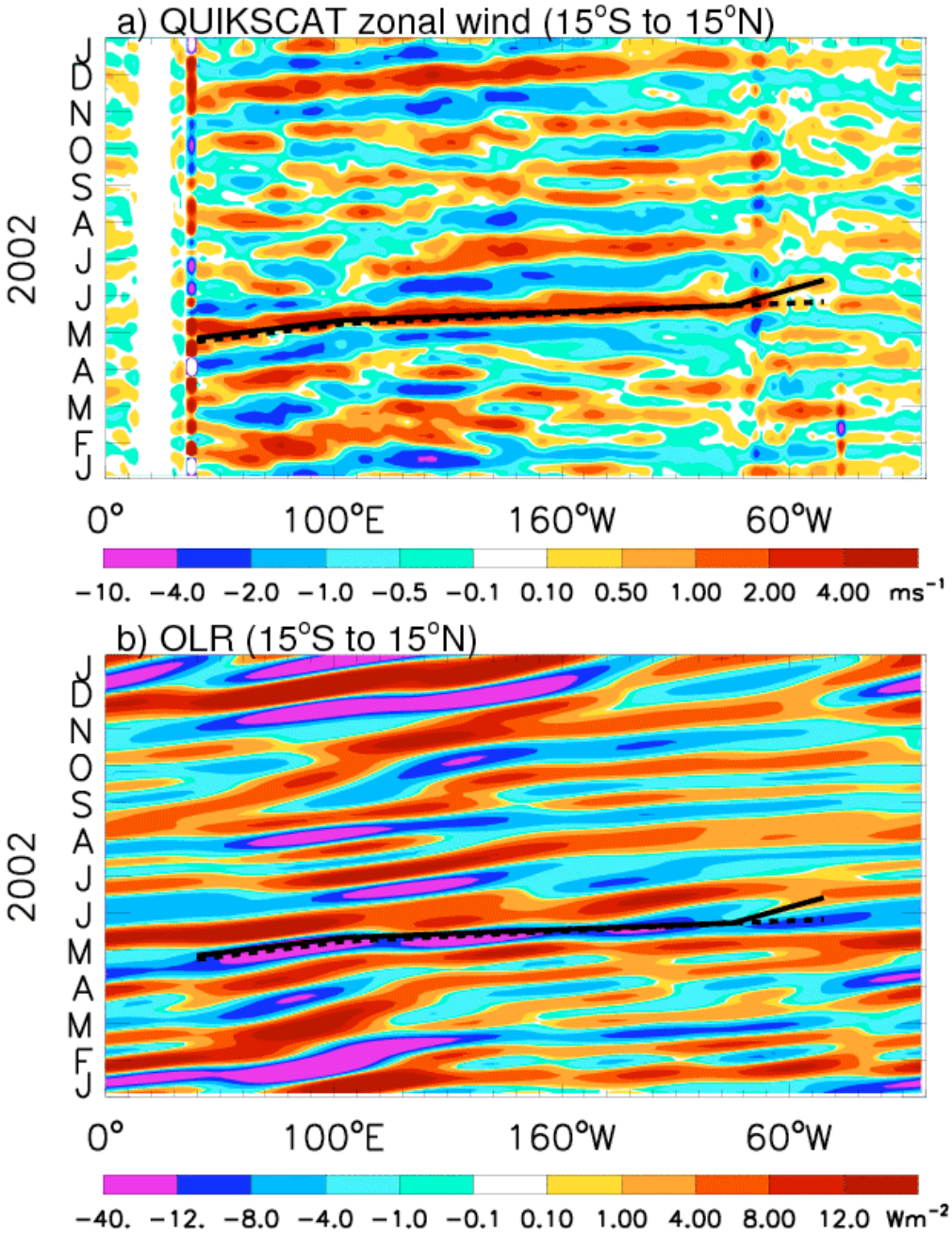

Figure 2.3. a) Same as Figure 2.2a, except for 20-100-day band-pass filer; b) Same as Figure 2.2b, except for 20-100-day band-pass filer, in which OLR data has been restrictively filtered to eastward wavenumbers 1-6.

In contrast, during boreal summer and fall of 2002, convection associated with the MJO is weaker in the western Atlantic Ocean compared to winter and spring. In the Eastern Equatorial Atlantic basin (20^{o}W to 0^{o}E), however, impacts of the westward propagating signals are observed during May-September (Figure 2.2a). The westward propagation of intraseasonal anomalies across the African monsoon region into the Atlantic has been suggested by previous studies (e.g. Matthews 2004, Janicot et al. 2009). In this Chapter, we focus on examining eastward propagating MJO influences, and will examine the Rossby waves, which contribute the westward propagation in Atlantic in Chapter III.

QuikSCAT winds cannot be retrieved over the South American Continent. The continuous eastward propagation of 30-70-day wind anomalies in Figure 2.2a and 2.3a across 70^{o}W is derived from comparatively fewer sampling points in the Caribbean Sea to the north of Colombia and Venezuela and near the Isthmus of Panama. This suggests that the MJO propagating signal is present in the surface winds near the Isthmus of Panama. An examination of ERA-Interim surface winds over the South American continent averaged from 10^{o}S to 10^{o}N does not indicate eastward propagation within the equatorial band (Figures 2.3c and 2.3d), indicating that MJO signals in surface winds may propagate into the Atlantic primarily through the Panama area. This point will be further demonstrated below.

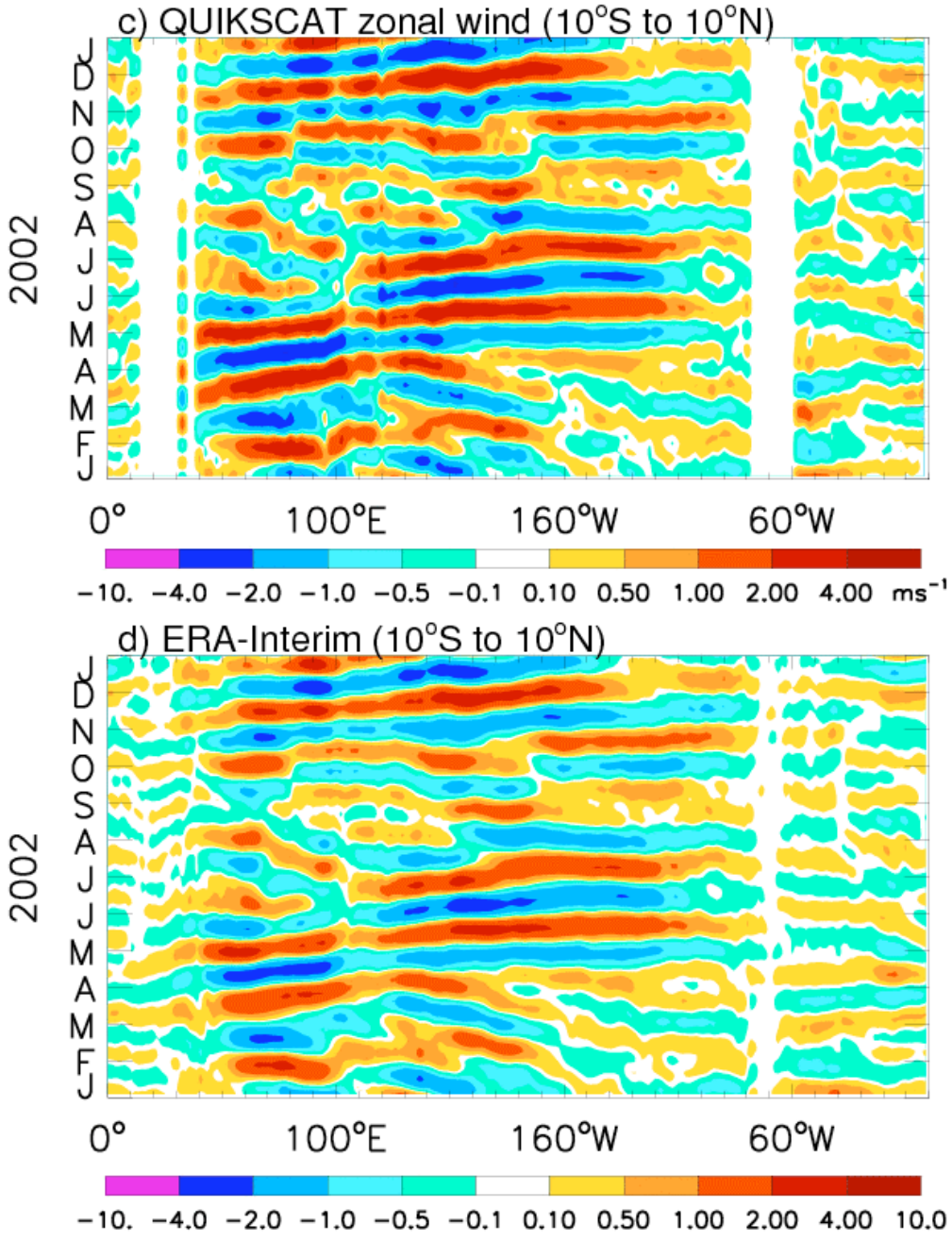

Figure 2.3. c) Longitude-time diagram of 30-70-day band-pass filtered QuikSCAT 10m zonal wind averaged from 10°S to 10°N during 2002; d) same as c) but for ERA-Interim data.

Figure 2.4 shows the time series of 30-70-day filtered surface zonal wind anomalies during 2002 averaged over three regions: 15°S to 15°N and 120°E to 160°E in the western Pacific (WP), 10°N to 20°N and 90°W to 70°W in the Caribbean Sea (CS), and 5°S to 5°N and 50°W to 30°W in the western equatorial Atlantic (WA). In the WP region, westerly wind anomalies associated with the MJO obtain large amplitudes (e.g., McPhaden 1999). The choice of the CS region is based on the propagation signal diagnosed in Figures 2.2 and 2.3, which suggests that the MJO enters the Atlantic through the Isthmus of Panama and CS. The WA region is chosen based on the observed 40-60-day zonal wind variability documented by Han et al. 2008 and shown in Figure 2.1. The phase lags from the WP to the CS and subsequently to the WA exhibit relatively consistent behavior from January to July. These lags indicate eastward propagation of the westerly wind anomalies from the WP to the WA through the CS, consistent with Figure 2.2. Note that Figure 2.2 is based on 15°S-15°N average, whereas Figure 2.4b is based on the three key regions shown in Figure 2.4a. Therefore, the two analyses may not be always consistent. From July to December, the clean phase progression differs from that in January to July, indicating that the MJO influence during boreal summer and fall is more complex. As mentioned above, in addition to the eastward pathway, the MJO can affect equatorial Atlantic winds by exciting westward propagating Rossby waves (Matthews 2004) from the Indian Ocean during summer and fall. Thorncroft et al. (2003) and Sultan et al. (2003) suggest that winds associated with the West African monsoon, which have biweekly and 25-60-day dominant periods, can significantly affect the tropical Atlantic Ocean through westward propagation. More detailed examination of

Rossby wave impacts on Atlantic and the sources of 10-100-day intraseasonal signals in African monsoon region will be provided in Chapter III.

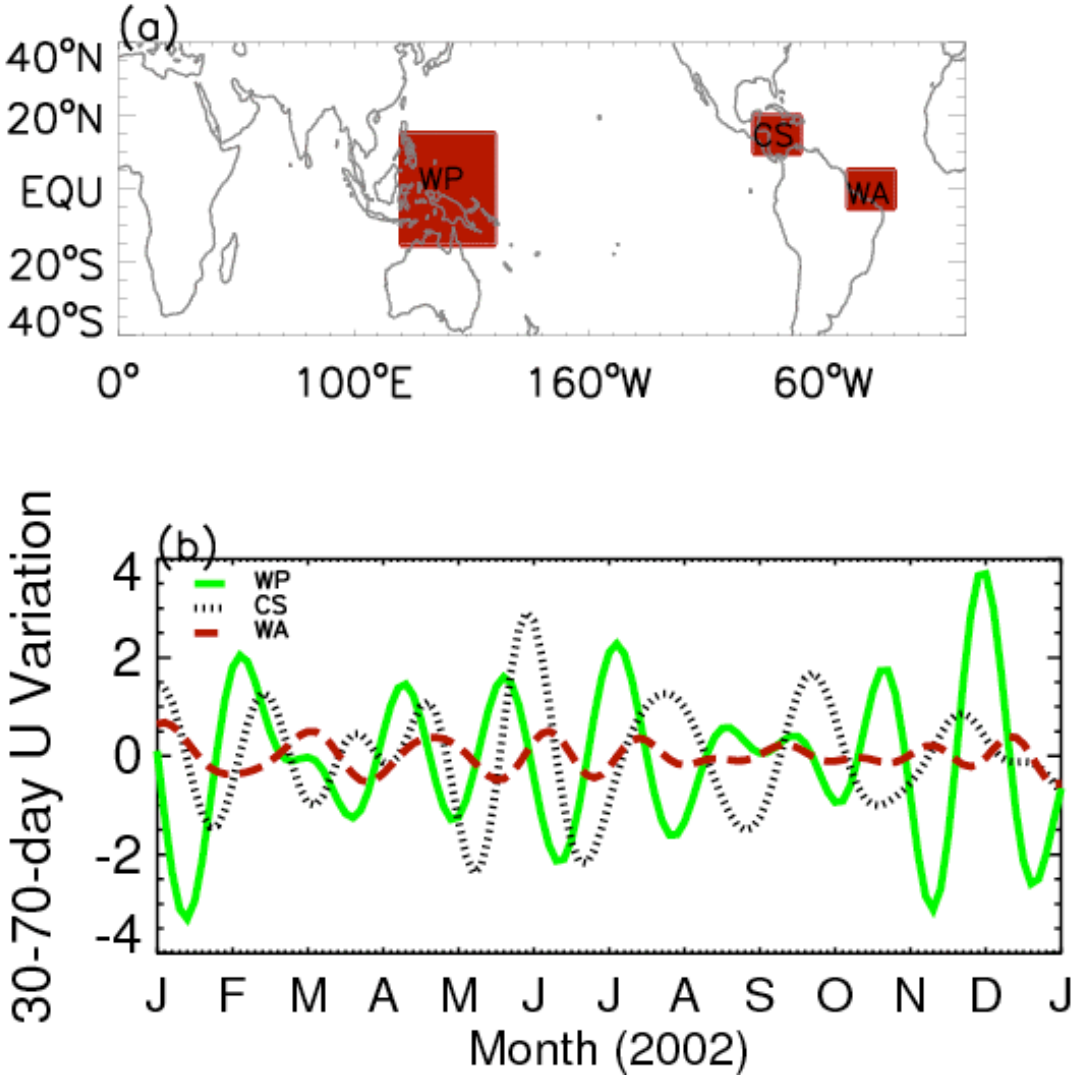

Figure 2.4. The time series of domain-averaged 30-70-day zonal wind variations from QuikSCAT. WP: 15°S to 15°N and 120°E to 160°E; CS: 10°S to 20°N and 90°W to 70°W; WA: 5°S to 5°N and 50°W to 30°W.

2.4 Evolution of the MJO during 2002

Figure 2.5a shows the time evolution of the 30-70-day filtered QuikSCAT wind and OLR anomalies during May 2002 associated with the strong MJO event that propagated into the Atlantic (see Figure 2.2). On May 1, in the tropical Indian Ocean, strong convection (large amplitude negative OLR anomaly) is symmetric about the equator. Associated with the convection, a westerly wind anomaly prevails in the central and western Indian Ocean. In subsequent days, the convective maximum accompanied by the westerly wind anomaly, moves into the central-western Pacific (e.g. May 13). Meanwhile, an off-equatorial convective maximum north of the equator in the central Pacific (near 160^{o}W, 20^{o}N) also moves eastward. By May 25, the strong convection and its associated westerly wind anomaly propagate into the NAM region and the Caribbean Sea. This signal is consistent with the work of Martin (2010), who showed using GPCP precipitation during 1997-2006 that intraseasonal precipitation variability in the Caribbean Sea is associated with variations in the Caribbean Low Level Jet, which is modulated by the MJO. Hurricane Alma formed in the east Pacific during this period was coincident with this MJO event. The evolution of tropical and subtropical convective activity shown by the OLR data above is further confirmed by using 30-70-day GPCP precipitation anomalies with 1^{o}x1^{o} resolution (Figure 2.5b). Consistent precipitation patterns are also obtained using 30-70-day, 2.5^{o}x2.5^{o} CMAP (Figure 2.5d) and 0.7^{o}x0.7^{o} ERA-Interim precipitation data (Figure 2.5e).

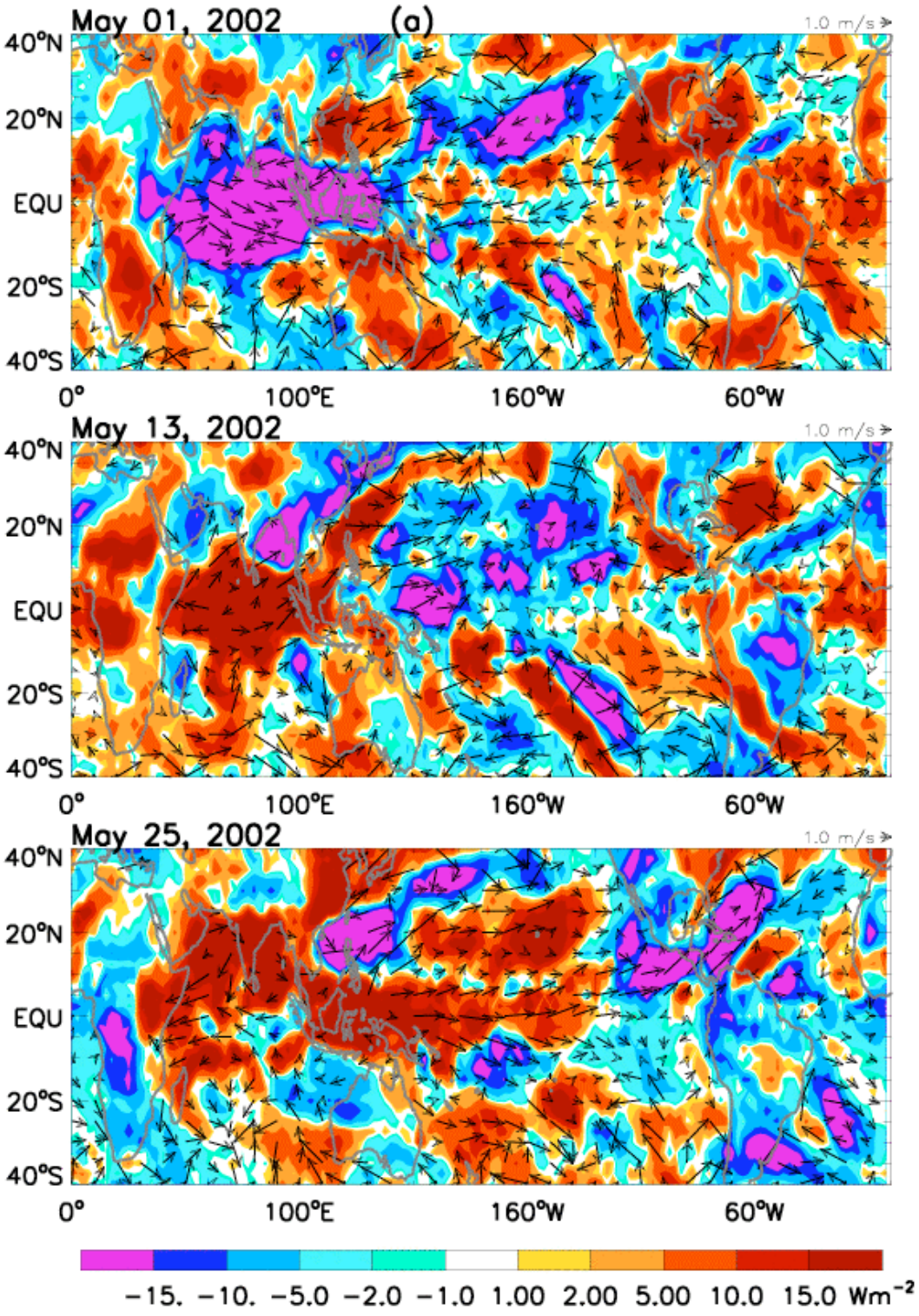

Figure 2.5. a) The 30-70-day band-pass filtered OLR (color contours) and QuikSCAT winds (arrows);

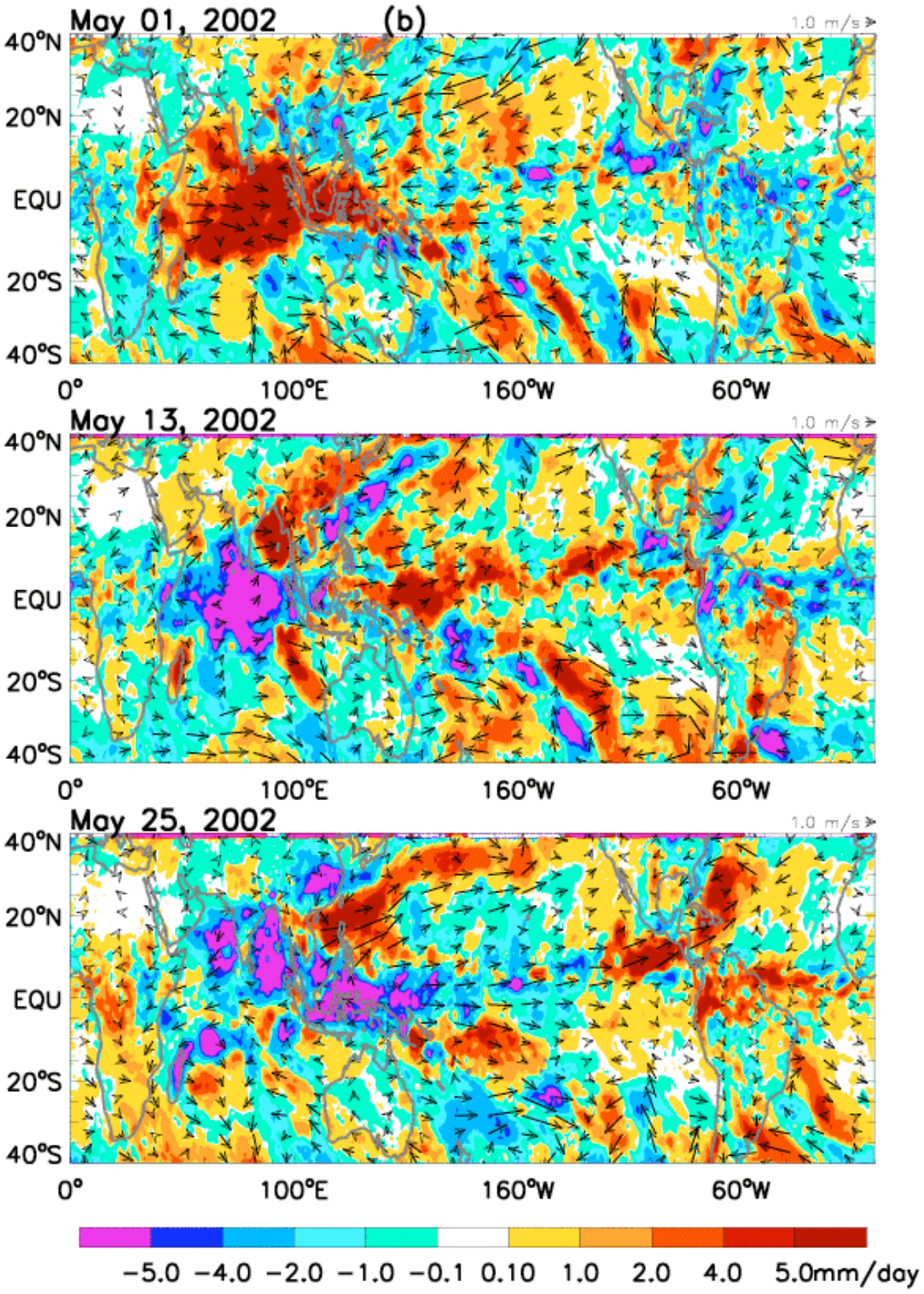

Figure 2.5 b) The 30-70-day band-pass filtered GPCP precipitation (color contours) and ERA-Interim winds (arrows);

To understand the role played by the MJO, 30-70-day bandpass filtered OLR and 850 mb wind anomalies from ERA-Interim data are further bandpass filtered to eastward zonal wave numbers 1-3 (Figure 2.5c). Anomalous 30-70-day convection and westerly surface winds shown in Figure 2.5a are associated with the strong May 2002 MJO event (see Figures 2.5c, 2.2b and 2.3b). This event was also prominent in the multivariate MJO index of Wheeler and Hendon (2004, see their Figures 5 and 12). On May 1, maximum convection together with westerly wind anomalies appears in the central and Eastern Equatorial Indian Ocean (Figures 2.5a-c, top panels), where anomalous convergence occurs at 850mb and divergence occurs at 200mb (not shown), consistent with the baroclinic structure of the MJO described by Jones and Carvalho (2006) and Hendon and Salby (1994). In the western equatorial Indian Ocean (50^{o}E), cyclonic surface wind circulations exist (centered near 50^{o}E, 25^{o}S and 60^{o}E, 25^{o}N), consistent with the Gill model of a Rossby wave response to the enhanced diabatic heating. East of the equatorial convective maximum, a tongue of negative equatorial OLR anomalies together with easterly wind and convergence anomalies that resemble a Kelvin wave extends eastward to the western Pacific. This scenario agrees well with the coupled Kelvin-Rossby wave packet structure associated with the MJO (e.g., Wang and Xie 1997). The dominance of wavenumber 1 on the equator and wavenumber 2 off the equator on May 1 (shown in Figure 2.5c) is also consistent with MJO structure (Hendon and Salby 1994).

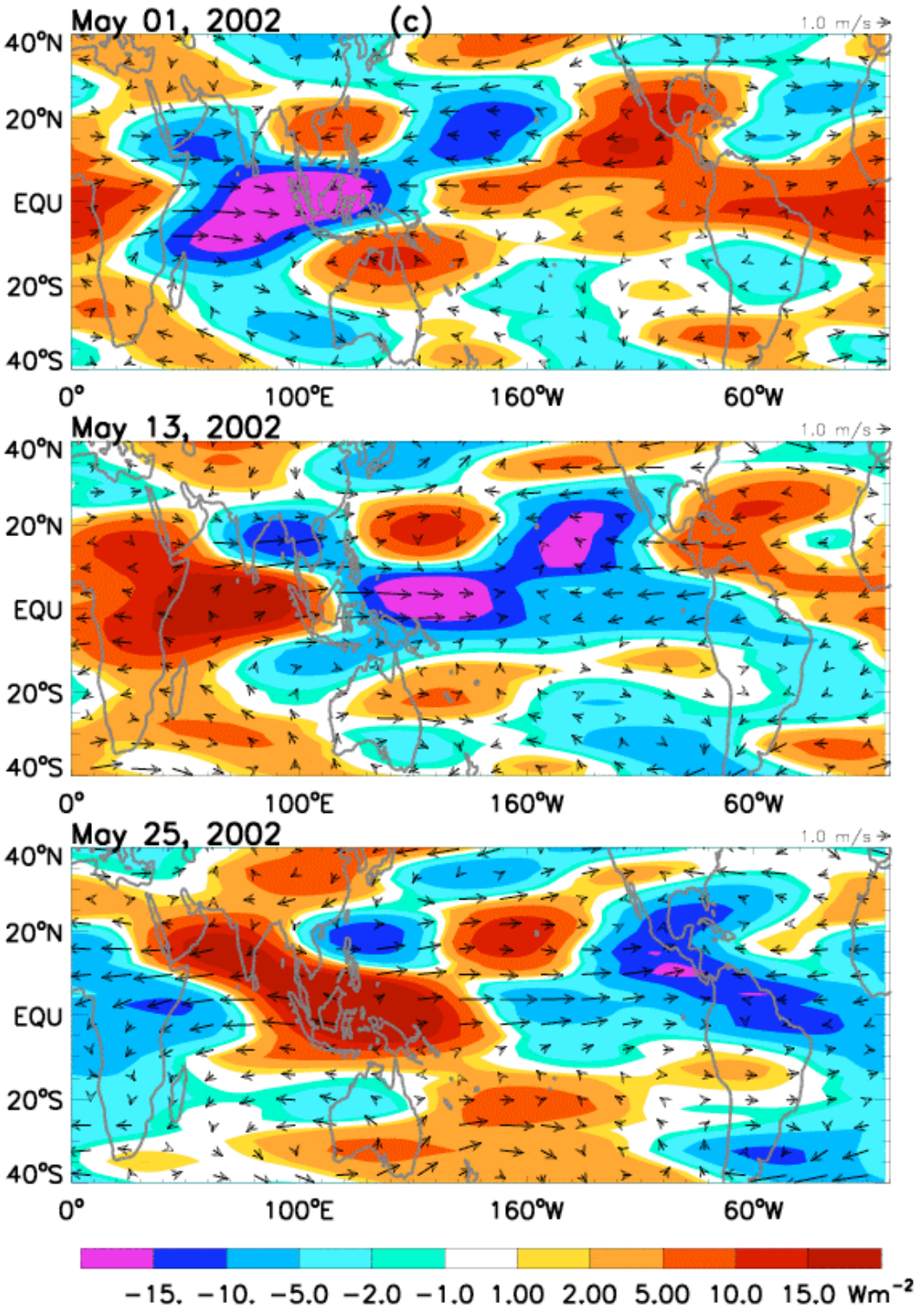

Figure 2.5 c) The 30-70-day band-pass filtered OLR (color contours) and 850 mb ERA-Interim winds (arrows) with eastward wavenumbers 1-3.

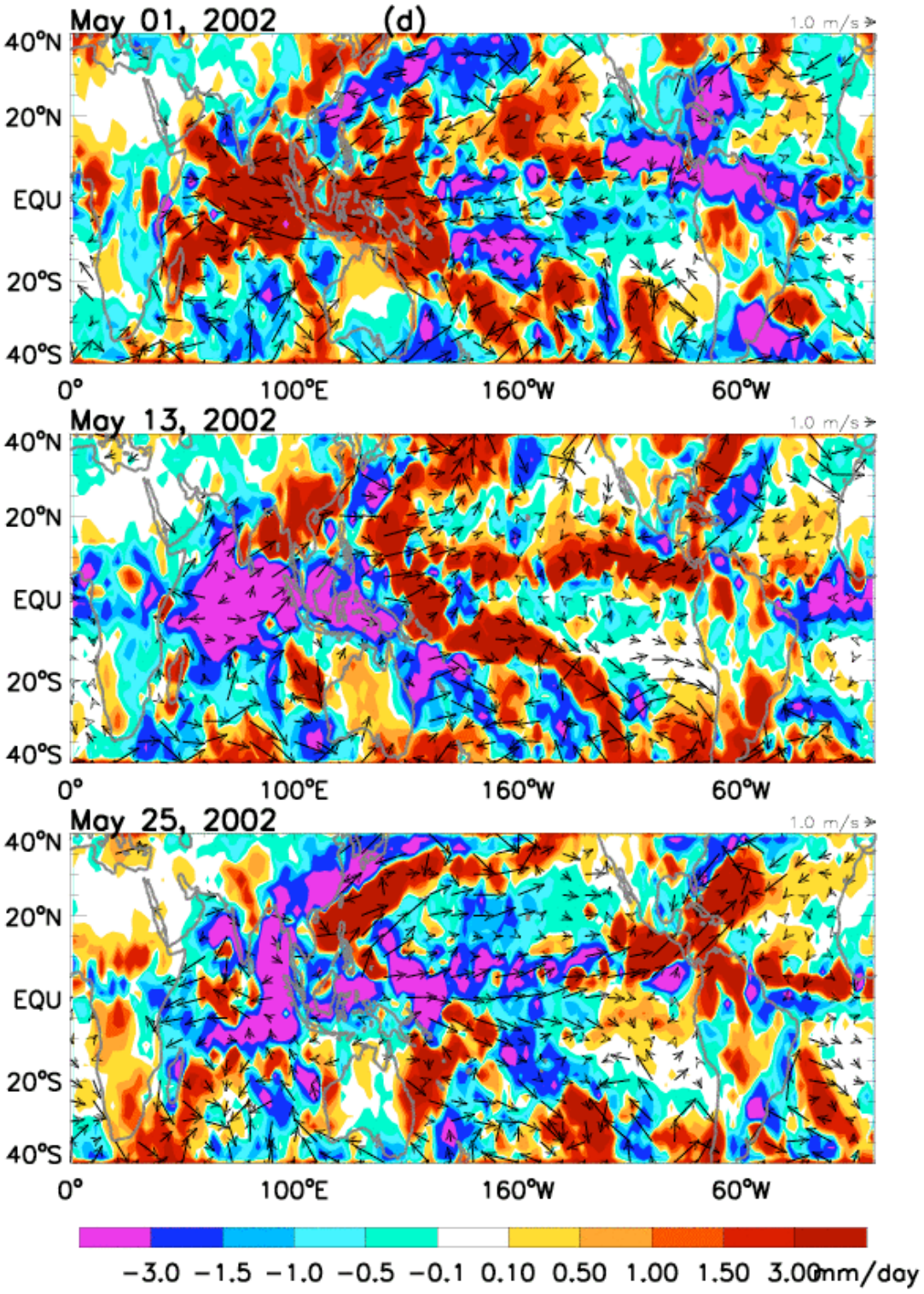

Figure 2.5 d). The 30-70-day band-pass filtered CMAP precipitation (color contours) and QuikSCAT winds (arrows).

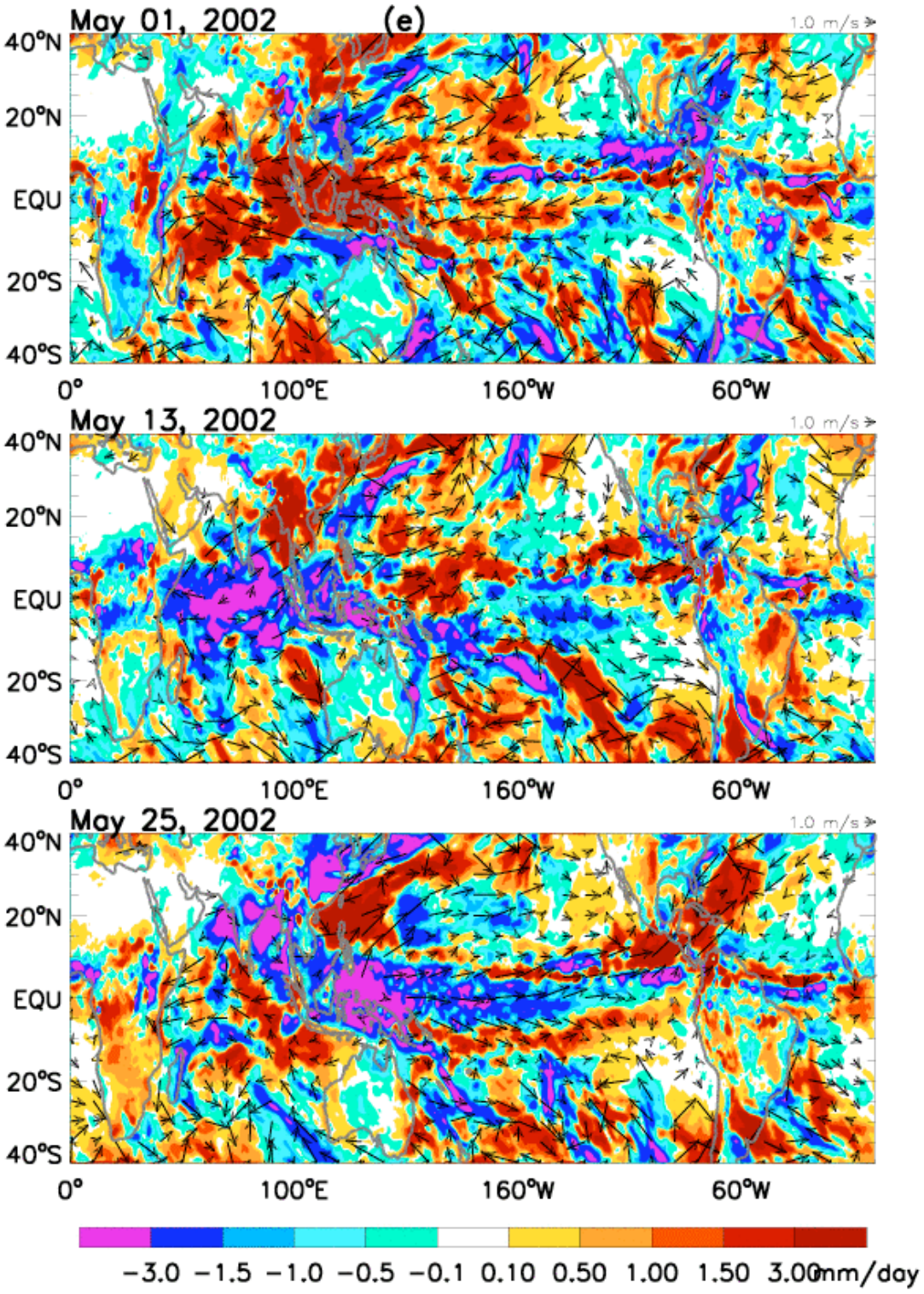

Figure 2.5 e). The 30-70-day band-pass filtered 0.7^{o}x0.7^{o} ERA-Interim precipitation (color contours) and QuikSCAT winds (arrows).

On May 13, the coupled Kelvin-Rossby wave packet discussed above propagates eastward into the western Pacific (Figure 2.5c middle panel). By May 25 the convection anomaly along the equator is significantly weakened east of the dateline and the disturbance propagates at a much faster speed into the Atlantic (bottom panel). This scenario is consistent with the global behavior of the MJO as seen in Matthews (2000) and other papers. Near the dateline, the fast equatorial Kelvin wave appears to decouple from the Rossby wave, which has two positive OLR maxima off the equator in the western Pacific warm pool and subsequently propagates eastward with a much slower speed. Since the low SST in the east Pacific cold tongue region inhibits convection, MJO signals in OLR become weak along the equator, while off-equatorial convection is strengthened to the east of the dateline and across the Panama Gap. The MJO propagates into the Caribbean Sea and northwestern subtropical Atlantic as indicated by the significant changes in wind anomalies in these regions. Specifically, in the Caribbean Sea, northeasterly wind anomalies prevailed on May 13 and southwesterly wind anomalies appeared on May 25, as shown in Figure 2.5a. This eastward propagation is consistent with the Hovmoller diagram derived from QuikSCAT and OLR anomalies as shown in Figures 2.2 and 2.3. The MJO that originates in the Indo-Pacific propagates eastward into the Atlantic, with its maximum influence occurring in the western tropical Atlantic basin, consistent with Foltz and McPhaden (2004).

The eastward propagation of the off-equatorial convection anomalies is intriguing. These anomalies appear near 160^{o}W, 20^{o}N in the Pacific on May 1 (top panels of Figures 2.5a-2.5c). With the eastward propagation of the MJO, the off-equatorial convective

anomalies are strengthened and enter the Atlantic via Central America and Isthmus of Panama with a wind anomaly magnitude above 2 m/s (Figures 2.5a-2.5c, bottom panels). The Central America and Isthmus of Panama pathway for the MJO surface wind and convection anomalies to enter the Atlantic is consistent among QuikSCAT surface winds, ERA-Interim surface winds, OLR, and precipitation data (Figures 2.5a-2.5c). These signals affect the NAM region and generate appreciable convective anomalies in the northwestern subtropical Atlantic Ocean. The eastward propagation during May-June of 30-70-day OLR anomalies averaged from 5^{o}N to 25^{o} N is evident from 160^{o}W to 60^{o}W in a Hovmoller diagram (Figure 2.6).

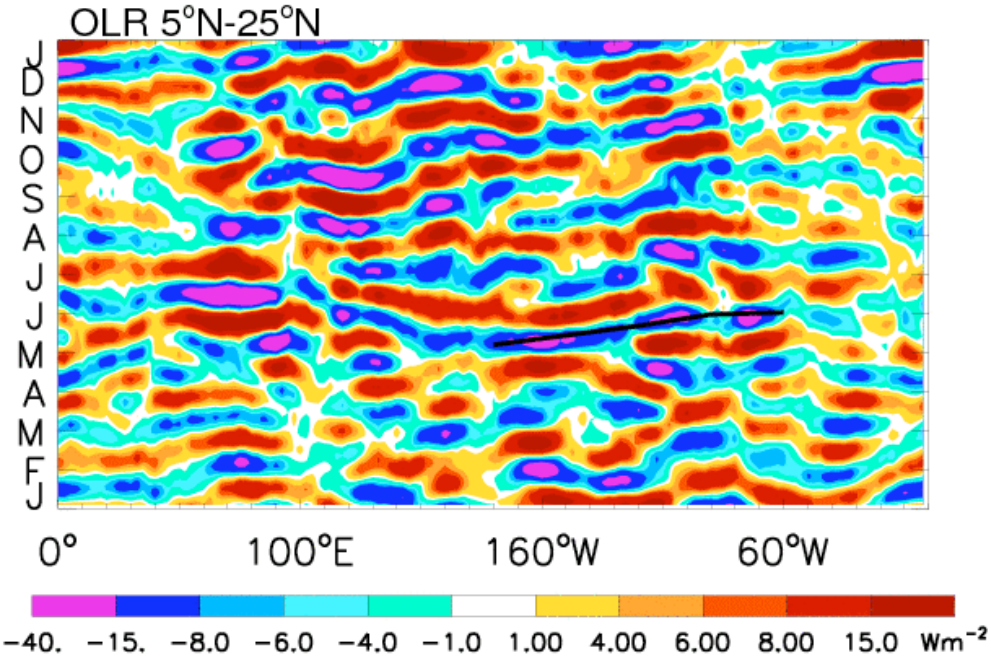

Figure 2.6. Same as Figure 2.2a except for 5°N to 25°N OLR data.

We further analyzed the 2002 period to document variability of OLR and precipitation for the region 5^{o}N to 25^{o}N and 180^{o}W to 170^{o}W to describe more specifically how off-equatorial convection and related precipitation anomalies in this region are related to the MJO. For example, it is possible that other mechanisms of subseasonal variability such as easterly waves dominate the OLR excursions in this region. In Figure 2.7, the daily unfiltered OLR time series during 2002 (mean removed) shows that strong convective events that occur in the central Pacific often correspond to negative 30-70-day eastward zonal wavenumber 1-3 bandpass filtered OLR anomalies (a good proxy for the MJO; Wheeler and Kiladis 1999), which are generally matched with the positive 30-70-day precipitation anomalies, indicating that strong convective events shown in daily OLR and the corresponding intraseasonal variations of precipitation are often associated with the MJO. Here the 30-70-day and wavenumber 1-3 filtered signals mainly reflect the MJO signals (Wheeler and Kiladis, 1999; also see Figure 3.1).

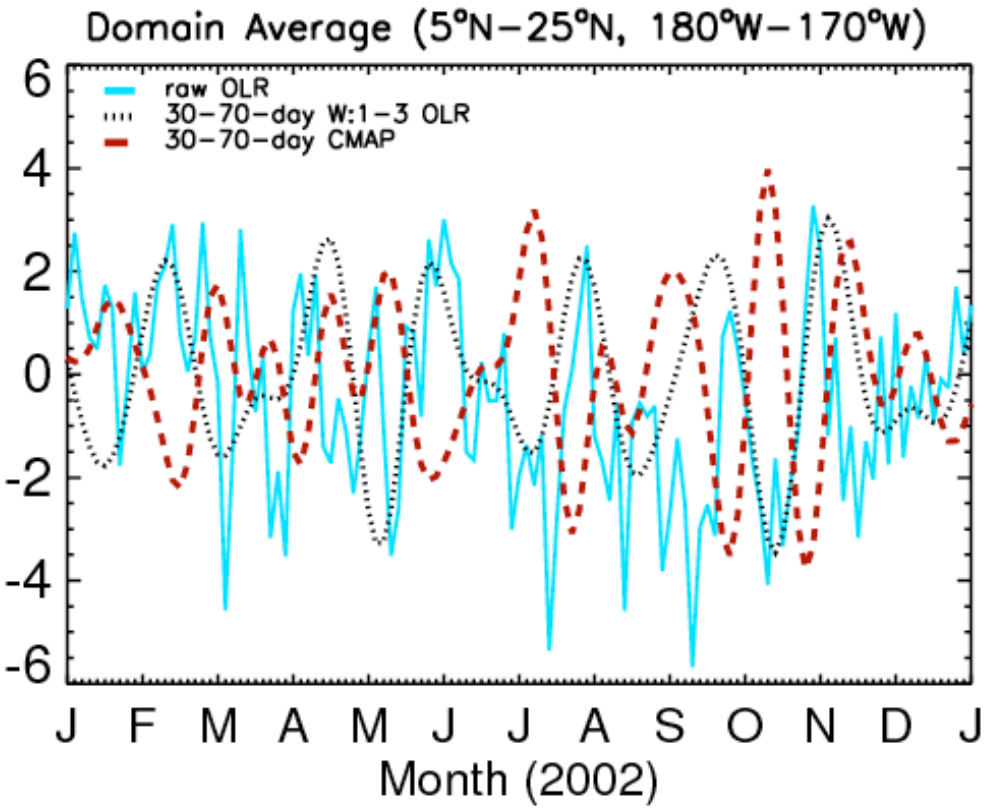

Figure 2.7 Domain-averaged OLR anomalies (5°N to 25°N and 180°W to 170°W) during 2002 from raw daily OLR anomaly with the mean removed (blue curve), 30-70-day eastward wavenumbers 1-3 filtered OLR (dotted black curve), and 30-70-day filtered CMAP data (dashed red curve). Units for daily OLR anomalies are 8^{-1}w m^{-2}, for filtered OLR anomalies are 3^{-1}w m^{-2}, and for filtered precipitation anomalies are mm day^{-1}.

Detailed analysis of MJO event evolution shows that off-equatorial convective anomalies exist in almost all of the MJO cycles. Why these off-equatorial anomalies propagate eastward with time is an unanswered question, as is the eastward propagation of the MJO in general. Recently, Pan and Li (2008) showed that the response pattern of wind and precipitation anomalies in the mid-latitudes shifts eastward when tropical heating moves eastward with the MJO. The connection between the off-equatorial convection maxima and OLR anomalies extending northeast and southeast into the mid-latitude north and south Atlantic (Figures 2.5a-2.5c), respectively, suggests that the gradual eastward shift of mid-latitude disturbances (Higgins and Mo, 1997) may also interact with this equatorial convection, possibly contributing to its eastward propagation. Higgins and Mo (1997) argued that while the MJO can cause mid-latitude anomalies through Rossby wave trains, the mid-latitude anomalies could feedback onto the tropical precipitation through modification of moisture transport. Eastward propagation in the Intertropical Convergence Zone (ITCZ) could also be affected by interactions between the large-scale MJO flow and tropical synoptic-scale disturbances, through their impacts on the tropospheric moisture budget (e.g. Maloney 2009). Further investigation of the dynamics that determine the eastward propagation of off-equatorial convection anomalies is beyond the scope of this study, and might be aided by modeling studies.

2.5 Spectral Coherence Analysis during 2002

An analysis of spectral coherence can diagnose the consistency of the phase relationship and amplitude ratio across spectral components in a frequency band for two

different time series. Following Maloney et al. (2008), we conduct such a spectral coherence analysis here using a reference time series of zonal wind stress averaged over (15^oS to 15^oN and 120^oE to 160^oE), where westerly wind anomalies associated with the MJO achieve large amplitudes (e.g., McPhaden 1999). Given that observed 40-60-day zonal wind anomalies in the western equatorial Atlantic are most prominent during 2002 from January to July and weaker from August to December (Figure 2.2; also see Figure 9a of Han et al 2008), we compute the coherence squared and phase in the 30-70-day band between the reference time series and the zonal wind stress at each grid point during January to July 2002 (Figure 2.8a) separately from August-December of 2002 (Figure 2.8b). A unit vector giving the phase relative to the reference time series is also derived for these periods. The direction of the phase vector indicates the phase relationship between the reference time series and the spatial location of interest. The phase vector of the reference time series is shown in the white area near 140^oE, 0^oN. A clockwise rotation of the vector indicates increasing phase, and thus the direction of phase propagation.

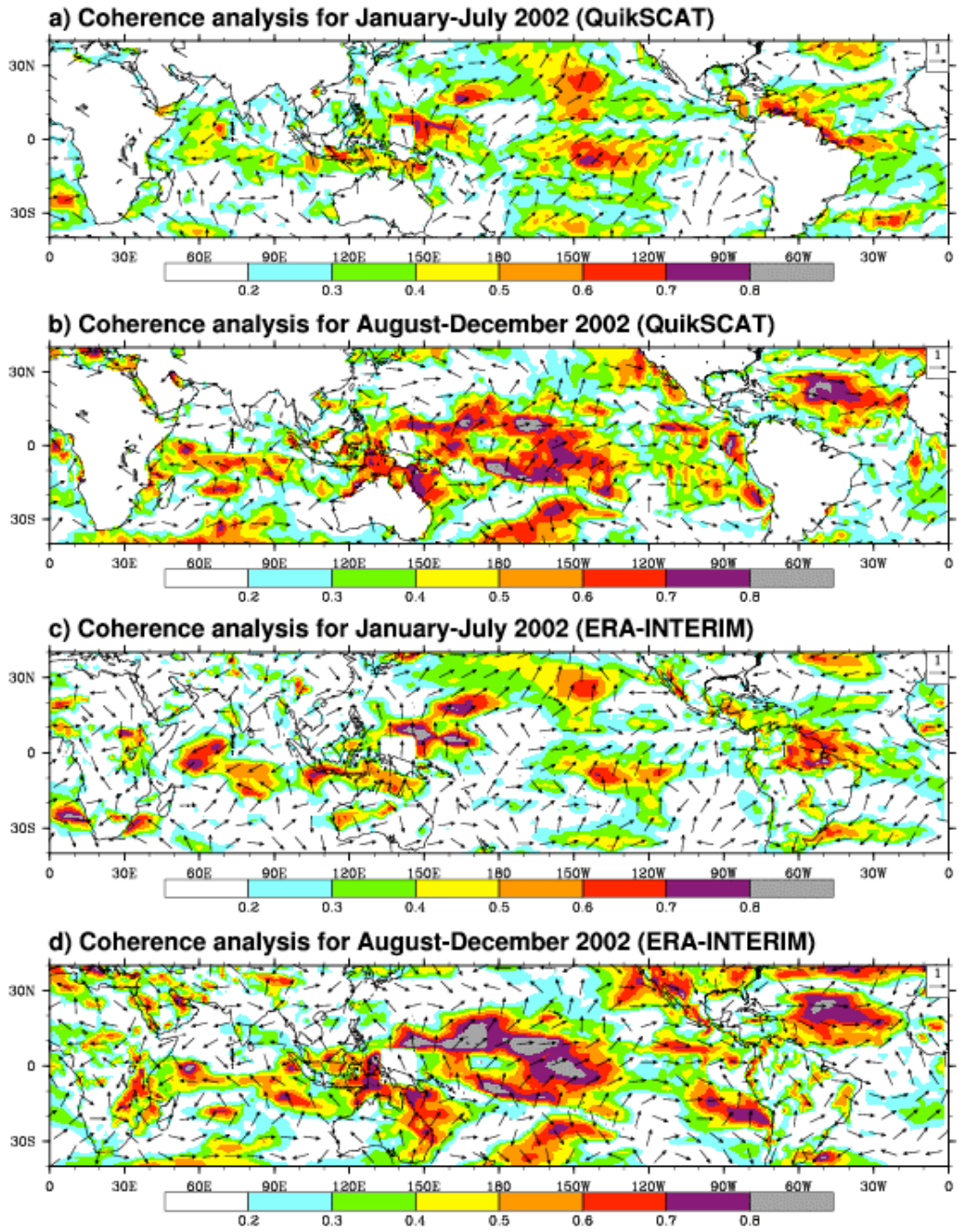

Figure 2.8 a) Averaged spectral coherence analysis from January to July 2002 in the 30-70-day band between a reference of surface zonal wind stress (15°S to 15°N and 120°E to 160°E averaged) and maps of surface zonal wind stress. Filled colors are the coherence squared. Vectors are the phase. The phase vector of the reference is located at the white area of 140°E at the equator. Clockwise rotation indicates phase propagation; b) same as a) but for the period from August to December 2002; c) same as a) but for 40-60-day band; d) same as b) but for 40-60-day band.

Coherence squared values exceed 0.5 from the western Pacific to the central Pacific for January-July (Figure 2.8a), with a phase lag of one-eighth to a quarter of a cycle relative to the reference point. Although a bit noisy, the general clockwise rotation of the phase vectors indicates eastward progression of zonal wind stress anomalies from the western Pacific to the central Pacific. Near 15^{o}N, zonal wind anomalies propagate from the central Pacific to the Caribbean and tropical north Atlantic basin through Central America and the Isthmus of Panama with coherence squared values of 0.3-0.6, indicating a direct influence of the MJO that propagates from the Pacific into the Atlantic Ocean. In the Atlantic, the coherence squared values exceed 0.5 from the Caribbean Sea to the central equatorial Atlantic basin along the South American coastline with surface wind stress anomalies lagging the reference point by somewhat less than one-quarter of a cycle in the Caribbean Sea to more than one-quarter of a cycle in the equatorial western Atlantic. The clockwise rotation of the phase vectors suggests MJO propagation along the northeast coastline of the South American Continent. One possibility to explore in future work is whether coastal topography in this region acts to propagate wind signals along the northern coast of South America in a similar manner to that of an oceanic Kelvin wave, with the coast to its right in the Northern Hemisphere. The significant surface zonal wind stress anomalies that propagate from the western Atlantic to the central Atlantic along the equator are consistent with the 40-60-day observed surface wind variations from January to July in Han et al (2008). In the southwest Atlantic, a large area of coherence above 0.3 can also be seen. This is consistent with the analysis of Jones and Schemm (2000) demonstrating that the South Atlantic Convergence Zone (SACZ) exhibits a wide range of intraseasonal variability, including 30-70 day variations that are

directly related to the MJO.

During August-December of 2002 (Figure 2.8b), large coherence squared values occur in the central Pacific and subtropical Atlantic. The clockwise rotation of the phase vectors and the coherence squared values above 0.4 also show propagation of surface zonal wind anomalies from the western Pacific to Panama. In the equatorial Atlantic, coherence squared values exceeding 0.5 are found in the central and eastern basins but with no obvious eastward propagation. This is consistent with the 40-60-day equatorial surface zonal wind structure during August-December shown by Han et al (2008). Again, the lack of eastward propagating surface wind signals during summer and fall may reflect the influences of westward propagating Rossby waves and the West African Monsoon (e.g., Grodsky and Carton 2001; Matthews 2004; Maloney and Shaman 2008). Some modest evidence exists for westward propagation along 10^{o}N, as well as some evidence for northward propagation in the Eastern Atlantic, consistent with previous studies (e.g. Maloney and Shaman 2008). Further analysis on the westward propagating signals is carried out in Chapter III.

The above analysis suggests that Atlantic equatorial winds can be strongly influenced by MJO events. Coherence maps for the narrower 40-60-day periods (Figures 2.8c and 2.8d; Figures 2.9c and 2.9d) are similar to Figure 2.8a and 2.8b, which have the same patterns but with somewhat higher coherence squared values. These suggest that the MJO events contribute to the 40-60-day zonal wind variability in the equatorial Atlantic discussed by Han et al. 2008. Figures 2.9a and 2.9b show coherence maps obtained using

the ERA-Interim 30-70-day surface winds that produces similar results to that from QuikSCAT. The coherence squared values and the clockwise rotation of the phase vectors show the MJO progression during boreal winter and spring of 2002 from the Eastern Pacific through Panama and into the western equatorial Atlantic along the South American coastline.

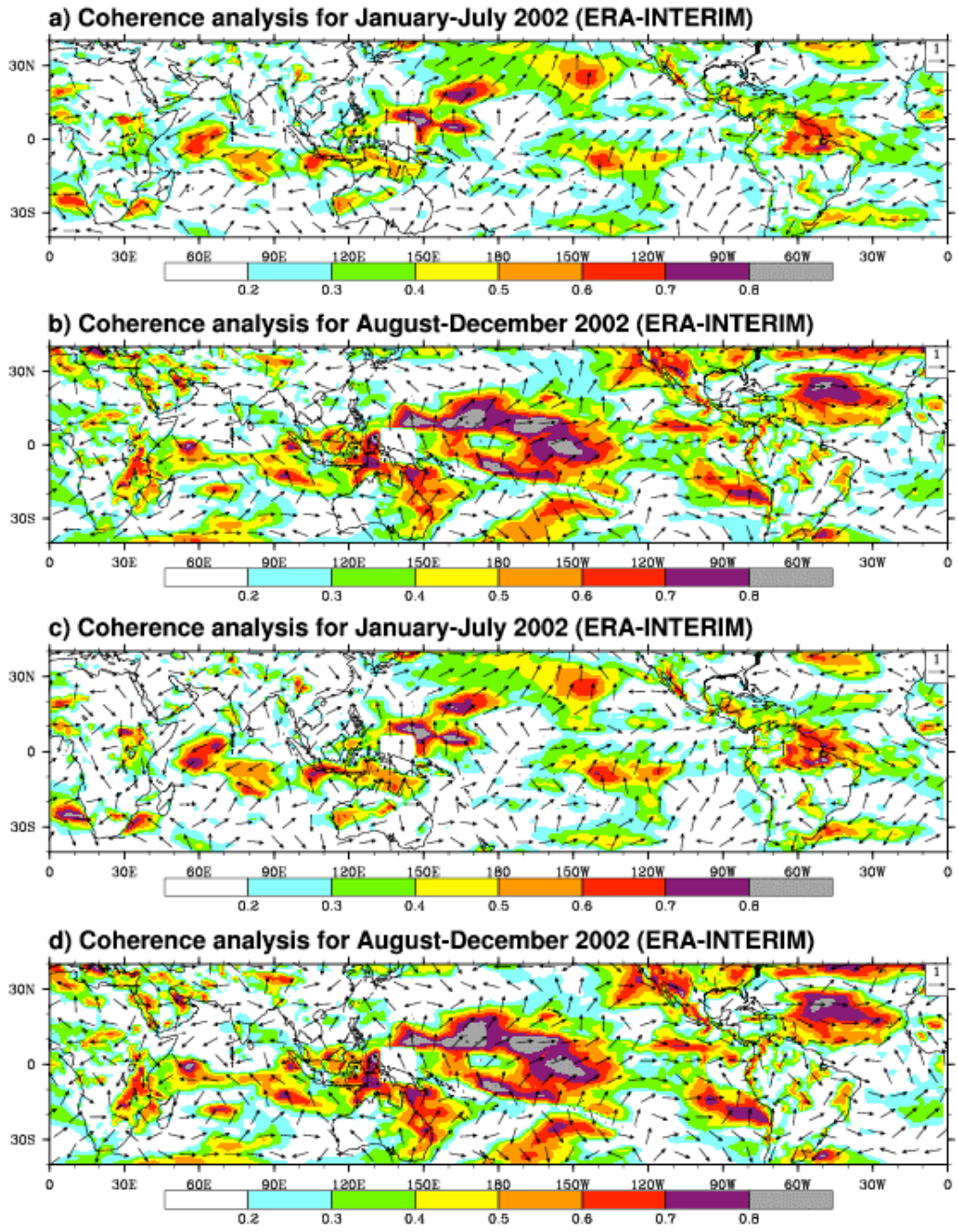

Figure 2.9 a) Averaged spectral coherence analysis from January to July 2002 in the 30-70-day band between a reference of surface zonal wind stress (15°S to 15°N and 120°E to 160°E averaged) and maps of surface zonal wind stress for ERA-Interim data. Filled colors are the coherence squared. Vectors are the phase. The phase vector of the reference is located at the white area of 140°E at the equator. Clockwise rotation indicates phase propagation; b) same as a) but for the period from August to December 2002; c) same as a) but for 40-60-day band; d) same as b) but for 40-60-day band.

2.6 Statistical Relationships

In the above, we focused on intraseasonal variability during 2002, a year when an Atlantic Nino event occurred and strong intraseasonal variability was observed in the equatorial Atlantic Ocean. Now, we perform coherence analysis for the 30-70-day band during 2000-06 period using QuikSCAT data (Figure 2.10) and ERA-Interim surface winds (Figure 2.11). This is done separately for December-May and June-November. We use these periods because the MJO propagation signal and statistics are most robust during these month bands and the nature of the MJO teleconnection to the Atlantic is very different between these two periods (although we did also test different periods [e.g. November-April and May-October]). We first obtained the coherence squared for each year in the season of interest, and then averaged these individual coherence estimates over all years. The phase vectors shown in Figures 2.10 and 2.11 represent the average of unit phase vectors during individual years across all seven years of the analysis. The amplitude of the phase vector thus represents the consistency of the phase relationship across all years. The eastward propagation of the surface wind anomalies is very obvious from the western Pacific into the Eastern Pacific, as indicated by the clockwise rotation of the phase vectors along 15^{o}N during December-May (Figures 2.10a and 2.11a), and along 10^{o}N during June-November but with much weaker coherence values (Figures 2.10b and 2.11b). During December-May (Figures 2.10a and 2.11a), the sizeable (>0.4) coherence squared values along the South American coastline to tropical Atlantic Ocean are similar to that of the 2002 case. During June-November, however, the small amplitudes of the phase vectors in Atlantic show the inconsistency of the phase

relationship relative to the reference point during 2000-06, suggesting substantial interannual variability and defined seasonality of the MJO teleconnection to the Atlantic. Note that ERA-Interim data show stronger coherence values than that of QuikSCAT wind in the Eastern Equatorial Pacific during June-November, but weaker coherences in the Central and Eastern Subtropical Pacific during December-May (compare Figures 2.10 and 2.11).

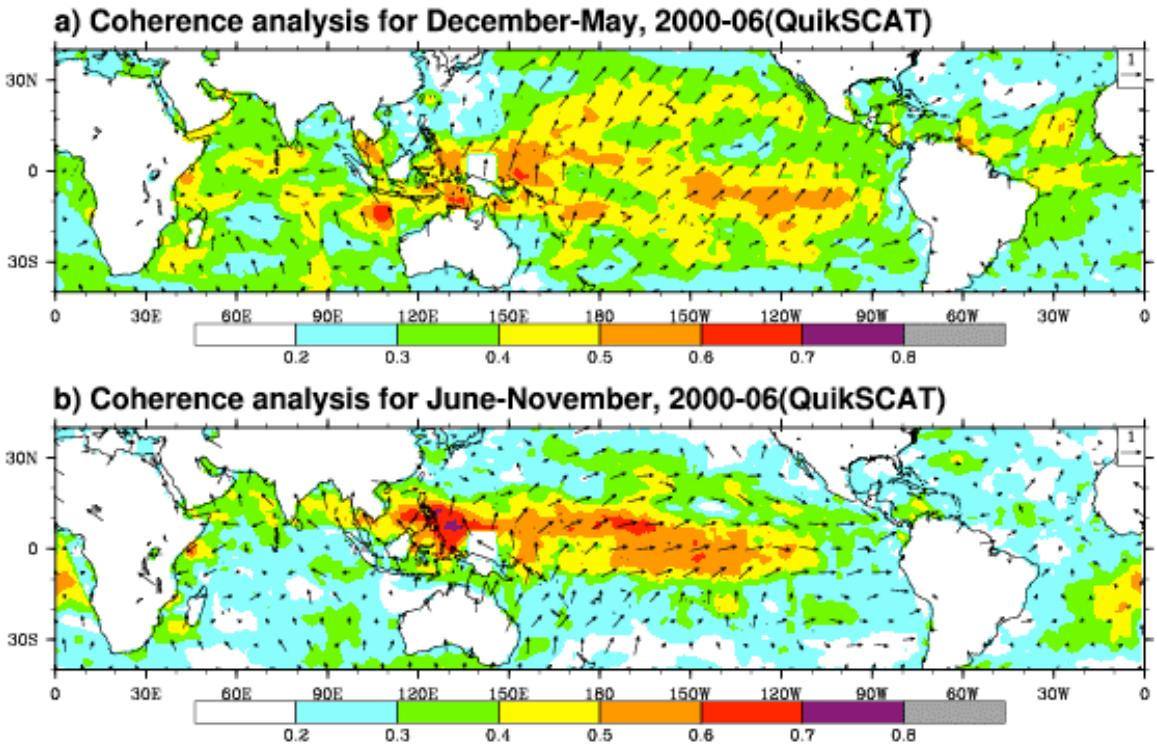

Figure 2.10. Same as Figure 2.8 except for longer period averaged 30-70-day QuikSCAT surface zonal wind during December-May and June-November.

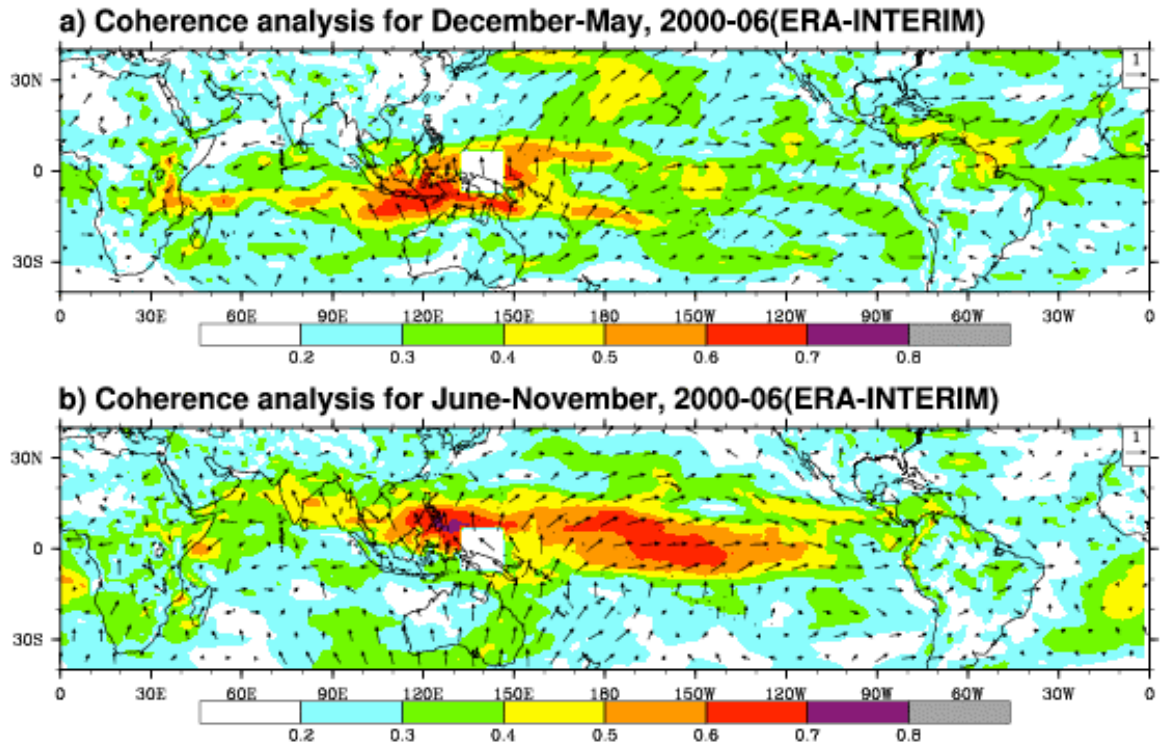

Figure 2.11. Same as Figure 2.8 except for longer period averaged 30-70-day ERA-Interim surface zonal wind during December-May and June-November.

For consistency with the coherence analysis shown in Figures 2.10 and 2.11 and to more precisely isolate the seasonal variations of the MJO teleconnection, we calculate the correlation coefficients for December-May and June-November between a reference time series of 30-70-day bandpass filtered zonal wind in the western Pacific (15^{o}S to 15^{o}N and 120^{o}E to 160^{o}E averaged) and zonal wind across the tropical oceans, using QuikSCAT surface winds during 2000–06 and ERA-Interim surface winds during 1990-2007. In Figure 2.12, correlation maps with the zonal wind index leading by 3 days, 9 days and 15 days, respectively, show a clear eastward progression during December-May and June-November with a maximum correlation coefficient exceeding 0.4 in the Eastern Pacific and Panama Gap area, and exceeding 0.3 in the Atlantic. These values define the 90% (95%) significance level for QuikSCAT (ERA-Interim) winds. During winter and spring, the MJO significantly affects the equatorial Atlantic and the western subtropical Atlantic Ocean, as indicated by the maximum correlation coefficient of above 0.4 for lags of 9 and 15 days.

When the lag is longer than 15 days, the MJO also has a significant influence on the subtropical northern Atlantic during summer and fall with correlation coefficients above 0.3. This delayed influence of MJO on the Atlantic during summer and fall may be due to the strong intraseasonal convective variability in the Western Hemisphere (e.g. Maloney et al. 2008), which makes MJO dynamical signals propagate more slowly due to convective coupling over the east Pacific warm pool. Alternatively, the delayed influence could be due to the different propagation pathways during boreal summer, such as the westward Rossby wave propagation from the Indian Ocean and African monsoon region

(Thorncroft et al. 2003; Sultan et al. 2003; Matthews 2004). Correlation maps using ERA40 winds for 1960-2001 period were also calculated and produced similar results especially during Northern winter and spring (Figure 2.13). During summer and fall, the MJO is seen to affect the Caribbean Sea region. Neither the ERA40 nor the ERA-Interim product shows continuous MJO propagation across the South American continent, consistent with the above coherence analysis, and further suggests that the Isthmus of Panama is a critical pathway for the surface signatures of the MJO to propagate into the Atlantic.

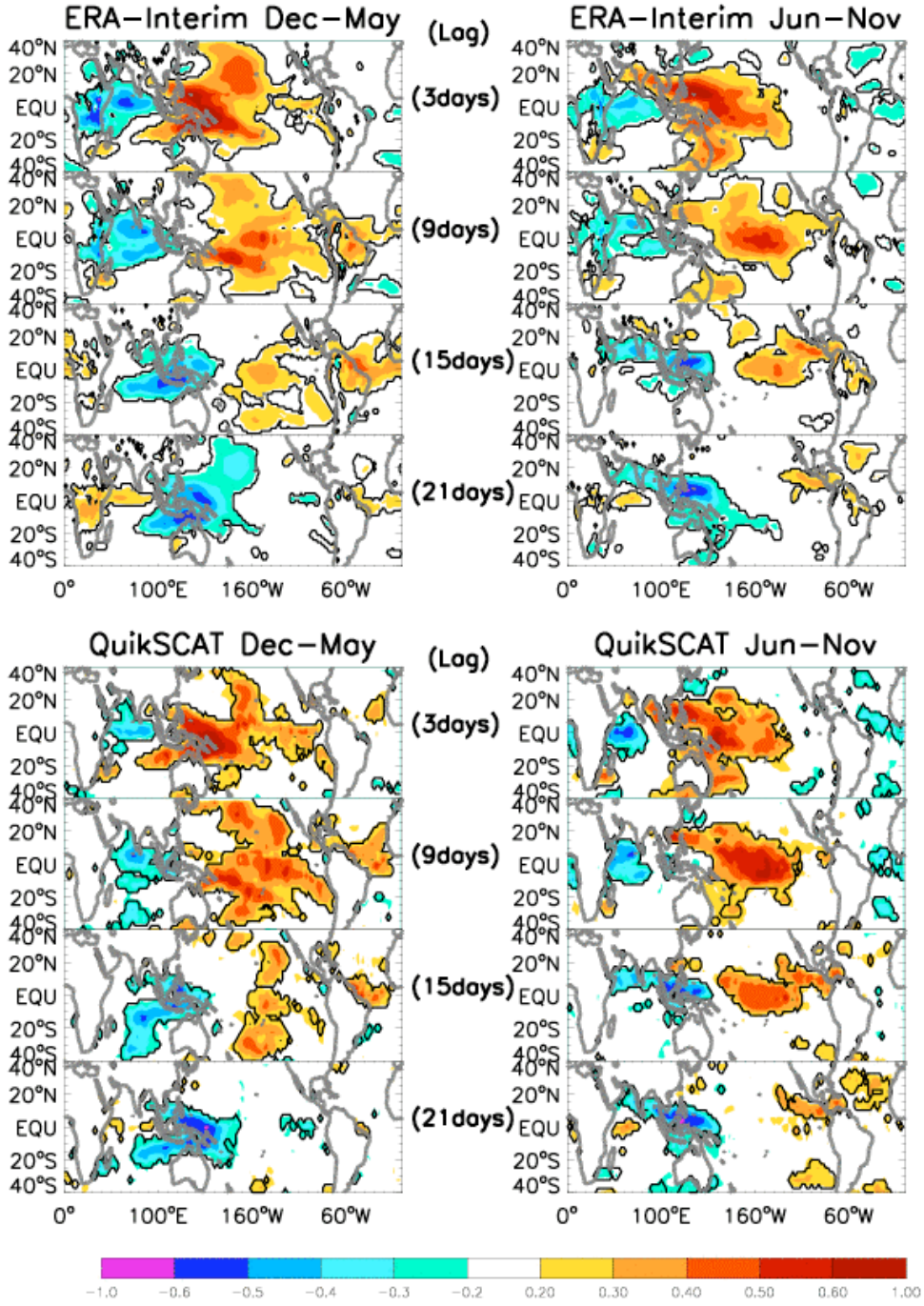

Figure 2.12. Correlation maps between time series of the 30-70-day zonal wind index of ERA-Interim (1990-2007) and QuikSCAT (2000-06) in the western Pacific averaged over (15°S to 15°N and 120°E to 160°E) and zonal wind at each location of 40°S-40°N oceans for lag=3, 9, 15 and 21 days. December-May (left), and June-November (right). Solid line shows that the correlation exceeds 90% (95%) significance level for QuikSCAT (ERA-Interim). Note that the significance test takes into account the reduced degree of freedom due to the filter [Livezey and Chen, 1983].

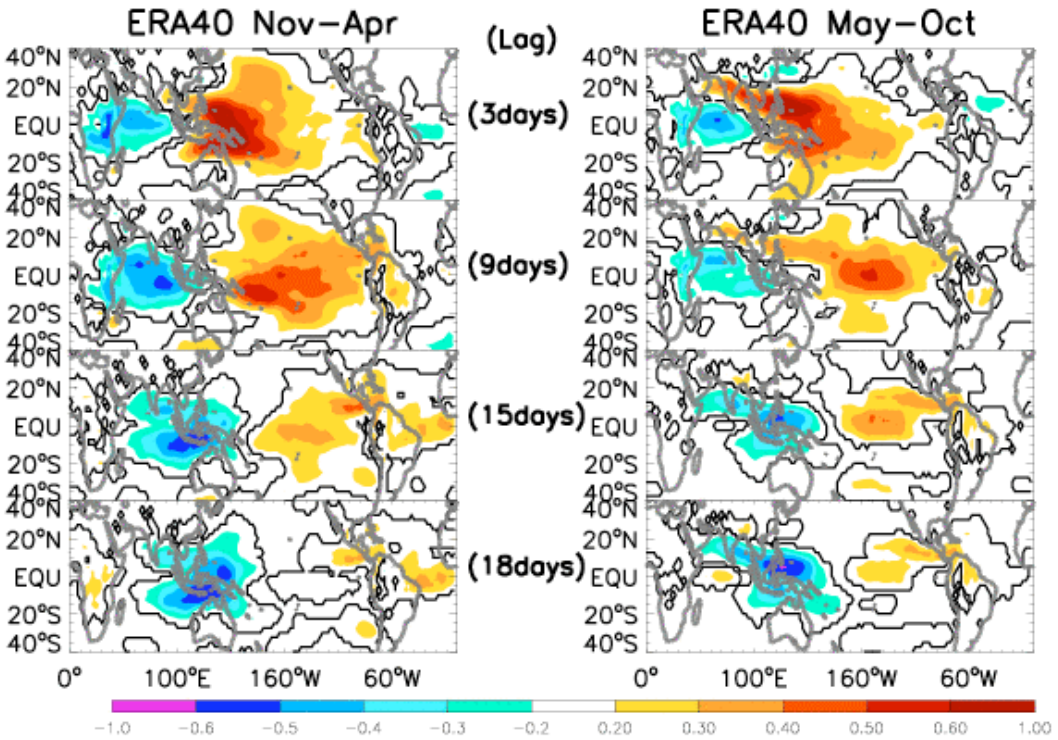

Figure 2.13. Same as Figure 2.12 but for ERA40 data during 1960-2001. Solid line shows that the correlation exceeds 95% significance level.

CHAPTER III

INFLUENCE OF THE MJO AND INTRASEASONAL WAVES ON SURFACE WIND AND CONVECTION OF THE TROPICAL ATLANTIC OCEAN

(Yu et al. 2011: JGR-Atmosphere, submitted)

3.1 Data and Method

The data used in this study are similar to those described in section 2.1. The 3-day mean, QuikSCAT ocean surface wind vectors, daily NOAA interpolated OLR, and daily European Center for Medium-Range Weather Forecasts (ECMWF) Reanalysis (ERA) Interim winds with 1.5^{o}x1.5^{o} resolution are used to diagnose intraseasonal variability. To minimize the influence of missing values due to incomplete sampling and rain contamination, we averaged the 0.25^{o}x0.25^{o} resolution QuikSCAT winds onto 2.5^{o}x2.5^{o} grids. To support inferences on convective activity provided by the OLR, we also analyzed the 1^{o}x1^{o} daily Global Precipitation Climatology Project (GPCP) precipitation data, and daily 1.5^{o}x1.5^{o} ERA-Interim reanalysis precipitation (Xie and Arkin 1997; Simmons et al. 2007).

Given that both the eastward- and westward-propagating atmospheric intraseasonal variability can impact the Atlantic Ocean, sources for the observed intraseasonal variability in the Atlantic are complex. To assess the relative importance of the MJO, intraseasonal Rossby and Kelvin waves, their signals need to be extracted. Based on the space-time spectral analysis of Wheeler and Kiladis (1999), the MJO and each type of the

equatorial waves have their dominant frequencies and wavenumbers (Figure 3.1). Space-time filter is applied to isolate the signals associated with each type of ISOs. Liebmann et al. (2009) used similar method to identify the convective events to study the mechanisms of the initiation of the Kelvin waves in South Africa. Here we focus on the propagation features in Atlantic for various intraseasonal signals. Specifically, to assess the MJO signals, OLR, precipitation and wind data were first filtered to 20-100-day periods with a Lanczos digital filter (Duchon 1979) and then further filtered to eastward wavenumbers 1-6, following the suggestion of the U.S. Climate Variability and Predictability Research Program (CLIVAR) MJO working group (CLIVAR MJO Working Group 2009). Based on the dispersion relation (Figure 3.1, taken from Wheeler and Kiladis 1999), the above filter primarily extracts the MJO signals. In addition, the MJO signals (OLR and surface winds) are also obtained by creating the multivariate global MJO index (Wheeler and Hendon 2004) using daily OLR and ERA-Interim 850mb and 200mb zonal winds during 2000-08.

Similarly, a 20-100-day filter with westward wavenumbers 1-6 is used to isolate the convectively coupled Rossby waves. A 10-25-day band-pass filter is applied to the above fields, to isolate the influence of quasi-biweekly oscillations from African monsoon region (Sultan and Janicot 2003a and 2003b). As can be seen from Figure 3.1, convective signals from these periods (10-25 days) result mainly from convectively-coupled, westward-propagating Rossby waves and eastward-propagating Kelvin waves. These data are further filtered to eastward wavenumbers 1-6 to extract the quasi-biweekly

Kelvin waves, and westward wavenumbers 1-8 to isolate the quasi-biweekly Rossby waves.

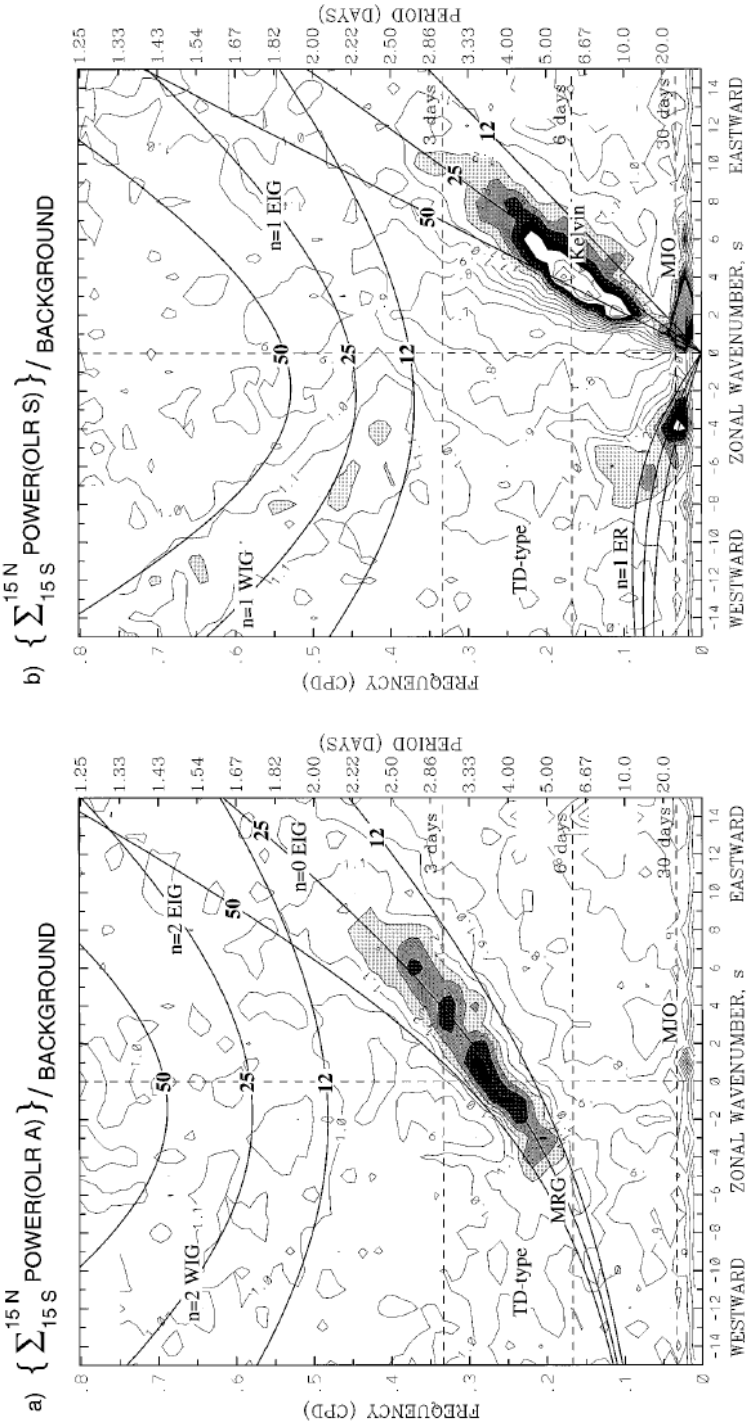

Figure 3.1. a) The antisymmetric OLR power divided by the background power. Contour interval is 0.1, and shading begins at a value of 1.1 for which the spectral signatures are statistically significantly above the background at the 95% level. Superimposed are the dispersion curves of the even meridional mode-numbered equatorial waves for three equivalent depths of h = 12, 25, and 50 m. b) Same as a) except for the symmetric component of OLR. Adapted from Wheeler and Kiladis (1999).

Composite analyses are performed to demonstrate each type of ISO impacts. First, we analyze the time series of total 20-100-day filtered OLR without wavenumber filtering, 20-100-day filtered OLR with east wavenumber 1-6 filtering (MJO) and west wavenumber 1-6 filtering (Rossby wave), respectively, for a specific region of the tropical Atlantic Ocean or West African monsoon during 2000-08. Indices of convective events are chosen when both the total 20-100-day OLR and the MJO (or Rossby wave) signal reach maxima and each exceeds one standard deviation (STD) of the time series. These events are referred to as "MJO-dominated" (or "Rossby wave-dominated"). To confirm the MJO-dominated events above, the multivariate global MJO index (Wheeler and Hendon 2004) is also used, and the two methods yield consistent MJO events. Similarly, the 10-25-day convectively coupled Kelvin- and Rossby wave-dominated events are selected.

Then, composite fields of 20-100-day (or 10-25-day) OLR, ERA-Interim and QuikSCAT winds, together with GPCP precipitation are created based on the indices obtained above. Note that even though indices are chosen based on both total 20-100-day OLR and the MJO (or Rossby wave) signal with wavenumber filtering, the composite fields shown later for the MJO-dominated (or Rossby wave-dominated) events are based on the total 20-100-day fields without further wavenumber filtering. This is also true for 10-25-day convective events. Intraseasonal variances and spectral coherence analysis were performed using OLR to demonstrate the effects of the MJO, Rossby and Kelvin waves on convections in the tropical Atlantic Ocean.

The rest of this Chapter is organized as follows. In section 3.2, we assess the effects of MJO, Rossby waves and their relative importance on 20-100-day variability of the tropical Atlantic Ocean and African monsoon region. In section 3.3, we examine the impacts of quasi-biweekly Kelvin and Rossby waves in the tropical Atlantic Ocean.

3.2 20-100-day Variability in Tropical Atlantic and African Monsoon Region

Figure 3.2 shows longitude-time diagrams of the 20-100-day bandpass filtered QuikSCAT surface zonal wind averaged from 15^{o}S to 15^{o}N during 2003 and 2005, which includes both the eastward-propagating MJO and westward-propagating Rossby wave signals. Similar eastward (westward)-propagating signals are also observed during other years. Consistent with Chapter II, the maximum wind anomalies are first observed in the Indian Ocean and Western Pacific during spring 2003, and then subsequently propagate into the Atlantic Ocean to 40^{o}W, and the Atlantic manifestation of the wind anomalies is weaker relative to the Indo-Pacific sector. Eastward propagating MJO events occur during boreal winter and spring, becoming weaker during summer. Similar situation exists for 2005, and the MJO signals are even stronger. During summer and fall, however, westward-propagating signals are evident.

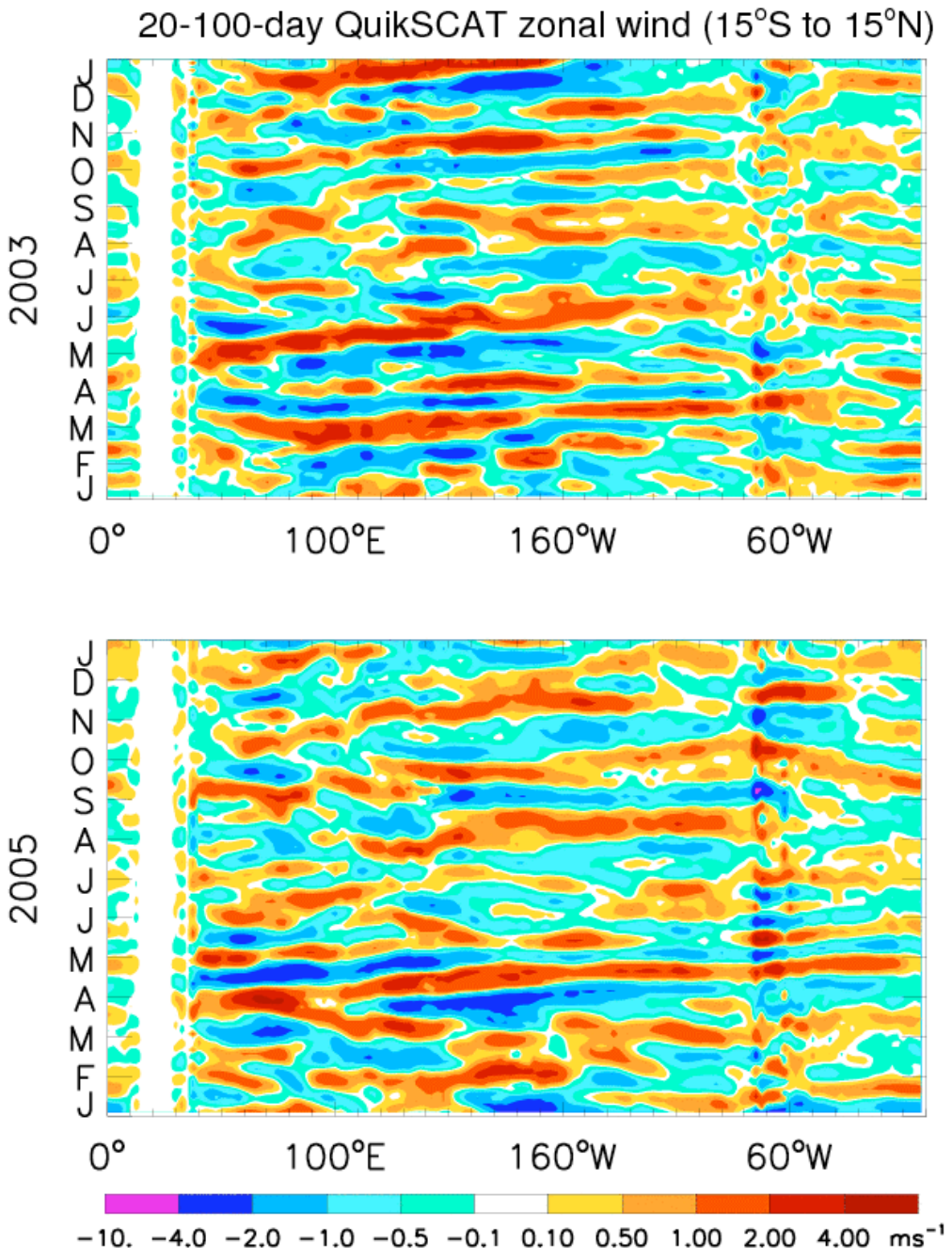

Figure 3.2. Longitude-time diagram of 20-100-day band-pass filtered QuikSCAT 10m zonal wind averaged from 15°S to 15°N during 2003 (top) and 2005 (bottom).

3.2.1 Effects of MJO

To further quantify the MJO influence, we create the multivariate global MJO index (e.g., Wheeler and Hendon 2004; Maloney et al. 2010) based on OLR data and ERA-Interim 850-mb and 200-mb zonal winds, each averaged over the latitudes of 15^{o}S-15^{o}N during 2000-08. The MJO is defined as the leading pair of EOFs. Zonal structures of the leading two EOFs of the combined fields of OLR, 850-mb and 200-mb zonal winds are presented in Figure 3.3. EOF1 and EOF2 explain 24.1% and 23.7% of the variance of the original atmospheric fields respectively. EOF1 shows the familiar MJO structures of its initiation phase (see phases 1-2, P1 and P2 of Figure 3.4), when the MJO produces enhanced convection (negative OLR anomalies) in the Eastern Equatorial Indian Ocean, with low level westerly wind anomalies located in the west and easterly wind anomalies in the east of the convection, which converges to the convective region. The 200-mb wind anomalies are in opposite direction to that of 850 mb. EOF2 has enhanced convection over the Eastern Indian and Western Pacific Oceans (see phases 3-4, P3 and P4 of Figure 3.4), and is associated with wind patterns that converge to the convective region, similar to those of EOF1.

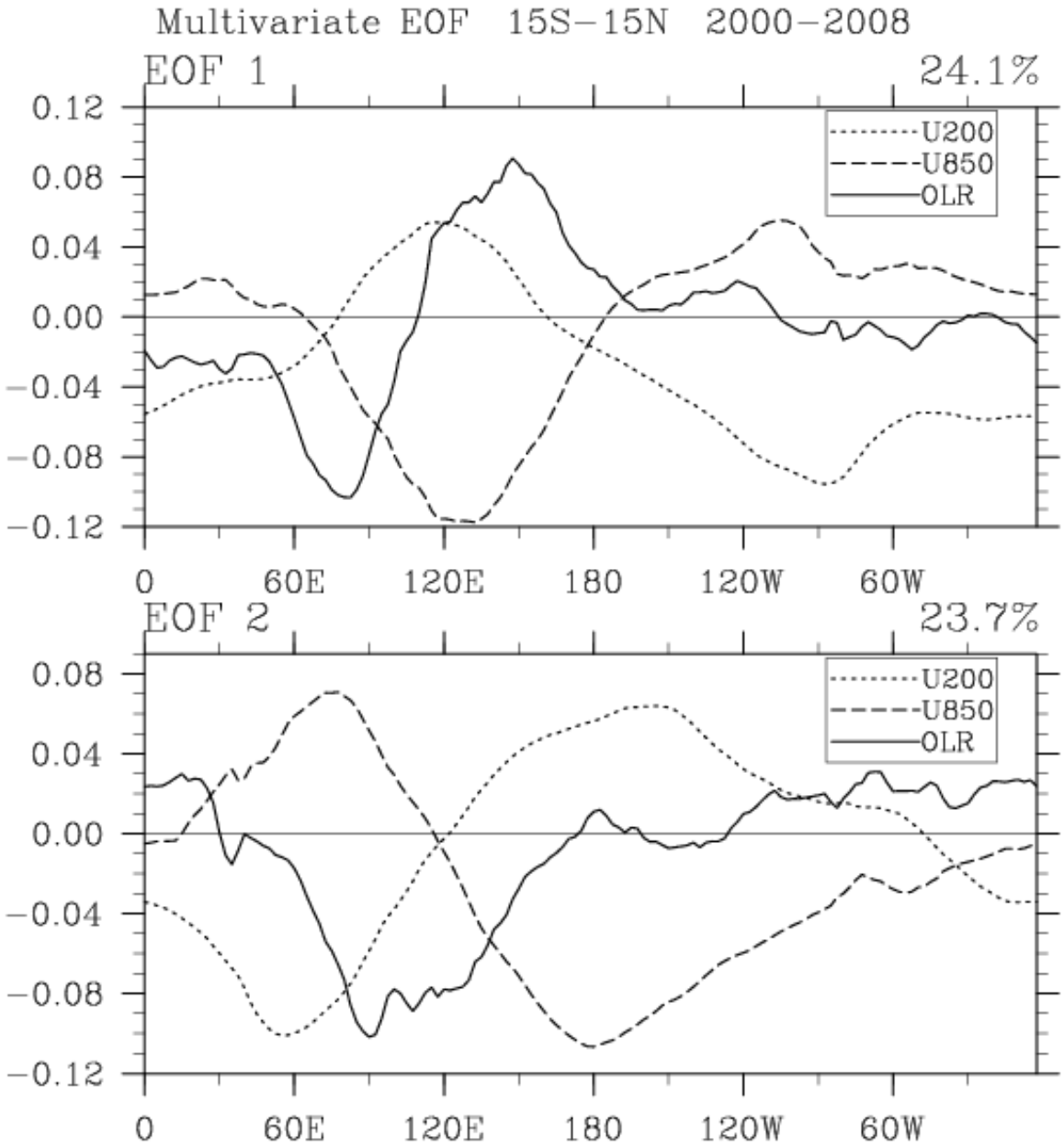

Figure 3.3. Multivariate EOF analysis during 2000-08 based on daily OLR, ERA-Interim 850-mb and 200-mb zonal winds. Averaged from 15^{o}S to 15^{o}N.

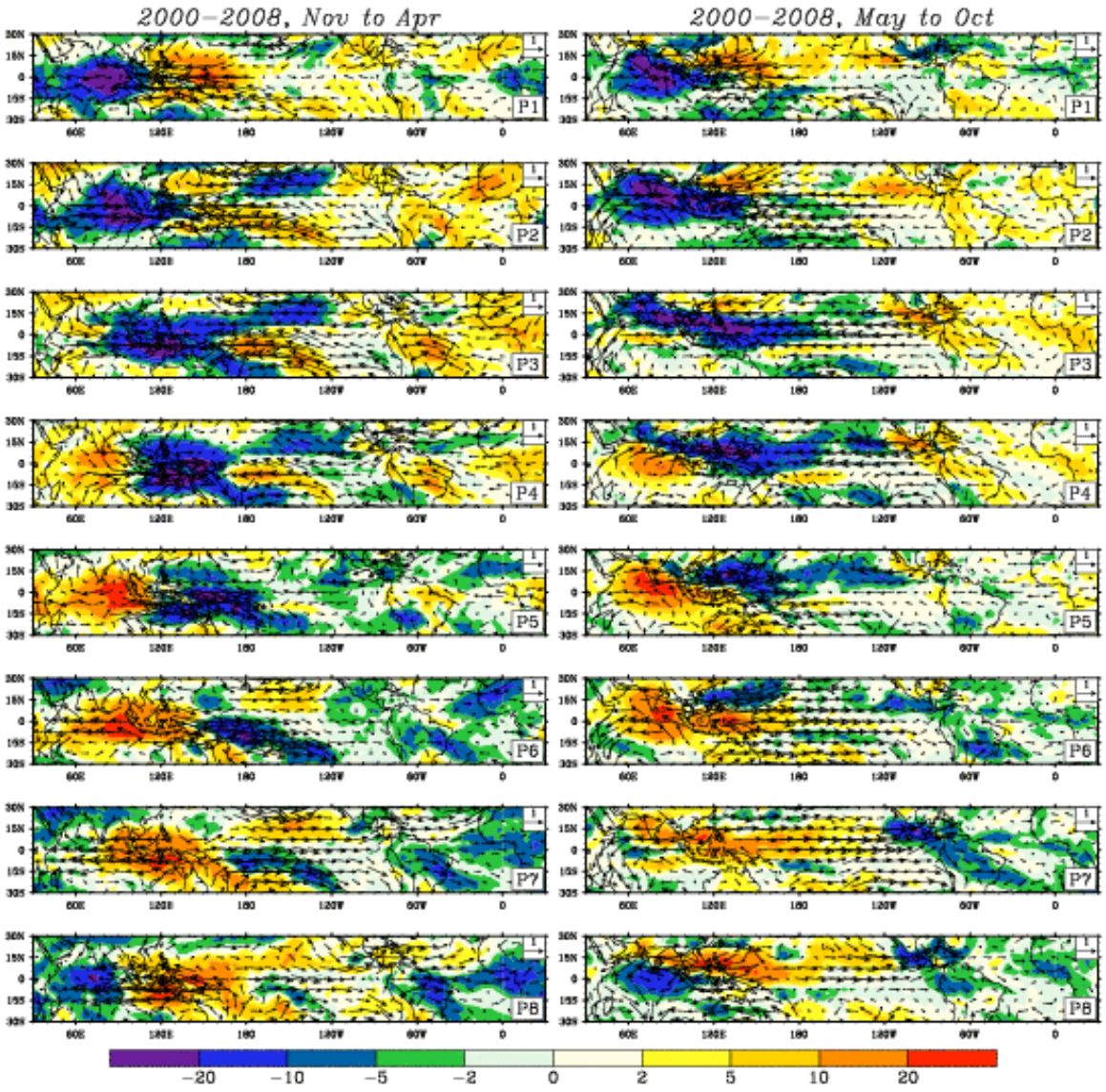

Figure 3.4. Composite maps based on the multivariate global MJO index for winter (left) and summer (right) MJO cycles during 2000-08. Filled colors are composite 20-100-day OLR variation. Wind vectors are 20-100-day 850-mb ERA-Interim wind variation.

Taken as a pair, these structures are consistent with those obtained by previous studies (Wheeler and Hendon 2004; Maloney et al. 2010). The time series of the first two principal components (PCs) of the EOFs are combined to derive the phase information. The phase space spanning 0^o to 360^o is partitioned into eight equal-angle ‘‘MJO phases’’ into which high amplitude events are binned based on phase information derived from the PCs. For each MJO phase, days with global MJO index (amplitude) exceeding 1 are averaged together to generate a composite event. Here the global MJO index is defined as the sum of the square of the first two principal components: $PC1^2 + PC2^2$. The composite maps of MJO cycles are shown in Figure 3.4, in which eight phases are shown with 45^o interval from 0^o-360^o to reveal the MJO propagation. For the winter MJO (Figure 3.4, left column), phases P1 and P2 show the familiar MJO convective dipole, with enhanced convection (negative OLR anomalies) in the Indian Ocean and reduced convection (positive OLR anomalies) in the Western Pacific. The westerly (easterly) wind anomalies are located to the west (east) of the enhanced convection, as discussed above. Associated with the eastward propagation of convection, the 850mb easterly and westerly wind anomalies propagate eastward, entering the Atlantic through Central America and Isthmus of Panama during phases P2-P4 and P5-P8, and affecting the tropical Atlantic Ocean. The negative convection anomalies of the MJO weaken in the Eastern Pacific and enhance in the Eastern Equatorial Atlantic and West Africa, suggesting the MJO impact on these regions (phases P6-P8 of Figure 3.4 left panels). In contrast, during boreal summer (Figure 3.4 right), even though surface wind and convection associated with the MJO have apparent influence on the tropical Atlantic, the amplitudes shown by OLR anomalies are weaker comparing to that of boreal winter. These results are consistent

with our discussion above (Figure 3.2) and the analysis of Chapter II.

3.2.2 Effects of Rossby waves

Interestingly, evident westward-propagating signals that are originated from West Africa are seen in the Eastern and Central Atlantic during most part of 2003 and during summer and fall of 2005 (Figure 3.2), a period while the MJO has weaker influence than winter and spring (Figures 3.2 and 3.4). To investigate these westward-propagating signals, which are most apparent during boreal summer and fall, we choose (5^{o}N-10^{o}N, 5^{o}W-0^{o}W) area from the West African monsoon region (e.g., Sultan and Janicot 2003a and 2003b) as a reference, and perform coherence analysis during May-October of 2000-08 (Figure 3.5). When we use the total 20-100-day filtered OLR data, significant coherence (with coherence squared values above 0.3) is trapped to the Eastern Tropical Atlantic without apparent westward propagation (Figure 3.5a). To exclude the MJO effect, we first extract the MJO signals by regressing the OLR data onto the global MJO index derived above (Figure 3.3), and then remove the MJO signals from the 20-100-day OLR field. After the MJO signals are removed, coherence squared values above 0.3 across the tropical Atlantic basin are observed and exhibit a westward phase propagation as shown by the clockwise rotation of phase vectors toward the west from the reference region (Figure 3.5b). For example, the phase vector is northward in West Africa, and is northeastward near 35^{o}W along the equator. These results indicate that intraseasonal convections of the West African Monsoon can affect the entire tropical Atlantic via westward-propagating Rossby waves. Indeed, the 20-100-day westward wavenumbers 1-

6 filtered OLR data (Figure 3.5c), which consist primarily of westward-propagating Rossby waves (Figure 3.1), show stronger coherence and clearer westward propagation from the West African monsoon region across the tropical Atlantic comparing to Figure 3.5b.

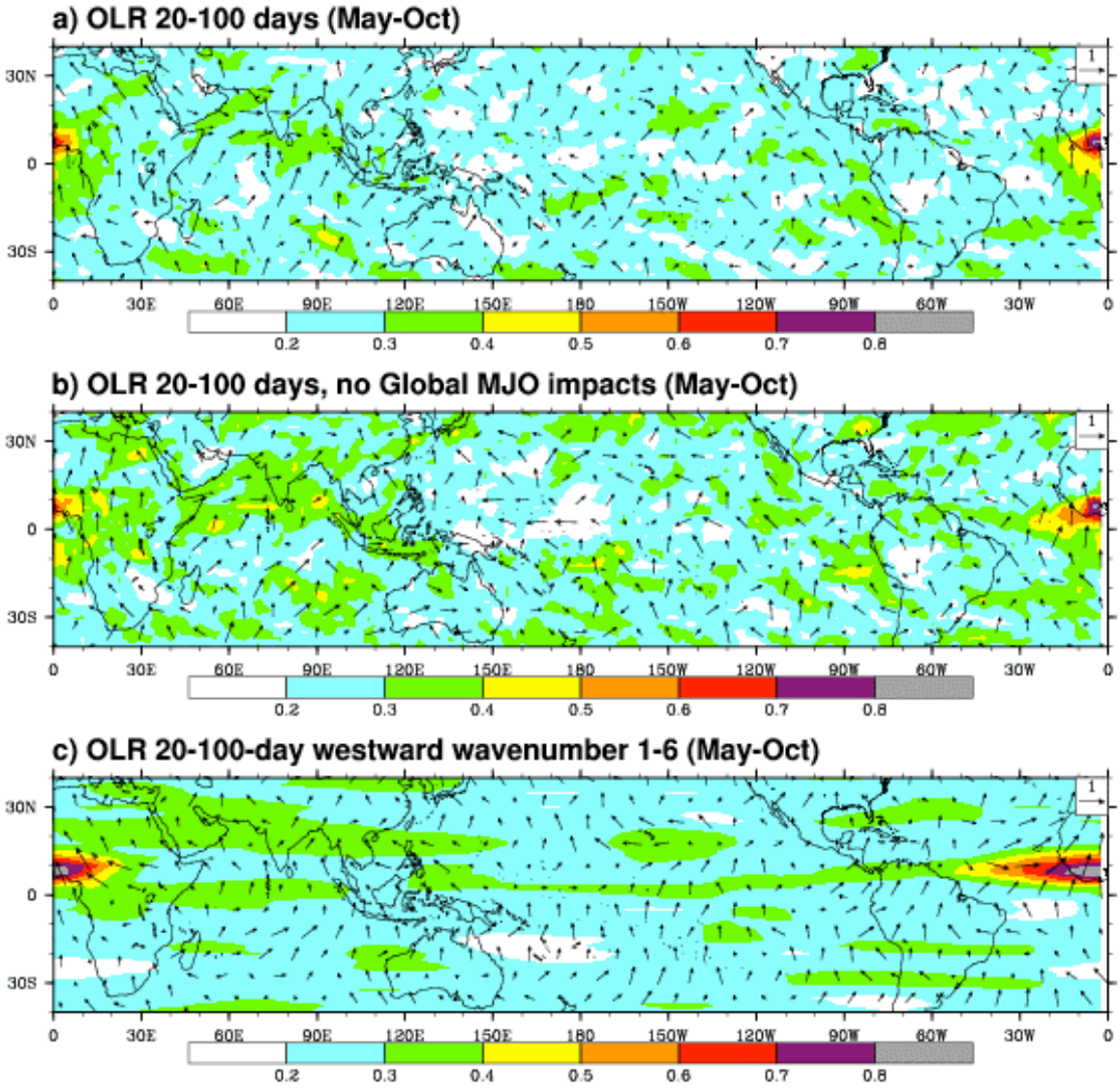

Figure 3.5. a) Averaged spectral coherence analysis from May to October during 2000-08 in the 20-100-day band between a reference of OLR (5°N-10°N, 5°W-0°W averaged) and global maps of OLR. Filled colors are the coherence squared. Vectors denote phases, with clockwise rotation toward the west indicating westward phase propagation; b) same as a) but for the OLR removing the global MJO signals extracted by regressing the OLR onto the multivariate global MJO index; c) same as a) but for the 20-100-day westward wavenumber 1-6 filtered OLR.

3.2.3 Relative Importance of MJO and Rossby Waves

To quantify the impacts of the MJO and Rossby waves, we choose 3 representative regions in the Western Atlantic (WA; 0^{o}N-15^{o}N, 50^{o}W-40^{o}W), Central Atlantic (CA; 5^{o}S-15^{o}N, 30^{o}W-20^{o}W) and African monsoon region (AF; 0^{o}N-14^{o}N, 10^{o}W-10^{o}E). Here we choose the African monsoon region (Sultan and Janicot 2003a; Redelsperger et al. 2002; Gu 2009). The WA region locates within the propagation path of MJO surface wind from Indo-Pacific to tropical Atlantic (Yu et. al. 2011). Geographic locations of these regions are shown in Figure 3.6a.

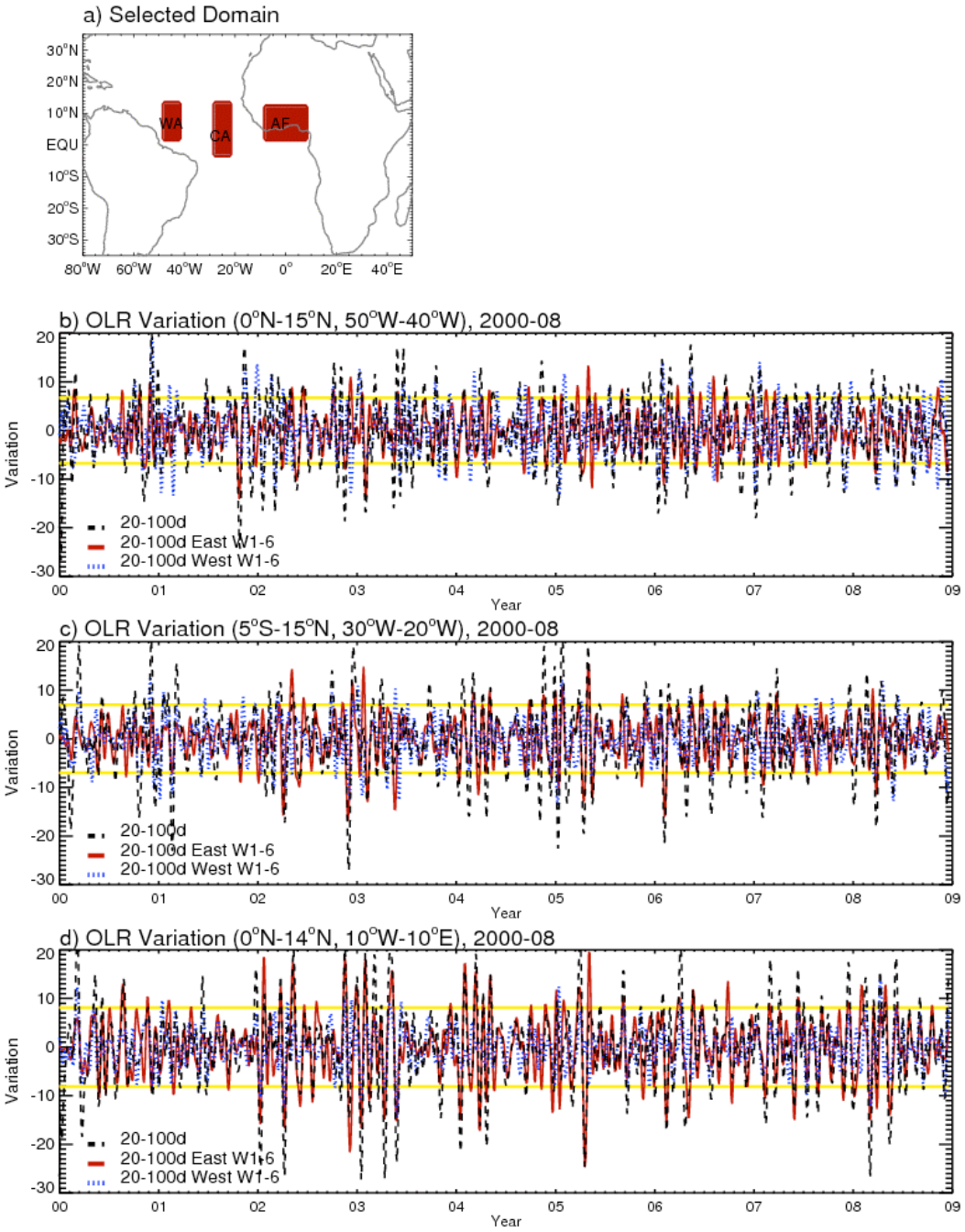

Figure 3.6 a) Selected domains: West Atlantic (WA; 0°N-15°N, 50°W-40°W), Central Atlantic (CA; 5°S-15°N, 30°W-20°W) and West African monsoon (AF; 0°N-14°N, 10°W-10°E); b) Time series of 20-100-day filtered OLR during 2000-2008 averaged for the WA region (dashed lines), 20-100-day eastward wavenumber 1-6 (solid lines), and 20-100-day westward wavenumber 1-6 (dotted lines). The constant solid lines show the standard deviation of 20-100-day filtered OLR. c) same as b) except for CA region; d) same as b) except for AF region.

Figures 3.6b-d show strong intraseasonal variations of 20-100-day filtered OLR above one STD (yellow line) occurred in the three regions (dashed black line), which are often correspond to either eastward wavenumbers 1-6 OLR anomalies (solid red line) that are primarily associated with the MJO and Kelvin waves (collectively referred to as the MJO here), or westward wavenumber 1-6 OLR anomalies (dotted blue line) that are associated with the Rossby waves. The standard deviation (STD) of MJO and Rossby waves comparing to the STD of 20-100-day OLR are 63% and 77% in Western Atlantic, 68% and 62% in Central Atlantic, and 83% and 50% in African monsoon region (Table 3.1), suggesting the comparable importance of the MJO and Rossby waves to intraseasonal variability in the tropical Atlantic Ocean. In the African monsoon region, however, MJO impacts are more important than Rossby waves, and almost all of the enhanced convective events above one STD correspond to significant MJO events (Figure 3.6d). The correlation coefficient between the 20-100-day OLR and the MJO (Rossby waves) during 2000-08 period is 0.51 (0.67) in Western Atlantic, 0.63 (0.59) in Central Atlantic and 0.8 (0.62) in African monsoon region. These results suggest that the strong enhanced convective events are more frequently related to MJO in the African monsoon region, to the Rossby waves in the Western Atlantic, and equivalently associated with MJO and Rossby waves in the Central Atlantic. The fact that both the eastward-propagating MJO and westward-propagating Rossby waves are important in the tropical Atlantic basin is consistent with the lack of propagation detected in Figure 3.5a.

Table 3.1. Domain-averaged 20-100-day variability. The percentage "%" is relative to the total 20-100-day OLR. Units: W M^{-2}.

		WA	CA	AF
Standard Deviation (STD)	20-100-day OLR	6.8	6.9	8.0
	MJO (percentage)	4.3 (63%)	4.7 (68%)	6.6 (83%)
	Rossby Wave (percentage)	5.2 (77%)	4.3 (62%)	4.0 (50%)
Correlation between 20-100-day OLR and	MJO	0.51	0.63	0.8
	Rossby wave	0.67	0.59	0.62

As shall be seen below, since MJO signals often strengthen while they cross the tropical Atlantic, MJO dominated convective events increase toward the east. Similarly, since the Rossby wave signals often enhance over the Atlantic Ocean while they propagate westward, and some even appear to be generated in the Eastern Atlantic basin, the Rossby wave dominated convective events increase toward the west.

In order to further quantify the relative contribution of MJO and Rossby waves, we first create the convective indices for different regions by choosing the date of the enhanced convective events when the domain averaged maximum negative 20-100-day OLR amplitudes exceed one STD, and then we further categorize these convective events as MJO dominated and Rossby wave dominated. The MJO (Rossby wave) dominated convective events are defined as the maximum negative 20-100-day with eastward (westward) wavenumbers 1-6 filtered OLR amplitudes exceed one STD of the total 20-100-day OLR time series and have the same phase. Finally, we calculate the time distribution of the convective index for May-Oct and Nov-Apr.

As shown in Table 3.2, the MJO and Rossby wave dominated convective events (relative to total 20-100-day events) are 17 (32%) and 29 (55%) in Western Atlantic, 18 (35%) and 20 (39%) in Central Atlantic, and 32 (62%) and 12 (23%) in African monsoon region. It implies that Rossby wave and MJO have different impacts in different regions across the tropical Atlantic Ocean, with more frequent Rossby wave dominated events in Western Atlantic and MJO dominated events in African monsoon region, and they are almost equally important in Central Atlantic. Given the fact that cold SST in the Eastern

Pacific inhibits convection and the continent of Central America blocks continuous air-sea interaction, MJO related convection is generally weaker in Western Atlantic after MJO propagates into the Atlantic than in the Indo-Pacific Ocean, consistent with Figure 3.4. Note that MJO dominated convective events are less frequent during May-Oct than during Nov-Apr, with 3 versus 14 events in Western Atlantic, 4 versus 14 in Central Atlantic and 10 versus 22 in African monsoon region (Table 3.2), consistent with the seasonal variation of MJO activities (Madden and Julian 1994; Jones et al. 2004; Matthews 2000; Maloney et al. 2008; Chapter II; Figure 3.2). In contrast, the Rossby wave dominated convective events are more evenly distributed during May-Oct and Nov-Apr in both Western Atlantic and Central Atlantic, with 14 versus 15 in Western Atlantic, and 9 versus 11 in Central Atlantic.

Table 3.2. Convective events for total 20-100-day OLR exceeding 1 STD, MJO dominated events when MJO associated convection exceeds 1 STD of total 20-100-day OLR with the same phase, and Rossby wave dominated events when Rossby wave associated convection exceeds 1 STD of total 20-100-day OLR. The "%" is relative to total 20-100-day OLR events.

		WA			CA			AF		
	Dominated	All	May-Oct	Nov-Apr	All	May-Oct	Nov-Apr	All	May-Oct	Nov-Apr
20-100-day convective events (exceeding 1 STD of total)	Total	53	26	27	51	23	28	52	20	32
	MJO dominated	17 32%	3	14	18 35%	4	14	32 62%	10	22
	Rossby wave dominated	29 55%	14	15	20 39%	9	11	12 23%	3	9

The development of MJO (Rossby wave) related deep convective anomalies over the tropical Atlantic and African monsoon region can be seen by a sequence of lagged composite maps of 20-100-day filtered fields during 2000-08, such as OLR, and surface wind fields, lagged with respect to OLR categorized convective index in different regions shown in Table 3.2 and Figure 3.6a. Day 0 corresponds to the time when convection attains its maximum strength. The categorized convective indices (Table 3.2) indicate that the 20-100-day deep convective anomalies are mainly MJO or Rossby wave dominated, consistent with the dispersion relation of tropical convective disturbances (Figure 3.1).

The composite 20-100-day filtered OLR and surface winds (Figures 3.7-3.9, left panels), based on the MJO dominated convective events in all three regions, show an eastward propagation and impact on the Atlantic. The maximum convective anomalies first appeared in the Indo-Pacific warm pool. Subsequently, the convective anomalies, together with the westerly wind anomalies to the west and easterlies to the east, propagate eastward (Figures 3.7-3.9, left panels; Milliff and Madden 1996; Matthews 2000), entering the Atlantic via Central America and Isthmus of Panama, across the Atlantic and affecting the Atlantic and African monsoon region.

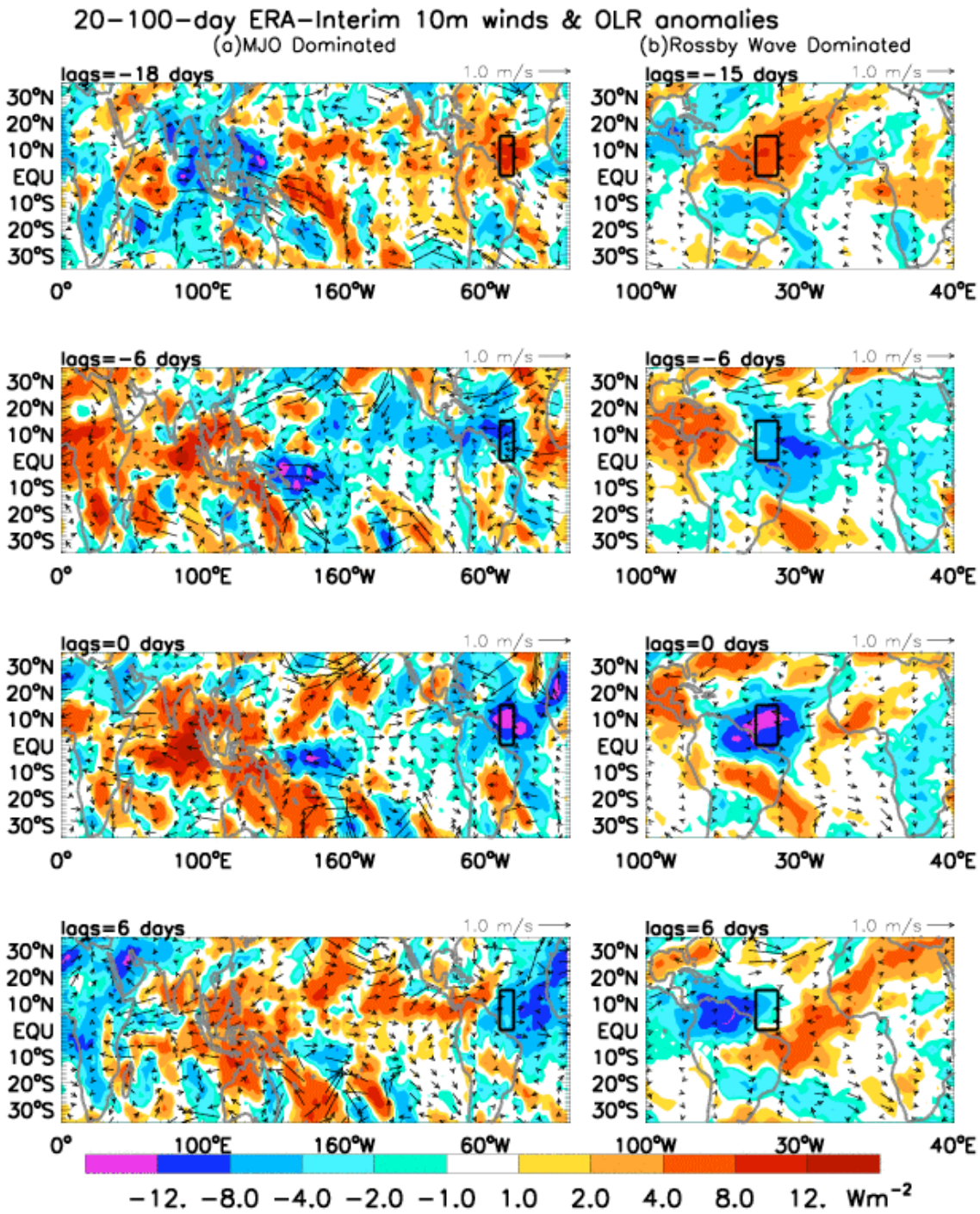

Figure 3.7. Composite fields of 20-100-day filtered ERA surface winds and OLR based on the MJO (a. left panels) and Rossby waves (b. right panels) dominated convective events in Western Atlantic region (the black box).

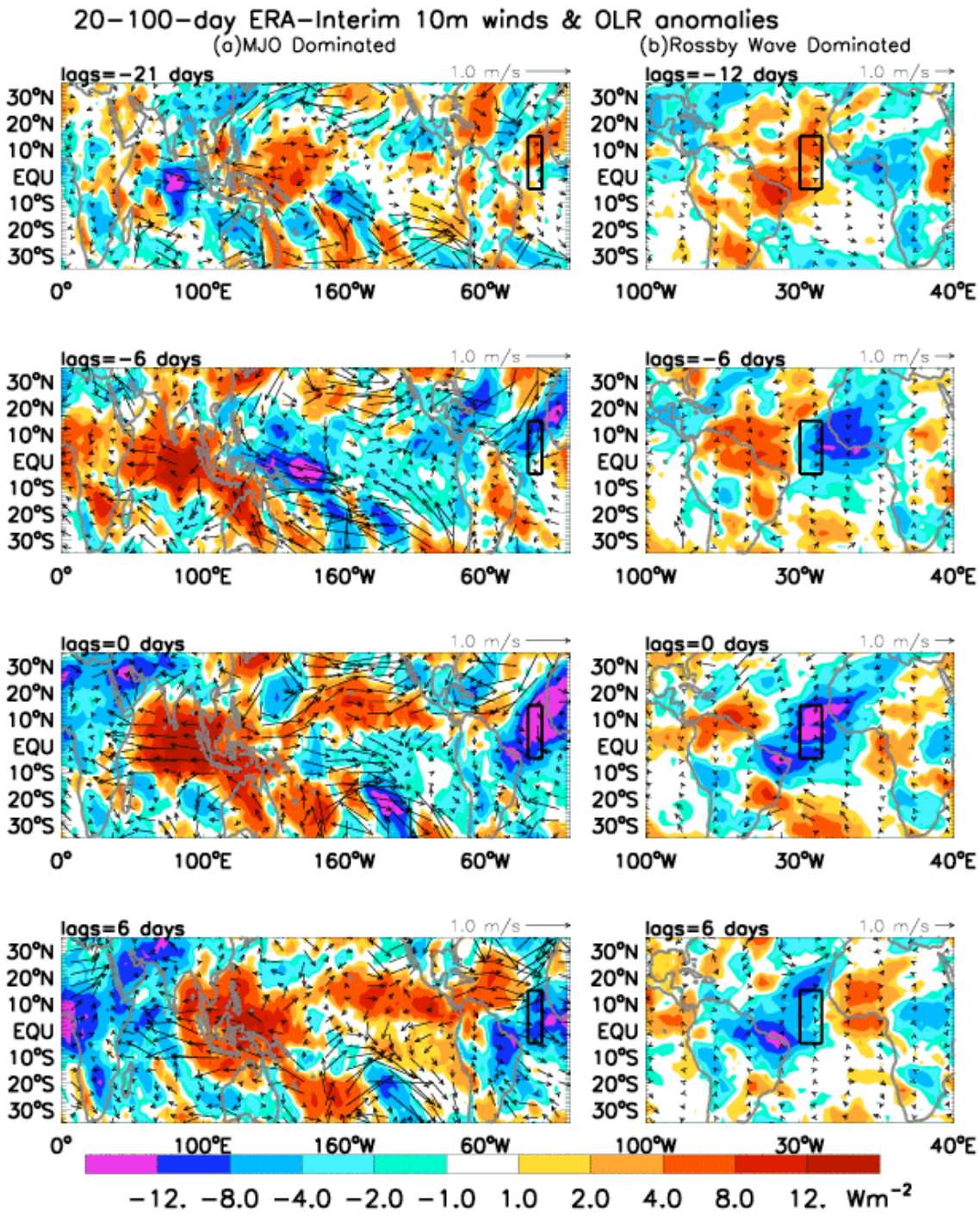

Figure 3.8. Same as Figure 3.7 except for convective events in Central Atlantic.

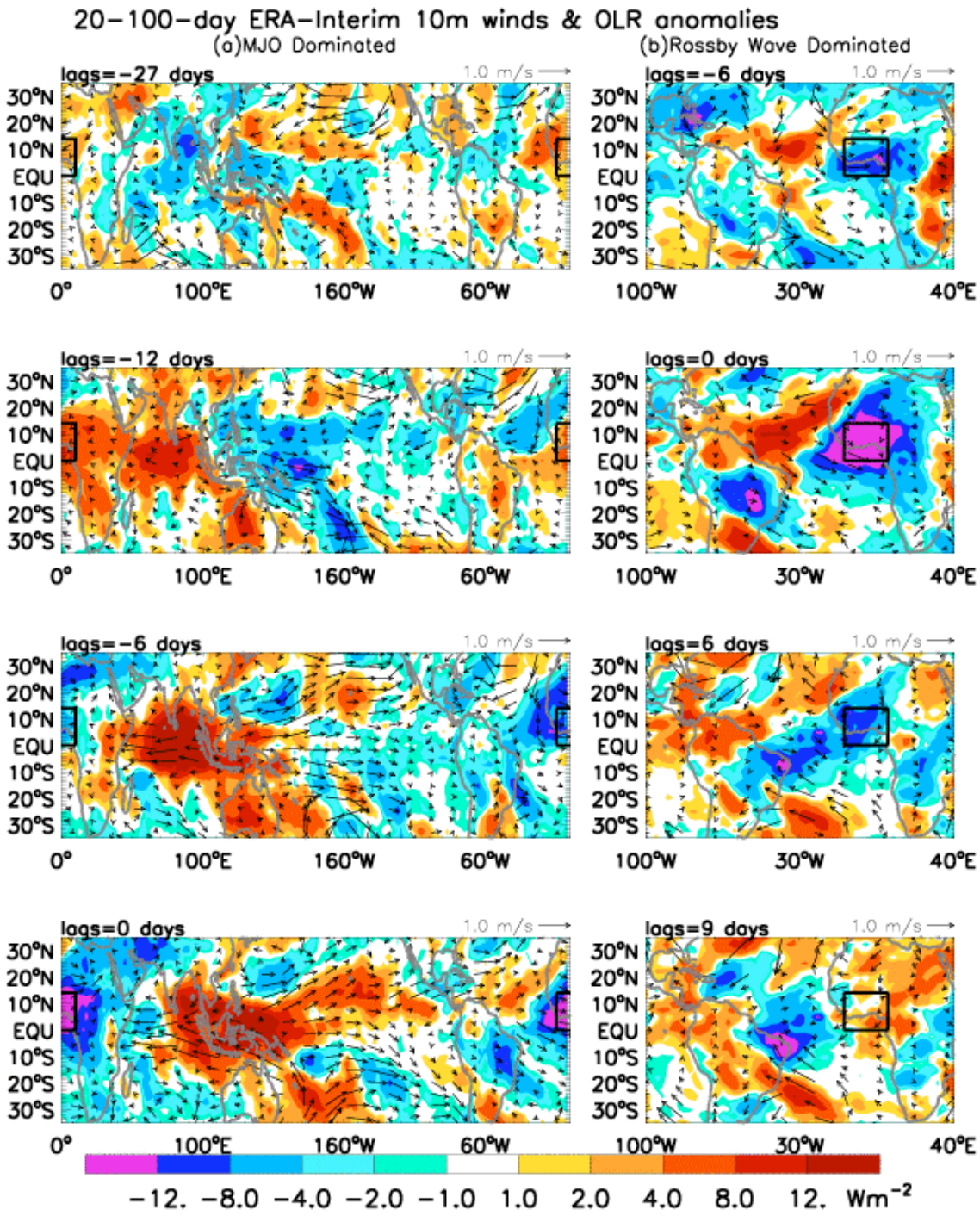

Figure 3.9. Same as Figure 3.7 except for convective events in African monsoon region.

Interestingly, the strength of the MJO convection varies following the MJO propagation from Western Atlantic to African monsoon region for different MJO events. For the MJO-dominated Western Atlantic events (Figure 3.7, left panels), convection obtains a large amplitude in the Western basin on day 0, and subsequently propagates eastward with weakened strength (day 6). These convective cases appear to be consistent with the MJO impacts examined in Chapter II, which obtain their largest impacts in the Western tropical Atlantic Ocean. For the Central Atlantic events (Figure 3.8, left panels), MJO convection propagates eastward without apparent change in strength.

In contrast, the situation for MJO-dominated convection in African monsoon region (Figure 3.9, left panels) is more complex. Convection first weakens from the western to the central Atlantic basin (from day -12 to -6), and then significantly enhances as it propagates to the African monsoon region by day 0. These evolutionary processes are more clearly seen in Figure 3.10 (left panels). This result suggests that the MJO impact on West African monsoon is not simply by direct eastward propagation of surface signatures. Rather, MJO can enhance likely due to upper-level atmospheric divergence, interaction with regional convective signals (Gu 2009), and possibly air-sea interaction over the Atlantic Ocean. All of which may contribute to an amplified influence in the West African monsoon region (Figure 3.6 and Table 3.1). Although the MJO dominated cases mainly occur during Nov-April, they can also happen in May-October during the West African monsoon season (Table 3.2). The possibility for air-sea interaction over the Atlantic Ocean to strengthen the MJO needs thorough investigation in our future research.

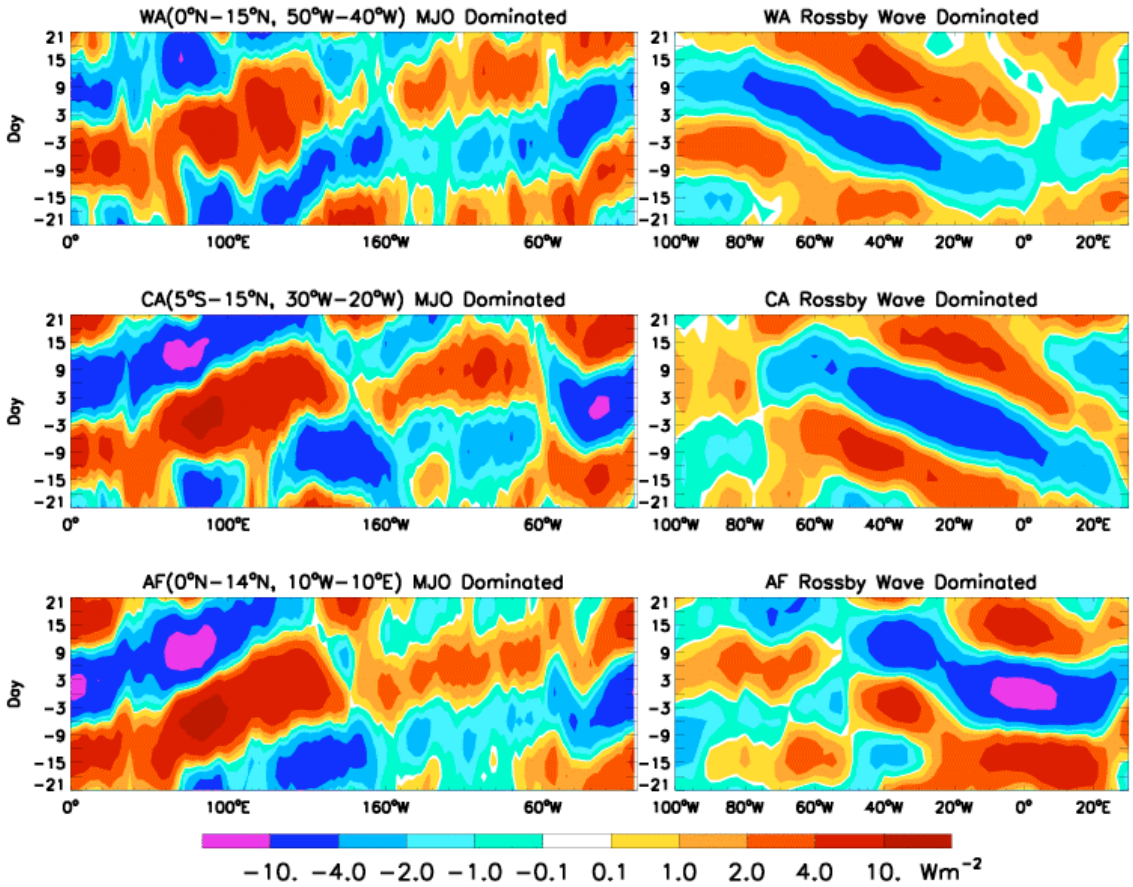

Figure 3.10. Longitude-time diagram of composite 20-100-day band-pass filtered OLR (averaged from 15°S to 15°N) based on the MJO (left panels) and Rossby wave (right panels) dominated convective events in WA (top), CA (middle) and AF (bottom).

Similarly, Rossby waves can have large impacts on intraseasonal surface winds and convection in the tropical Atlantic Ocean. Figure 3.7b shows the development and propagation of the Rossby wave dominated convective events in the Western Atlantic basin. First, weak convective anomaly appears in the Eastern Equatorial Atlantic basin (day -15). In the following days, convection enhances while it propagates westward along the equator, reaches its maximum strength in the Western Atlantic region by day 0, and further progresses westward on day 6, affecting the Caribbean Sea and Central America. The Rossby wave dominated events in the Central Atlantic are quite similar, except that convective anomaly is first initiated over the African continent, subsequently enhances in the eastern and central equatorial Atlantic basin, and then weakens in the western basin. These results suggest that Rossby waves can be generated in the Eastern Equatorial Atlantic and intensify as they propagate westward (Figure 3.7b), or they can be generated over the African continent and subsequently strengthen over the equatorial Atlantic Ocean (Figure 3.8b). These evolution processes are more clearly seen in Figure 3.10 (right panels), in which the impact of Rossby wave indicated as negative OLR anomalies can extend to 70^{o}W. The reason for their intensification over the Atlantic Ocean needs further investigation. Very likely candidate processes are air-sea interaction.

In contrast, for the Rossby wave dominated convective events in the West African monsoon region, their influence on surface wind and convection in the Atlantic Ocean are due to westward-propagating Rossby waves generated in the monsoon region. Convection anomalies weaken, rather than enhance, as they propagate westward to the Central and Western Atlantic basin. The westerly wind anomalies to the west of the

convective maxima exhibit apparent equatorial Rossby wave structure, with maximum westerly wind along the equator and two cyclonic wind shears off equator (Figure 3.9b on day 0).

Furthermore, we investigated the relationship between the MJO dominated convective events and the phase of the Rossby waves. About 82% of the MJO dominated convective events interfere constructively with the Rossby waves in Western Atlantic, and 94% in both Central Atlantic and West African Monsoon regions. This suggests that the MJO and Rossby waves together can amplify their impacts on convection and surface winds over the tropical Atlantic Ocean and African monsoon region.

At 25-60-day periods, the eastward-propagating signals result mainly from the MJO, and westward-propagating signals from Rossby waves (Figure 3.1). Here, composites of 25-60-day filtered OLR and ERA surface winds for both the MJO and Rossby waves are also analyzed for the West African monsoon region and we obtain similar results as those for the 20-100-day fields discussed above. These further suggest that the observed 25-60-day peak of African monsoon precipitation (Sultan and Janicot 2003a) can be affected by the MJO, consistent with previous studies (e.g., Foltz and McPhaden 2004; Matthews 2004; Maloney and Shaman 2008; Janicot et al. 2009; Gu 2009). On the other hand, Rossby waves associated with 25-60-day precipitation of African monsoon can propagate westward affecting the tropical Atlantic.

To verify the MJO dominated indices from Table 3.2, we compare all of the MJO dominated convective events in different regions (Table 3.2) with the selected MJO events from global MJO index used in configuring the composite maps for Figure 3.4. The results show that 91% of the MJO dominated convective events (Table 3.2) are picked up by the global MJO index and 78% are located in phase 6, 7 and 8. This result indicates that the categorized MJO dominated convective events in Table 3.2 are subset from the EOF based global MJO index. The former can effectively reveal the regional variability of the MJO impacts in the Atlantic and African monsoon regions.

3.3 Quasi-biweekly Oscillation of Tropical Atlantic and African Monsoon

Figure 3.11a shows the spectral analysis of OLR in the three regions shown in Figure 3.6a. Spectral peaks at 10-25-day periods are observed in all three regions and are more significant in the Eastern and Central Atlantic basins. The 25-60-day peaks are observed in all three regions and more evident in African monsoon region, consistent with our above discussion (Figure 3.6 and Table 3.1). In the western Atlantic, the 40-45-day peak is below the 80% significance level, and this could be related to the relative weak convective anomalies in this region. To confirm this, we perform spectral analysis using QuikSCAT zonal wind during 2000-08 in the same Western Atlantic region. The 50-60-day peak in the surface zonal wind (Figure 3.11b) is obvious, consistent with the correlation and coherence analysis in Section 2. Similar to Figure 3.11a, we analyze the ORL data with longer period during 1990-2008, and the 50-60-day peak becomes evident (Figure 3.11c). It indicates that there is a decade variation of OLR data in the Western Atlantic region for the 40-60-day intraseasonal signals. The 10-25-day and 25-60-day spectral peaks of OLR in African monsoon region are consistent with the observed two dominant periods of the African monsoon precipitation (Sultan and Janicot 2003a). Below, we focus on discussing the Quasi-biweekly variability, which is excluded by the 20-100-day filter discussed above.

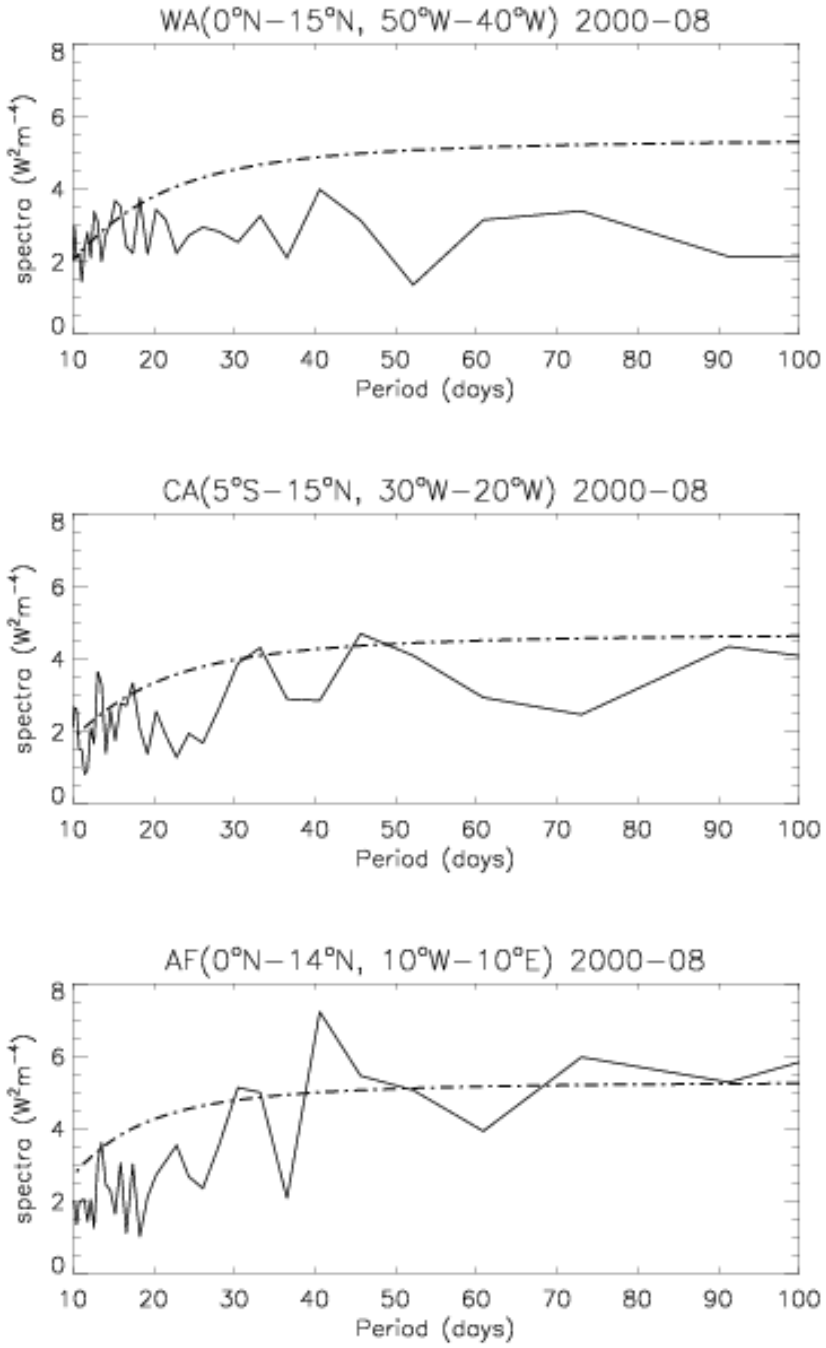

Figure 3.11a. Spectral analysis of OLR during 2000-08 for WA (top), CA (middle) and AF (bottom), see Figure 3.6a for geographic regions. Dot-dashed lines show 80% significance level.

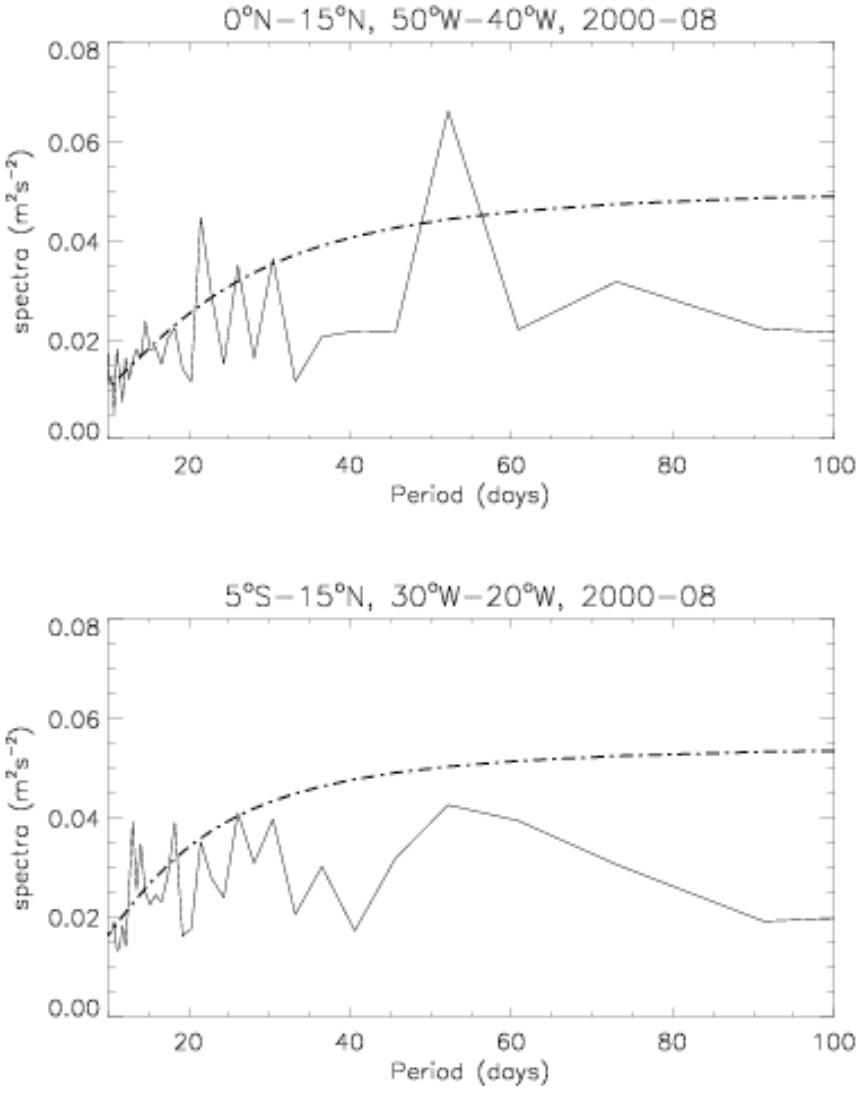

Figure 3.11b. Spectral analysis of QuikSCAT zonal wind during 2000-08 for WA (top), CA (middle), see Figure 3.6a for geographic regions. Dot-dashed lines show 80% significance level.

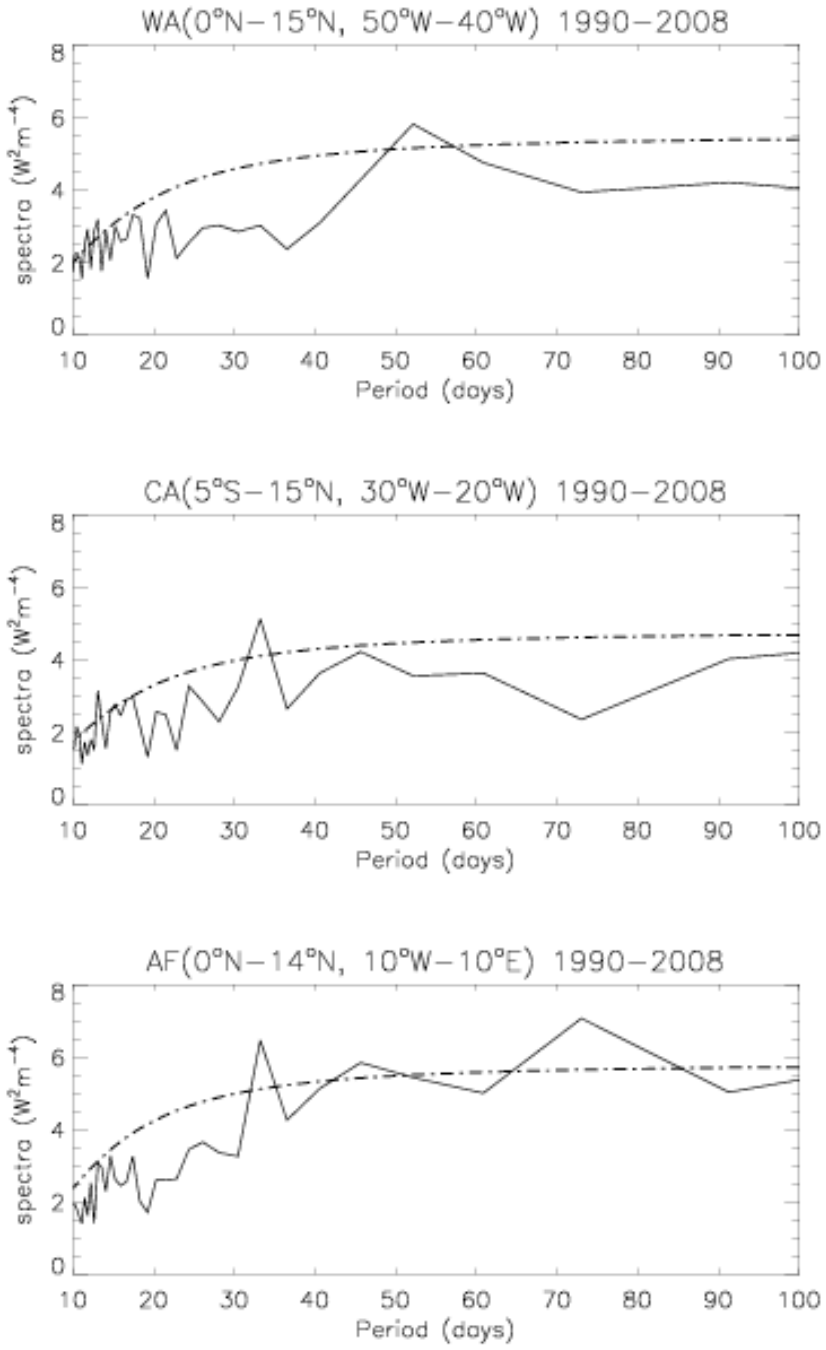

Figure 3.11c. Spectral analysis of OLR during 1990-2008 for WA (top), CA (middle) and AF (bottom), see Figure 3.6a for geographic regions. Dot-dashed lines show 80% significance level.

As shown in Figure 3.1, at 10-20-day periods, convection is associated with eastward Kelvin wave (near 10 days) and westward Rossby wave (near 20 days). Tables 3.3 and 3.4 show STDs of 10-25-day variability in Western Atlantic, Central Atlantic and African monsoon region (Figure 3.6a). The 10-25-day Rossby waves are filtered with zonal wavenumbers 1-8 (Figure 3.1). The STDs of Kelvin waves and Rossby waves comparing to the STD of 10-25-day OLR are 56% and 68% in Western Atlantic, 64% and 66% in Central Atlantic, and 71% and 61% in monsoon region (Table 3.3), suggesting the comparable importance of both the Kelvin waves and Rossby waves to 10-25-day intraseasonal variability in all three regions, with somewhat more frequent Rossby wave dominance in the Western Atlantic and Kelvin wave in the African monsoon region.

Table 3.3 The STD of domain-averaged 10-25-day filtered OLR The "%" is relative to the total 10-25-day OLR.

		WA	CA	AF
Standard Deviation (STD)	10-25-day OLR	7.8	6.7	7.2
	Kelvin Wave (percentage)	4.4 (56%)	4.3 (64%)	5.1 (71%)
	Rossby Wave (percentage)	5.3 (68%)	4.4 (66%)	4.4 (61%)
Correlation between 10-25-day OLR and	Kelvin Wave	0.56	0.67	0.75
	Rossby wave	0.67	0.55	0.69

Table 3.4. Convective events for total 10-25-day OLR exceeding 1 STD, Kelvin wave dominated events when Kelvin wave associated convection exceeds 1 STD of total 10-25-day OLR with the same phase, and Rossby wave dominated events when Rossby wave associated convection exceeds 1 STD of total 10-25-day OLR. The "%" is relative to total 10-25-day OLR events.

		WA			CA			AF		
	Dominated by	All	May-Oct	Nov-Apr	All	May-Oct	Nov-Apr	All	May-Oct	Nov-Apr
10-25-day convective events (beyond STD)	Total	127	58	69	120	42	78	117	44	73
	Kelvin wave	23 18%	5	18	47 39%	9	38	59 50%	15	44
	Rossby wave	45 35%	18	27	40 33%	11	29	40 34%	13	27

The correlation coefficient between the 10-25-day OLR and the Kelvin (Rossby) waves during 2000-08 period is 0.56 (0.67) in Western Atlantic, 0.67 (0.55) in Central Atlantic and 0.75 (0.69) in African monsoon region. As shown in Table 3.4, the Kelvin and Rossby wave dominated convective events (relative to total 10-25-day events) are 23 (18%) and 45 (35%) in Western Atlantic, 47 (39%) and 40 (33%) in Central Atlantic, and 59 (50%) and 40 (34%) in African monsoon region. This distribution is similar to the MJO versus Rossby wave effects at the 20-100-day periods. Similar to that of MJO activities (Table 3.2), the 10-25-day Kelvin wave dominated convective events are more frequent during Nov-Apr. Different from the 20-100-day Rossby waves, the 10-25-day Rossby wave dominated convective events occur more frequently during May-Oct than during Nov-Apr in all three regions.

Figures 3.12a-3.14a show the 10-25 day composite maps for the 10-25 day Kelvin wave dominated convective events (Table 3.4). The enhanced convection is first observed in the Amazon region and then propagates across the Atlantic, affecting the African monsoon region. Liebmann et al. (2009) discussed various mechanisms of the convectively coupled Kelvin waves in South America and Western Atlantic. Among which, the preexisting of the Kelvin waves in eastern Pacific and the precursor convection related to the cold surge in South America are more important. However, it remains unclear about the maintenance and propagation of the Kelvin waves in Atlantic, since the convectively coupled Kelvin waves could dissipate or strengthen when they propagate across the Atlantic as demonstrated in this study (Figures 3.12a-3.14a). Except

the large-scale dynamics, SST could be an important factor, and this will be addressed in our future studies with model experiment.

Figures 3.12b-3.14b show the 10-25-day composite maps for the westward convective events. Similar to 20-100-day Rossby waves (Figures 3.7b-3.9b), the 10-25-day convective anomalies first appear in the Eastern Equatorial Atlantic and West African equatorial region, and then strengthen in Central and Western Atlantic while they propagate westward (Figures 3.12b-3.13b), affecting the Western Atlantic and Caribbean Sea. Figure 3.14b demonstrates the case that 10-25-day convective anomalies reaches maximum in African monsoon region, and then propagates westward across the Atlantic with reduced strength.

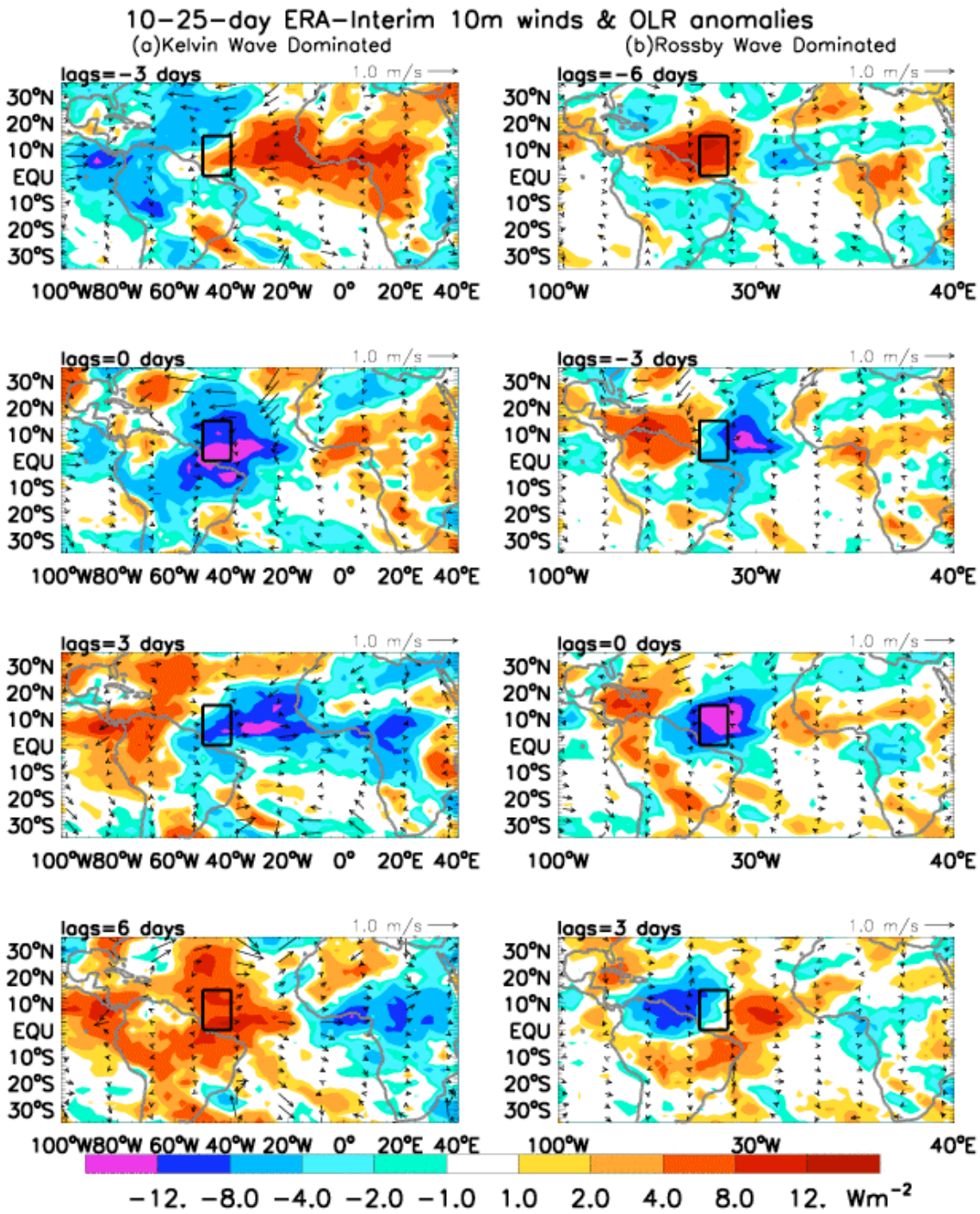

Figure 3.12. Composite fields of 10-25-day filtered ERA surface winds and OLR based on the 10-25-day Kelvin waves with zonal wavenumber 1-6 (a. left panels) and 10-25-day Rossby waves with zonal wavenumber 1-8 (b. right panels) dominated convective events in Western Atlantic (the black box).

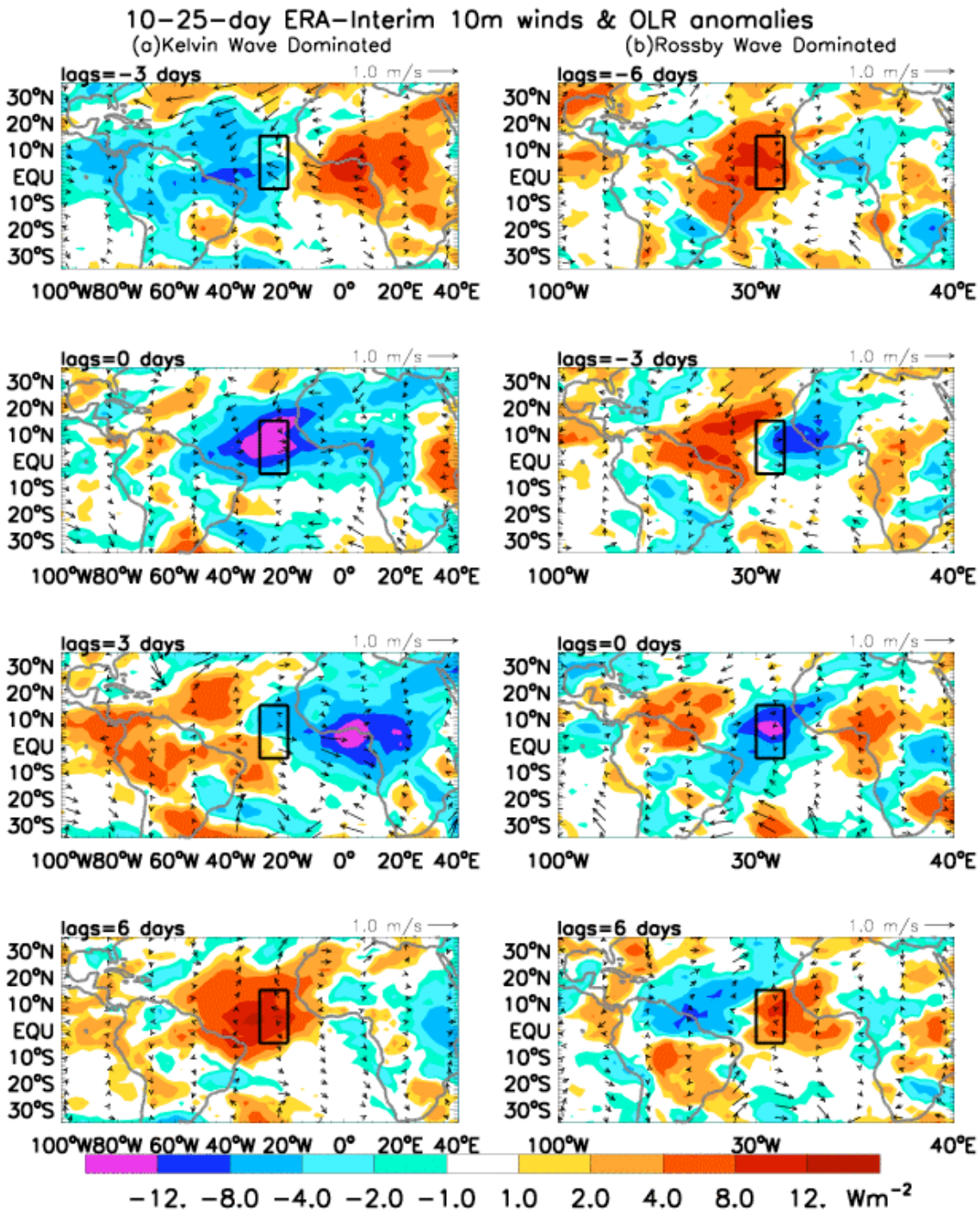

Figure 3.13. Same as Figure 3.12 except for convective events in Central Atlantic.

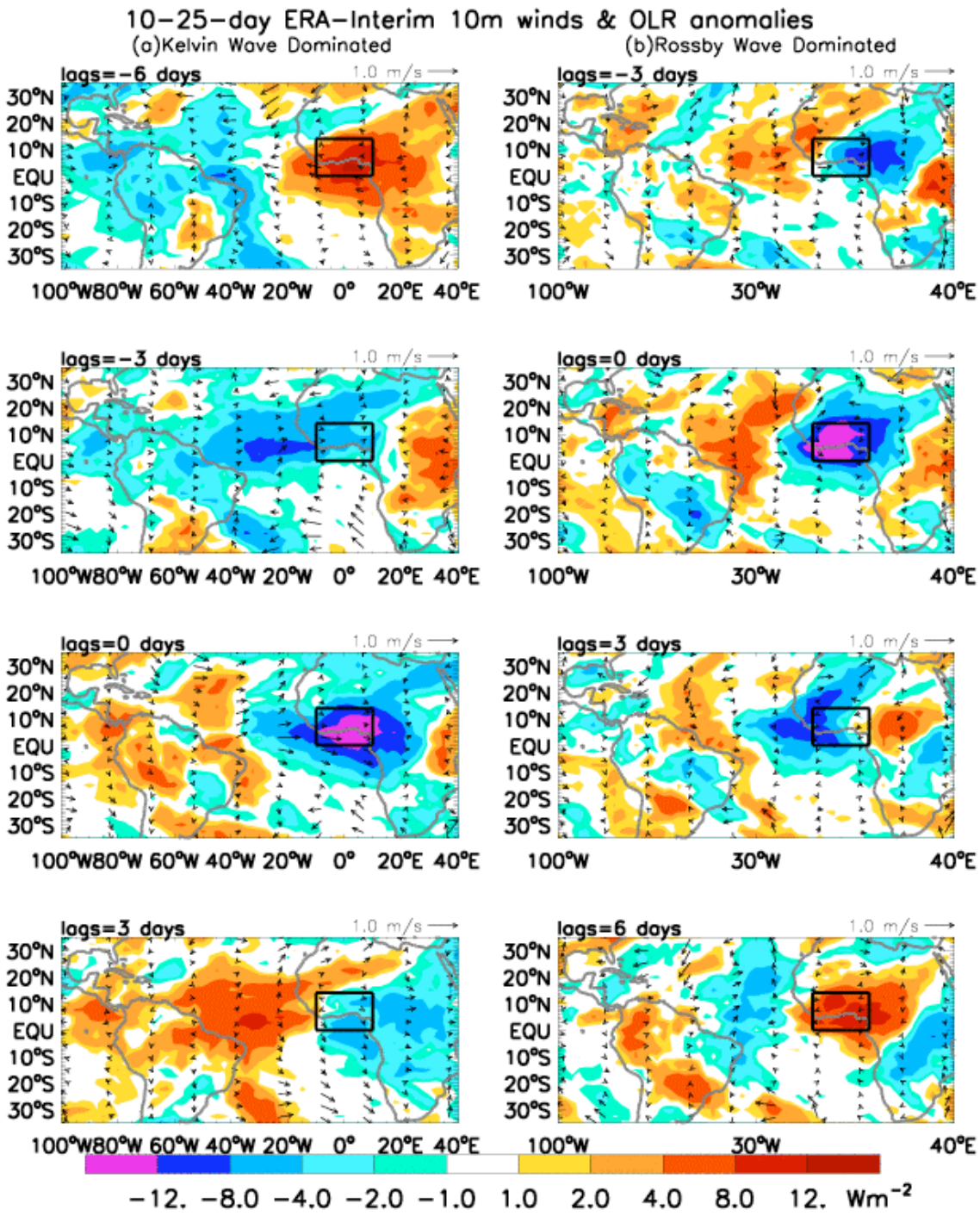

Figure 3.14 Same as Figure 3.12 except for convective events in African monsoon region.

The above results show that the eastward-propagating convective anomaly signals, both MJO and 10-25-day Kelvin waves, can be strengthened in the tropical Atlantic and have significant impacts in African monsoon region. On the other hand, the 10-100-day Rossby waves developed in the Atlantic can have significant impacts in Western Atlantic, Caribbean Sea and Central America. The Rossby wave dominated convective events, which reach maximum in African monsoon region, show less impact on the Western Atlantic due to the reduced strength during their westward propagation.

Previous studies have shown different mechanisms of the Rossby waves from African monsoon (Gu and Alder 2004; Gu 2009; Janicot et al. 2010; Taylor, 2008 and 2011). Figure 3.14b is consistent to the "Sahel" mode (Janice et al., 2010) for the bi-weekly Rossby waves and Figure 3.9b is similar to the observation of Sultan and Janicot (2003b) for the 25-60-day westward intraseasonal signals. Both show the dissipated Rossby waves from African monsoon region. However the cases that the Rossby waves strengthen or even originate over Atlantic ocean (Figures 3.7b, 3.8b, 3.12b and 3.13b) are not addressed. The related large-scale circulations and SST impacts on the maintenance, development and propagation of the intraseasonal signals over Atlantic remain unclear, and will be explored in our future studies.

Figures 3.12-3.14 suggest that the quasi-biweekly Kelvin waves originate from the Amazon region, consistent with Liebmann et al. (2009). Are the 10-25-day convection anomalies in Amazon region also related to the warm pool convection? To answer this question, we perform spectral analysis of OLR for the Amazon region (15^{o}S

to 5°N and 75°W to 45°W). The 10-25-day spectral peaks are evident and exceed 90% significance level (Figure 3.15). The spectral power, however, is weaker than that in the Western Atlantic basin (Figure 3.11a). This implies that the 10-25-day convective events originated from the Amazon can intensify in the Western Atlantic, or they can be generated by large-scale convection that spans the Amazon and Western Atlantic region, as shown by Figures 3.12-3.14 (right panels).

The lag correlation coefficients between a time series of 10-25-day OLR averaged in the Amazon region and 10-25-day OLR at each grid point, using OLR data during 2000-08, show that 10-25-day convection over Amazon does not seem to be directly correlated with convection in the Western Pacific warm pool (Figure 3.16). The maximum coefficients above 0.3 in the Eastern Pacific off Panama on day -2 and the maximum coefficients above 0.5 in Amazon area on day 0 suggest that the 10-25-day convective variability in the Amazon and Western Atlantic region is mainly generated locally and subsequently propagates eastward (Figures 3.16 and 3.11).

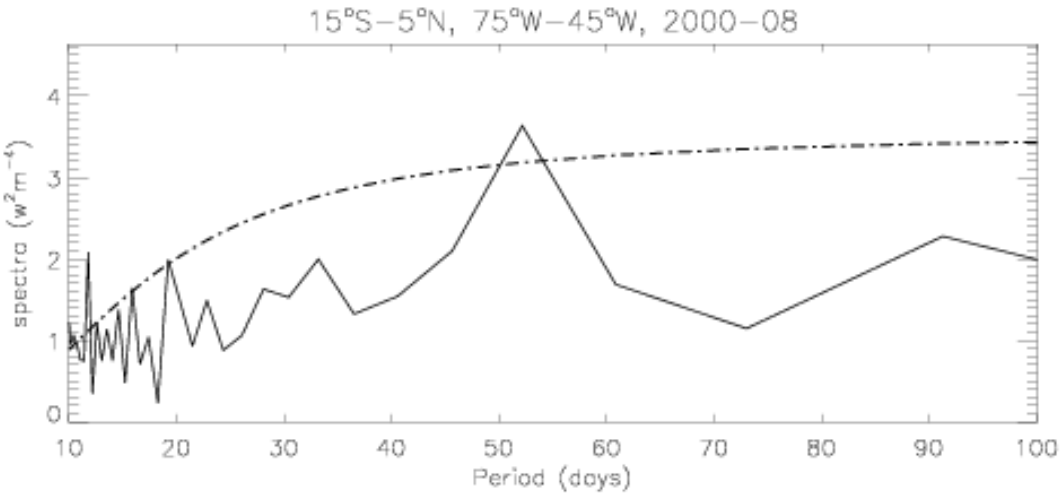

Figure 3.15. Spectral analysis of OLR during 2000-08 for Amazon region 15°S to 5°N and 75°W to 45°W). Dot-dashed line shows 90% significance level. Its topographic location is shown in Figure 3.16.

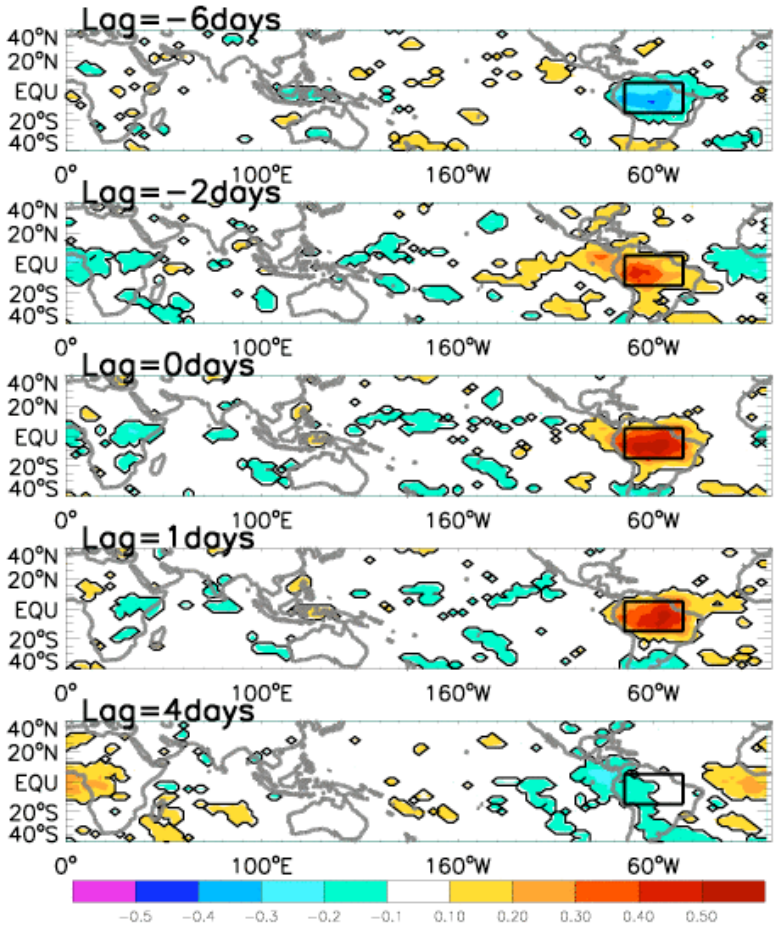

Figure 3.16. Correlation maps between time series of the 10-25-day OLR index of 2000-08 in the Amazon region (15°S to 5°N and 75°W to 45°W, black solid box) and 10-25-day OLR at each location of 40°S-40°N for lag= -6, -2, 0, 1 and 4 days. Solid line shows that the correlation exceeds 95% significance level. Note that the significance test takes into account the reduced degree of freedom due to the filter [Livezey and Chen, 1983].

CHAPTER IV

SUMMARY AND CONCLUSIONS

Intraseasonal variability (10-100-day periods) of surface wind and convection in the tropical Atlantic is analyzed using satellite wind, outgoing longwave radiation (OLR), precipitation, and ERA-interim reanalysis products for the period of 2000-2008. The ERA reanalysis winds for longer periods (ERA40 for 1960-2001 and ERA-Interim for 1990-2007) are also analyzed to confirm the statistical relationship. Both westward- and eastward-propagating intraseasonal signals are observed from surface winds, OLR and precipitation fields. The MJO dominates the 20-100-day eastward-propagating signals, quasi-biweekly Kelvin wave dominates the 10-25-day eastward-propagating signals and Rossby wave dominates the 10-100-day westward-propagating signals (Figure 3.1).

During 2002, spectral coherence and correlation analysis using QuikSCAT and ERA-Interim winds show that surface signatures of the MJO propagate from the western Pacific into the tropical Atlantic through Central America and the Panama gap, and with further propagation along the northern coastline of South America from the Caribbean Sea to the equatorial Atlantic (Figures 2.8 and 2.9). MJO events thus appear to be the primary cause of the observed 40-60-day bandpass filtered zonal surface wind anomalies in the equatorial Atlantic discussed by Han et al. (2008).

In the case study of 2002, strong convection and westerly wind anomalies associated with the MJO first propagate eastward into the western Pacific at a speed of about 5m/s as a Rossby-Kelvin wave packet. Near the dateline, the Rossby and Kelvin waves decouple, with the Kelvin wave propagating eastward along the equator into the Atlantic at a much faster speed. The off-equatorial convection maxima associated with the Rossby wave also propagates eastward, but at a slower rate (Figures 2.2, 2.3 and 2.5). The eastward propagation associated with off-equatorial features is accompanied by the eastward shift of mid-latitude convective anomalies, with possible feedbacks onto tropical convection. Another possible mechanism for the eastward propagation of OLR anomalies in the east Pacific ITCZ is the interaction of tropical eddies and the large-scale MJO flow (Maloney, 2009). These possibilities will be explored in future research.

Statistical calculations using QuikSCAT winds for 2000-06 and ERA-Interim surface data for 1990-2007 (Figure 2.12) show that Atlantic equatorial zonal surface winds are significantly correlated with the intraseasonal zonal winds in the western equatorial Pacific Ocean, a region where westerly wind anomalies associated with the MJO are strong. The maximum correlations exceed 0.4 (significant at the 90% confidence level for QuikSCAT and 95% confidence level for ERA-Interim) in the equatorial Atlantic region during boreal winter and spring, when the equatorial Atlantic winds lag the western Pacific winds by 9-15 days. The Isthmus of Panama and Central America appear to be an important pathway for the MJO to propagate from the Pacific into the Atlantic, consistent with the spectral coherence analysis during 2002 (Figures 2.8 and 2.9). The MJO impact on Atlantic surface winds during boreal summer and fall is

delayed relative to boreal winter and spring, with significant lag correlations apparent after 15 days, which suggests that interactions between the MJO and strong convective variability in the Western Hemisphere may delay MJO impacts. These results are consistent with previous studies showing that the character of the MJO has strong seasonality (Madden and Julian 1994; Jones et al. 2004; Matthews 2000), and were also verified using a long record of ERA40 reanalysis winds for 1960-2001. ERA products show scant evidence of MJO propagation across South America continent, which further suggests that surface winds associated with the MJO likely propagate into the Caribbean Sea across the Isthmus of Panama and Central America.

The results also show that generally, the MJO generated in Indo-Pacific Ocean (Figures 3.2-3.4 and left panels of Figures 3.7-3.10) and quasi-biweekly Kelvin waves related to the convection in Amazon-Western Atlantic area (left panels of Figures 3.12-3.14) can propagate across the equatorial Atlantic to impact the African monsoon. On the other hand, Rossby waves generated in the Eastern Equatorial Atlantic or African monsoon region propagate westward (Figure 3.5 and right panels of Figures 3.7-3.10), affecting the entire tropical Atlantic basin and even Caribbean Sea and Central America. Of particular interest is that the MJO and Kelvin wave can enhance over the tropical Atlantic Ocean while they propagate eastward, amplifying their impacts on the African monsoon (Figures 3.8a, 3.9a, 3.13a and 3.14a); Rossby waves can strengthen while they propagate westward, amplifying their effects in the west (Figures 3.7b, 3.8b, 3.12b and 3.13b).

The relative contributions from westward and eastward signals related to different atmospheric processes vary in different regions. At 20-100-day periods, the MJO has a larger contribution to convection and more frequently dominates the observed strong convective events in the African monsoon region than Rossby waves, with STD of OLR variability of 6.6 W/m^2 versus 4.0 W/m^2 (Tables 3.1 and 3.2), while Rossby waves are more important in Western Atlantic Ocean than MJO, with STD of 5.2 W/m^2 versus 4.3 W/m^2 (Tables 3.1 and 3.2). Both of the MJO and Rossby waves contribute approximately equally in the Central Atlantic basin.

The impacts of atmospheric intraseasonal variability in the Atlantic and African monsoon regions have significant seasonality. While the MJO is more intense during Nov-Apr than May-Oct in all three regions defined in Figure 3.6, the 20-100-day Rossby waves are stronger during Nov-Apr only in the African monsoon region, and they are comparable for the two seasons in the Western and Central Atlantic basins (Table 3.2). Indeed, there are more Rossby-wave dominated convective events during May-Oct in the Western and Central Atlantic (Table 3.2), which account for the observed westward-propagating signals of the 20-100-day OLR for this season (Figure 3.2).

In contrast, at 10-25-day periods, Rossby waves contribute more to the convective variability and more frequently dominate strong convective events in the Western Atlantic Ocean than the quasi-biweekly Kelvin wave, with OLR STD of 5.3 W/m^2 versus 4.4 W/m^2, while the quasi-biweekly Kelvin waves are more important in the African Monsoon region than Rossby waves, with OLR STD of 5.1 W/m^2 versus 4.4 W/m^2. Both

contribute almost equally in the Central Atlantic basin. Similar to the MJO, quasi-biweekly Kelvin waves are much more intense during Nov-Apr than May-Oct in all three regions. Different from the 20-100-day Rossby waves, which are equally important for both seasons in the Western and Central Atlantic, the quasi-biweekly Rossby waves are evidently stronger in Nov-Apr in all three regions, like the Kelvin waves (Table 3.4).

Results presented here support the notion that the MJO can propagate eastward affecting the African monsoon precipitation system. The results also support previous studies that Rossby waves from African monsoon precipitation can propagate westward to affect the tropical Atlantic Ocean. In addition, this study presents a few new findings. Firstly, results here show that the strong equatorial intraseasonal zonal wind variations of 2002 result largely from the MJO. Surface wind and convection associated with the MJO can propagate into the Atlantic through the Isthmus of Panama and Central America, affecting the subtropical Atlantic and equatorial region. Secondly, the relative importance of MJO and Rossby waves in causing intraseasonal variability of convection and surface wind are quantitative assessed in the tropical Atlantic Ocean and African monsoon region. Thirdly, some strong convective events associated with the MJO and quasi-biweekly Kelvin waves (Rossby waves) can enhance while they propagate eastward (westward) across the Atlantic Ocean. Interestingly, our results indicate that Rossby waves can also be generated in the Eastern Equatorial Atlantic Ocean, not only in the African monsoon region; the quasi-biweekly Kelvin waves appear to be generated in Amazon and Western Atlantic basin, consistent with previous studies (e.g., Liebmann et

al. 2009), which show various mechanisms of origin of convectively coupled Kelvin waves over South America.

Under what conditions do the MJO, Kelvin wave and Rossby wave strengthen, and what are the roles played by air-sea interaction over the Atlantic Ocean? What are the generating mechanisms for the Rossby waves from the Eastern Equatorial Atlantic basin? Since the MJO and equatorial waves play important roles in causing intraseasonal variations of surface wind and convection over the Atlantic Ocean, model experiments using high resolution weather research and forecasting (WRF) model may help to explore the detailed processes of air-sea interaction, local topography forcing, as well as the impacts of the large-scale atmospheric system related forcing. The strength variations of the intrapersonal signals in Atlantic could be controlled by the large-scale circulations and affected by SST. The WRF model experiments will focus on the SST variation and explore the large-scale dynamics. To what extent could SST affect the strength of convection, the propagation and even the origins of the convectively coupled equatorial Rossby waves? First, we will analyze the large-scale circulations for three regions (Western Atlantic, Central Atlantic and African monsoon area) when intraseasonal signals reach maximum, as well as the related SST anomalies and the possible mechanism. The WRF model simulation will be conducted to provide detailed dynamic information. Secondly, the WRF model experiments will focus on the intraseasonal variability of SST. Increasing, decreasing or removing the intraseasonal variations from the real SST data will show the impacts and importance of the SST related to the development and propagation or even origins of the intraseasonal signals in Atlantic.

Other extreme SST situations can also be tested, such as the fixed colder or warmer SST. Finally, the WRF model output will provide detailed evolution and propagating signatures, as well as the dynamic features. Analysis of those data could explore more interesting results. Through the WRF model experiments and analysis we would like to explore the related dynamics and SST conditions that the Rossby waves from African monsoon region can impact the western Atlantic and even NAM. Similar experiments can also be conducted and analyzed for the eastward propagating signals.

BIBLIOGRAPHY

Allan, Richard P., Brian J. Soden, Viju O John, William Ingram, and Peter Good (2010), Current changes in tropical precipitation, Environ. Res. Lett. 5, 025205

Arkin, P. A. and Ardanuy, P.E. (1989), Estimating climatic-scale precipitation from space: A review, J. Climate, 2, 1229-1238.

Avila , L. A. and R. J. Pash, (1995), Atlantic tropical systems of 1993, Monthly Weather Review, vol. 123, pp. 887–896.

——, and —— (1992), Atlantic tropical systems of 1992, Monthly Weather Review, vol. 120, pp. 2688–2696.

Barlow, M. and D. Salstein (2006), Summertime influence of the Madden-Julian oscillation on daily rainfall over Mexico and Central America, Geophys. Res. Lett., 33, doi:10.1029/2006GL027738.

Burpee, R. W. (1974), Characteristics of North African easterly waves during the summers of 1968 and 1969, Journal of the Atmospheric Sciences, vol. 31, pp. 1556–1570.

Chang, C. P., and H. Lim (1988), Kelvin wave-CISK: A possible mechanism for the 30 – 50 day oscillations, J. Atmos. Sci., 45, 1709 – 1720.

CLIVAR Madden Julian Oscillation Working Group (2009), MJO Simulation Diagnostics, J. Climate, 22, 3006-3030.

Duchon, C.E. (1979), Lanczos filtering in one and two dimensions, J. Appl. Sci., 61, 1004-1023.

Emanuel, K. A. (1987), An air-sea interaction model of intraseasonal oscillations in the tropics, J. Atmos. Sci., 44, 2324–2340.

Foltz, G.R., and M. J. McPhaden (2004), The 30-70 day oscillations in the tropical Atlantic, Geophys. Res. Lett., 31, L15025, doi:10.1029/2004GL020023.

Fu, Rong, M. Young, H. Wang, and W. Han (2007), Investigate the influence of the Amazon rainfall on westerly wind anomalies and the 2002 Atlantic Nino using QuikScat, Altimeter and TRMM dat. The NASA OVWST 2007 Meeting, 2007 EUMETSAT Meteorological Satellite Conference and the 15th American Meteorological Society Satellite Meteorological & Oceanography Conference, Amsterdam, The Netherlands, September 28, 2007.

—, B. Zhu, and R. Dickinson (1999), How do the atmosphere and land surface influence the seasonal changes of convection in tropical Amazon?, J. Climate, 12, 1306–1321.

Fu, Xiouhua, Bo Yang, Qing Bao, and Bin Wang (2008), Sea Surface Temperature Feedback Extends the Predictability of Tropical Intraseasonal, Oscillation. Monthly Weather Review 136:2, 577-597.

Garreaud, R. D. and J. M. Wallace (1998), Summertime incursions of midlatitude air into subtropical and tropical South America, Mon. Wea. Rev., 126, 2713–2733.

— (2000), Cold air incursions over subtropical South America: Mean structure and dynamics, Mon. Wea. Rev., 128, 2544–2559.

Goldenberg, S. B. Goldenberg and L. J. Shapiro (1996), Physical mechanisms for the association of El Nin˜o and West African rainfall with Atlantic major hurricane activity, Journal of Climate, vol. 9, no. 6, pp. 1169–1187.

Grabowski, Wojciech W. (2006), Impact of Explicit Atmosphere–Ocean Coupling on MJO-Like Coherent Structures in Idealized Aquaplanet Simulations, J. Atmos. Sci., 63, 2289–2306.

Grodsky, S.A., and J.A. Carton (2001), Coupled land/atmosphere interactions in the West African Monsoon, Geophys. Res. Lett., 28(8), 1503-1506.

Gu, G. (2009), Intraseasonal variability in the equatorial Atlantic-West Africa during March–June, Climate Dynamics 32:4, 457-471.

—, and R. F. Alder (2004), Seasonal evolution and variability associated with the west African monsoon system, J. Climate, 17, 3364-3377.

Hsu, H.-H., B. J. Hoskins, and F.-F. Jin (1990), The 1985/86 intraseasonal oscillation and the role of the extratropics, J. Atmos. Sci., 47, 823–839.

Han, W., P. J. Webster, J.-L. Lin, W. T. Liu, R. Fu, D. Yuan, and A. Hu (2008), Dynamics of intraseasonal sea level and thermocline variability in the equatorial Atlantic during 2002-2003, J. Phys. Oceanography, 38, 945-967.

—, T. Shinoda, L. Fu, and J.P. McCreary (2006), Impact of atmospheric intraseasonal oscillations on the Indian Ocean Dipole during the 1990s, J. Phys. Oceanography, 36, 670-690.

Held, I.M., and B. J. Hoskins (1985), Large-scale eddies and the general circulation of the troposphere, Adv. Geophysics, 28, 3–31, doi: 10.1016/S0065-2687(08)60218-6.

Hendon, H. H. and M. L. Salby (1994), The life cycle of Madden-Julian oscillation, J. Atmos. Sci., 51, 2225-2237.

Higgins, R.W., and W. Shi (2001), Intercomparison of the principal modes of interannual and intraseasonal variability of the North American monsoon system, J. Climate, 14, 403-417.

── and K. C. Mo (1997), Persistent North Pacific circulation anomalies and the tropical intraseasonal oscillation, J. Climate, 10, 3028–3046.

Hoskins, B. J., and G.-Y. Yang (2000), The equatorial response to higher-latitude forcing, J. Atmos. Sci., 57, 1197–1213.

Janicot, S., F. Mounier, N. M. J. Hall, S. Leroux, B. Sultan, and G. N. Kiladis, 2009: Dynamics of the west African monsoon: Part IV: Analysis of 25-90 day variability of convection and the role of the Indian monsoon. J. Climate, 22, 1541-1565.

── and B. Sultan (2001), Intra-seasonal modulation of convection in the West African monsoon, Geophys. Res. Letter, vol.28, 3, 523-526.

Jones, C., (2009), A homogeneous stochastic model of the Madden–Julian oscillation, J. Climate, in press.

──, and M. V. Carvalho (2006), Changes in the activity of the Madden–Julian Oscillation during 1958–2004, J. Climate, 19, 6353-6370.

──, M. V. Carvalho, R. W. Higgins, D. E. Waliser, and J. K. E. Schemm (2004), Climatology of tropical intraseasonal convective anomalies: 1979-2002, J. Climate, 17, 523-539.

──, and J. E. Schemm (2000), The influence of intraseasonal variations on medium- to extended-range weather forecasts over South America, Mon. Wea. Rev., 128, 486-494.

──, and B. C. Weare (1996), The role of low-level moisture convergence and ocean latent heat flux in the Madden-Julian Oscillation: An observational analysis using ISCCP data and ECMWF analyses, J. Clim., 9, 3086–3104.

Kessler, W. S., and R. Kleeman (2000), Rectification of the Madden-Julian oscillation into the ENSO cycle, J. Climate, 13, 3560-3575.

Kleeman, R. (1989), A modeling study of the effect of the Andes on the summertime circulation of tropical South America, J. Atmos. Sci., 46, 3344–3362.

Kiladis, G. N., K. H. Straub, and P. T. Haertel (2005), Zonal and vertical structure of the Madden-Julian Oscillation, J. Atmos. Sci., in press.

Knutson, R. R., K. M. Weickmann, and J. E. Kutzbach (1986), Global-scale intraseasonal oscillations of outgoing longwave radiation and 250 mb zonal wind during Northern Hemisphere summer, Mon. Weather Rev., 114, 605–623.

Krishnamurti, T. N., and D. Subramanyam (1982), The 30-50 day mode at 850 mb during MONEX, J. Atmos. Sci., 39, 2088-2095.

Landsea, C. W. (1993), A climatology of intense (or major) Atlantic hurricanes, Monthly Weather Review, vol. 121, no. 6, pp. 1703–1713.

Lau, K.M. and D.E. Waliser (eds) (2005), Intraseasonal Variability in the Atmosphere -Ocean Climate System, Praxis. Springer Berlin Heidelberg.

──, P.-J. Sheu, and I.-S. Kang (1994), Multiscale low- frequency circulation modes in the global atmosphere, J. Atmos. Sci., 51, 1169–1193.

──, and L. Peng (1987), Origin of low frequency (intraseasonal) oscillations in the tropical atmosphere. Part I: Basic theory, J. Atmos. Sci., 44, 950–972.

Lawrence, D. M., and P. J. Webster (2001), Interannual variations of the intraseasonal oscillation in the south Asian summer monsoon region, J. Climate, 14, 2910-2922.

Liebmann, B., and C. A. Smith, L. M. V. Carvalho, C. Jones, C. S. Vera, I. Blade´, and D. Allured (2009), Origin of convectively coupled Kelvin waves over South America, J. Climate, 22, 300–315.

──, and ── (1996), Description of a complete (interpolated), outgoing longwave radiation dataset, Bull. Am. Meterol. Soc., 77(6), 1275-1277.

──, and D. L. Hartmann (1984), An observational study of tropical midlatitude interaction on intraseasonal time scales during winter, J. Atmos. Sci., 41, 3333–3350.

Linter, Benjamin R. and J. David Neelin (2008), Time Scales and Spatial Patterns of Passive Ocean–Atmosphere Decay Modes, Journal of Climate 21:10, 2187-2203.

Livezey, R.E., and W.Y. Chen (1983), Statistical field significance and its determination by Monte-Carlo Techniques, Mon. Weather Rev. 111 (1), 46-59.

Lorenz, D.J. and D.L. Hartmann (2006), The effect of the MJO on the North American Monsoon, J. Climate, 333-343.

Madden, R. A., and P.R. Julian (1994), Observations of the 40-50 day tropical oscillation A review, Mon. Wea. Rev., 122, 814-837.

── (1986), Seasonal variations of the 40 – 50 day oscillation in the tropics, J. Atmos. Sci., 43, 3138–3158.

—, and P.R. Julian (1972), Description of global-scale circulation cells in the tropics with a 40-50 day period, J. Atmos. Sci., 29, 1109-1123.

—, and P.R. Julian (1971), Detection of a 40-50 day oscillation in the zonal wind in the tropical Pacific, J. Atmos. Sci., 28, 702-708.

Magana, V., and M. Yanai (1991), Tropical midlatitude interaction on the time scale of 30 to 60 days during the northern summer of 1979, J. Clim., 4, 180–201.

Majda, Andrew J., and Samuel N. Stechmann (2009), The skeleton of tropical intraseasonal oscillations, PNAS May 26, 2009 vol. 106 no. 21 8417–8422.

—, and J. A. Biello (2004), A multiscale model for tropical intraseasonal oscillation, Proc. Natl. Acad. Sci. U. S. A., 101, 4736–4741.

—, and R. Klein (2003), Systematic multiscale models for the Tropics, J. Atmos. Sci., 60, 393–408, doi: 10.1175/ 1520-0469(2003)060,0393:SMMFTT.2.0.CO;2.

Maloney, E. D., Adam H. Sobel and Walter M. Hannah (2010), Intraseasonal Variability in an Aquaplanet General Circulation Model, J. Adv. Model. Earth Syst., Vol. 2, Art. #5, 24 pp.

—, (2009), The moist static energy budget of a composite tropical intraseasonal oscillation in a climate model, J. Climate, 22, 711-729.

—, and J. Shaman (2008), Intraseasonal variability of the West African monsoon and Atlantic ITCZ, J. Climate, 21, 2898–2918.

—, D. B. Chelton, and S. K. Esbensen (2008), Subseasonal SST variability in the tropical Eastern North Pacific during boreal summer, J. Climate, 21, 4149-4167.

—, and D. L. Hartmann (2000), Modulation of Eastern North Pacific hurricanes by the Madden–Julian oscillation, J. Climate, 13, 1451–1460.

—, and D. L. Hartmann (1998), Frictional Moisture Convergence in a Composite Life Cycle of the Madden–Julian Oscillation, J. Climate, 11, 2387-2403.

Martin, E. (2010), Caribbean precipitation and the MJO, 29th Conference on Hurricanes and Tropical Meteorology, 10-14 May 2010, Tucson, AZ.

Matthews, Adrian J. (2004), Intraseasonal variability over tropical Africa during northern summer, J. Climate, 17, 2427-2440.

— (2000), Propagation mechanisms for the Madden-Julian Oscillation, Q. J. R. Meteorol. Soc. 2000, 126, 2637-2651.

——, and G. N. Kiladis (1999), The tropical-extratropical interaction between high frequency transients and the Madden-Julian Oscillation, Mon. Weather Rev., 127, 661–677.

——, B. J. Hoskins, and J. M. Slingo (1996), Development of convection along the SPCZ within a Madden-Julian Oscillation, Q. J. R. Meteorol. Soc., 122, 669–688.

McPhaden, M. J. (1999), Genesis and evolution of the 1997-98 El Niño, Science, 283, 950-954.

Milliff, R.F., and R.A. Madden (1996), The existence and vertical structure of fast, eastward-moving disturbances in the equatorial troposphere, J. Atmos. Sci., 53, 586-597.

Moore, A. M., and R. Kleeman (1999), Stochastic forcing of ENSO by the intraseasonal oscillation, J. Climate, 12, 1199-1200.

Mounier, F., S. Janicot, and G. N. Kiladis (2008), The West African monsoon dynamics. Part III: The quasi-biweekly zonal dipole, J. Climate, 21, 1911–1928.

Neelin, J. D., I. M. Held, and K. H. Cook (1987), Evaporation-wind feedback and low frequency variability in the tropical atmosphere, J. Atmos. Sci., 44, 2341–2348.

Nicholson, S. E. and Grist, J. P. (2003), The seasonal evolution of the atmospheric circulation over West Africa and equatorial Africa, J. Climate, 16, 1013–1030.

Pan, LL and Tim Li (2008), Interactions between the tropical ISO and midlatitude low-frequency flow, Clim Dyn, 31, 375-388.

Park, Chung-Kyu and Siegfried D. Schubert (1993), Remotely forced Instraseasonal Oscillations over the Tropical Atlantic, J. Atmos. Sci., 50, 89-103.

Rao, S.A., and T. Yamagata (2004), Abrupt Termination of Indian Ocean Dipole Events in Response to Intraseasonal Oscillations, Geophys. Res. Lett., 31, doi:10.1029/2004GL020842.

Raymond, D. J., and Eljka Fuchs (2009), Moisture Modes and the Madden–Julian Oscillation, J. Climate, 22, 3031-3046.

—— (2001), A new model of the Madden-Julian oscillation, J. Atmos. Sci., 58, 2807–2819, doi: 10.1175/ 1520-0469(2001)058,2807:ANMOTM.2.0.CO;2.

Redelsperger, J.-L., A. Diongue, A. Diedhiou, J. P. Ceron, M. Diop, J. F. Gueremy, and J. P. Lafore (2002), Multi-scale description of a Sahelian synoptic weather system representative of the West African monsoon, Quart. J. Roy. Meteor. Soc., 128, 1229–1258.

Salby, M. L., R. R. Garcia, and H. H. Hendon (1994), Planetary- scale circulations in the presence of climatological and wave- induced heating, J. Atmos. Sci., 51, 2344–2367.

Shapiro, L. J., and S. B. Goldenberg (1993), Intraseasonal Oscillations over the Atlantic, J. Climate, 6, 677-699.

── (1986), The three-dimensional structure of synoptic scale disturbances over the tropical Atlantic, Monthly Weather Review, vol. 114, no. 10, pp. 1876–1891.

Sikka, D. R., and S. Gadgil (1980), On the maximum cloud zone and the ITCZ over Indian longitudes during southwest monsoon, Mon. Wea. Rev., 108, 1840-1853.

Simmons, A., S. Uppala, D. Dee, and S. Kobayashi (2007), ERA-Interim: New ECMWF reanalysis products from 1989 onwards, ECMWF Newsletter, 110, 25–35.

Small, R. J., S.-P. Xie, E. D. Maloney, S. P. deSzoeke, and T. Miyama (2010), Intraseasonal Variability in the far-east Pacific: Investigation of the role of air-sea coupling in a regional coupled model, Clim. Dyn., 34, 24pp, DOI 10.1007/s00382-010-0786-2.

Sobel, A. H., E. D. Maloney, Bellon, G., and D. M. Frierson (2010), Surface fluxes and tropical intraseasonal variability: a reassessment. J. Adv. Model. Earth Syst., 2, Art. #2, 27 pp., doi: 10.3894/JAMES.2010.2.2.

── , E. D. Maloney, Bellon, G., and D. M. Frierson (2008), The role of surface fluxes in tropical intraseasonal oscillations, Nature Geoscience, 1, 653–657, doi: 10.1038/ ngeo312.

── , J. Nilsson and L. M. Polvani (2001), The weak temperature gradient approximation and balanced tropical moisture waves, J. Atmos. Sci., 58, 3650–3665, doi: 10.1175/ 1520-0469(2001)058,3650:TWTGAA.2.0.CO;2.

Sperber, K. R. (2003), Propagation and the vertical structure of the Madden-Julian Oscillation, Mon. Weather Rev., 131, 3018–3037.

Sugiyama, M. (2009a), The moisture mode in the quasi-equilibrium tropical circulation model. Part I: Analysis based on the weak temperature gradient approximation, J. Atmos. Sci., 66, 1507–1523, doi: 10.1175/ 2008JAS2690.1.

──, M. (2009b), The moisture mode in the quasi-equilibrium tropical circulation model. Part II: Nonlinear behavior on an equatorial beta-plane, J. Atmos. Sci., 66, 1525–1542, doi: 10.1175/2008JAS2691.1.

Sultan, B., and S. Janicot (2003a), The West African monsoon dynamics. Part I: Documentation of intraseasonal variability, J. Climate, 16, 3389-3406.

—, and — (2003b), The West African monsoon dynamics. Part II: The "Preonset" and "Onset" of the summer monsoon, J. Climate, 16, 3407-3427.

—, —, and A. Diedhiou (2003), The West African monsoon dynamics. Part 1: Documentation of intraseasonal variability, J. Climate, 16, 3389–3406.

Takayabu, Y. N., T. Iguchi, M. Kachi, A. Shibata, and H. Kanzawa (1999), Abrupt termination of the 1997-98 El Niño in response to a Madden-Julian oscillation, Nature, 402, 279-282.

Thorncroft, C.D., D. J. Parker, R. R. Burton, M. Diop, J. H. Ayers, H. Barjat, S. Devereau, A. Diongue, R. Dumelow, D. R. Kindred, N. M. Price, M. Saloum, C. M. Tayor, and A. M. Tompkins (2003), The JET2000 Project, Aircraft observations of the African easterly jet and African easterly waves, Bull. Amer. Meteor. Soc., 79, 815-829.

Wang, B., and X. Xie (1997), A model for the boreal summer intraseasonal oscillation, J. Atmos. Sci., 54, 72-86.

—, and T. Li (1994), Convective interaction with boundary layer dynamics in the development of the tropical intraseasonal system, J. Atmos. Sci., 51, 1386–1400.

—, and H. Rui (1990), Dynamics of the coupled moist Kelvin-Rossby wave on an equatorial beta plane, J. Atmos. Sci., 47, 397–413.

Webster, P. J. (1983), Mechanisms of monsoon transition: Surface hydrology effects, J. Atmos. Sci., 40, 2110-2124.

Weickmann, K. M., G. R. Lussky, and J. E. Kutzbach (1985), Intraseasonal (30 – 60 day) fluctuations of outgoing longwave radiation and 250 mb stream function during northern winter, Mon. Weather Rev., 113, 941–961.

Wheeler, M. C., and H. H. Hendon (2004), An all-season real-time multivariate MJO index: Development of an index for monitoring and prediction, Mon. Weather Rev., 132, 1917–1932.

—, and G. N. Kiladis (1999), Convectively Coupled Equatorial Waves: Analysis of Clouds and Temperature in the Wavenumber-Frequency Domain, J. Atmos. Sci., 56, 374-399.

Xie P., and P. A. Arkin (1997), Global precipitation: a 17-year monthly analysis based on gauge observations, satellite estimates, and numerical model outputs, Bull. Amer. Meteor. Soc., 78, 2539-2558.

Yanai, M., B. Chen, and W. W. Tung (2000), The Madden-Julian Oscillation observed during the TOGA COARE IOP: Global view, J. Atmos. Sci., 57, 2374–2396.

—, and M.-M. Lu (1983), Equatorially trapped waves at 200 mb and their association with meridional convergence of wave energy flux, J. Atmos. Sci., 40, 2785–2803.

Yasunari, T. (1981), Structure of an Indian summer monsoon system with around 40-day period, J. Meteor. Soc. Japan, 59, 336-354.

— (1979), Cloudiness fluctuations associated with the Northern Hemisphere summer monsoon, J. Meteorol. Soc. Jpn., 57, 227–242.

Yu, W., W. Han, E. D. Maloney, D. Gochis, and S. Xie (2011), Observations of eastward propagation of atmospheric intraseasonal oscillations from the Pacific to the Atlantic, J. Geophys. Res., 116, D02101, doi:10.1029/2010JD014336.

Zhang, Chidong (2005), Madden–Julian Oscillation, Reviews of Geophysics, 43, RG2003, 36 PP., 2005 doi:10.1029/2004RG000158.

— and H.H. Hendon (1997), Propagating and stationary components of the intraseasonal oscillation in tropical convection, J. Atmos. Sci., 54, 753-767.